The Reimagined Nummulites Factory, Using Machine Learning and Artificial Intelligence to Model Reservoir Sweet Spots in the Kirthar Formation of Jacobabad-Khairpur High, Southern Indus Basin Pakistan: Beyond the Microscope to Unlock the Diagenetic Features and Sequence Stratigraphy

Muhammad Haris[1], Syed Kamran Ali[1], Humza Tariq[2], Muhammad Zaheer[3], Tariq Mehmood[5]

[1] Institute of Geology, University of Azad Jammu & Kashmir, Muzaffarabad, Pakistan.
[2] Department of Geology, Hazara University, Mansehra, Pakistan.
[3] Geoscientist, Excellence Logging Turkey.
[5] Oil & Gas Development Company Limited, Islamabad, Pakistan.
* Harismuhammad873@yahoo.com.

DOI: 10.29322/IJSRP.16.08.2026.p17608
https://dx.doi.org/10.29322/IJSRP.16.08.2026.p17608

Paper Received Date: 25th June 2026
Paper Acceptance Date: 26th July 2026
Paper Publication Date: 8th August 2026

ABSTRACT

The Jacobabad-Khairpur High, a prominent structural feature within the Sukkur Rift Zone, delineates the boundary between the Central and Southern Indus Basins of Pakistan. This study presents an integrated analysis of the Middle to Late Eocene Kirthar Formation, based on a detailed 28.8 m measured section at Rohri, near Sukkur. The investigation combines outcrop analysis, petrography, and quantitative modeling using ML and AI to elucidate the depositional environments, diagenetic history, and reservoir potential of this economically significant carbonate succession. Four distinct lithofacies were identified in the field, ranging from coarse-grained, fossiliferous limestones to algal dolomitic limestones. Petrographic analysis of fourteen thin sections revealed six microfacies associations: (1) Benthonic Foraminiferal Nummulites Packstone, (2) Algal Foraminiferal Wackstone, (3) Foraminiferal Nummulites Wackstone-Packstone, (4) Benthonic Foraminiferal Wackstone/Oo-Biomicrite, (5) Planktonic Foraminiferal Nummulites Packstone, and (6) Bioclastic Carbonate Mudstone. These facies, classified using Dunham, Folk's, and Flügel schemes, indicate deposition on a homoclinal carbonate ramp, with environments spanning from inner-ramp shoals to lower-energy mid- and outer-ramp settings. The faunal assemblage, dominated by Large Benthic Foraminifera (LBF) such as Nummulites and Assilina, alongside red algae, confirms a shallow, warm-water marine setting. The overall progradational stacking pattern suggests deposition during a third-order regression (Regressive Systems Tract) within a broader second-order transgression. The Kirthar Formation has undergone a complex diagenetic history involving marine (micritization, fibrous cements), burial (compaction, stylolitization, blocky calcite cementation, neomorphism, dolomitization), and meteoric (dissolution, fracturing) phases. Reservoir quality is fundamentally controlled by the interplay between primary depositional fabric and subsequent diagenetic overprint. The best reservoir potential is identified in the grain-dominated packstone facies where secondary dissolution has created significant moldic and vuggy porosity. Conversely, porosity has been occluded in mud-dominated facies by compaction and extensive cementation. Stylolitization plays a dual role, acting as a barrier to vertical fluid flow while potentially serving as a conduit for lateral migration. This study demonstrates that understanding the paleotopographic control of the Jacobabad-Khairpur High on facies distribution, coupled with a detailed diagenetic model, is critical for predicting reservoir sweet spots in the Eocene carbonates of the Southern Indus Basin. Not only this, by integrating this diagenetic model with modern data science and quantitative ML and AI algorithms we have gone beyond the traditional microscopic petrography and qualitative interpretations, to provide a reliable, rigid and predictive data frame to identify the reservoir potential.

Keywords: Jacobabad-Khairpur High, Kirthar Formation, Microfacies, Carbonate Ramp, Diagenetic History, Reservoir Characterization, Sequence Stratigraphy, Southern Indus Basin, Machine Learning, Sweet Spots.

1. INTRODUCTION

1.1. The Eocene Carbonate Systems of the Neo-Tethys Margin

The Eocene epoch represents a critical interval in Earth's history, characterized by warm greenhouse conditions and the development of extensive carbonate platforms along the margins of the closing Neo-Tethys Ocean. (1) These platforms were dominated by Large Benthic Foraminifera (LBF), particularly the genus *Nummulites*, which formed vast accumulations of bioclastic sediment. (2) These Nummulitic limestones, extending from the Atlantic to the West Pacific, are not merely of academic interest; they constitute major hydrocarbon reservoirs in numerous basins across North Africa, the Mediterranean, and the Middle East. (3) The excellent reservoir qualities are often linked to the preservation of primary intraparticle porosity within the complex chambers of the foraminiferal tests, which can be significantly enhanced or degraded by subsequent diagenetic processes. (2) Consequently, understanding the depositional architecture and post-depositional evolution of these Eocene carbonate systems is paramount for global hydrocarbon exploration and production (Figure 1.1).

1.2. Geological Context and Hydrocarbon Significance of the Southern Indus Basin

The Southern Indus Basin of Pakistan, situated on the northwestern margin of the Indo-Pakistan Plate, is a prolific hydrocarbon province with a complex Mesozoic-Cenozoic history of rifting, drifting, and collision. (4) The basin hosts significant reserves in various stratigraphic units, including Cretaceous sandstones and Eocene limestones.[6]

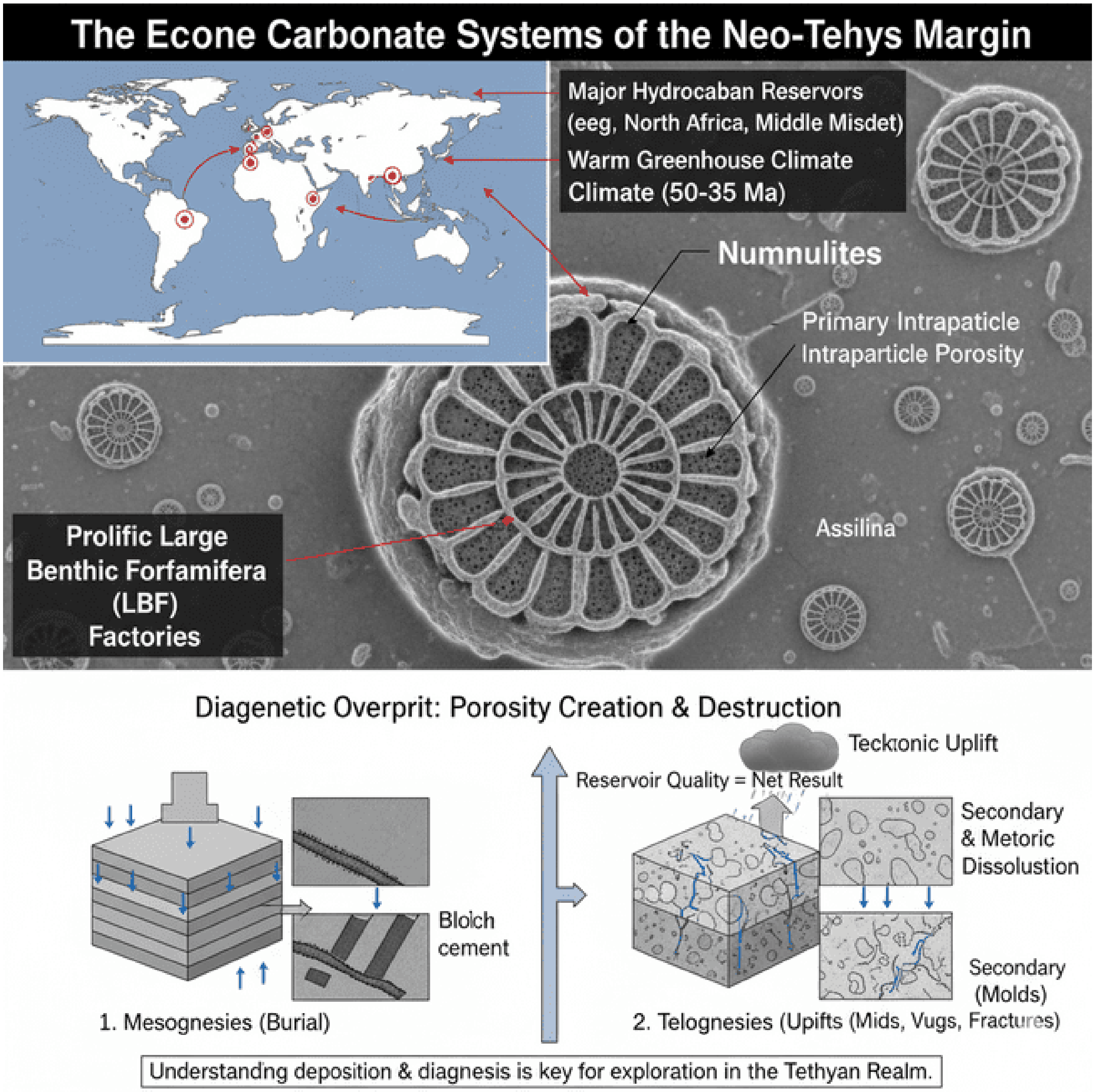

Figure 1.1: A geological infographic illustrating how Eocene carbonate systems of the Neo-Tethys margin, built by large benthic foraminifera (like Nummulites), form major hydrocarbon reservoirs and how their porosity is altered by subsequent diagenetic processes (burial and uplift).

The Eocene Kirthar Formation, a thick and widespread carbonate unit, is a key component of the regional petroleum system and has been a target for exploration. (7)

This study focuses on an outcrop of the Kirthar Formation in the vicinity of the Jacobabad-Khairpur High (JKH). The JKH is a major NNW-SSE trending basement-involved structural high, part of the Sukkur Rift Zone, which has exerted a profound influence on sedimentation patterns since at least the Jurassic.[9] As a long-lived paleotopographic feature, the JKH created elevated, shallow-water conditions on the Eocene shelf, providing an ideal setting for the proliferation of LBF and the development of high-energy carbonate facies. The structural and stratigraphic complexities associated with such basement highs make them critical areas for understanding facies distribution, diagenetic trends, and the localization of potential hydrocarbon reservoirs (Figure 1.2). (11)

1.3. Research Gaps and Study Objectives

While the stratigraphy, tectonics, and rich foraminiferal fauna of the Kirthar Formation and the Southern Indus Basin have been documented by numerous researchers (12), a detailed, integrated study linking depositional facies, diagenetic evolution, and quantitative reservoir characterization at the micro-scale is lacking for the Kirthar Formation on the strategically important Jacobabad-Khairpur High. Previous work has often been regional in scope or focused primarily on biostratigraphy. This study aims to address this gap by providing a comprehensive analysis of the Kirthar Formation at a well-exposed section in Rohri. The primary objectives are to:

1. Identify and characterize the lithofacies and microfacies of the Kirthar Formation using established carbonate classification schemes (Dunham, 1962; Folk, 1959; Flügel, 2004).
2. Reconstruct the paleo-depositional environment and develop a robust carbonate platform model based on facies analysis and faunal assemblages.
3. Establish a comprehensive diagenetic history, including a detailed paragenetic sequence of post-depositional alterations, and assess their impact on the rock fabric.
4. Evaluate the controls on reservoir potential by systematically analyzing the evolution of the pore system as a function of primary depositional facies and subsequent diagenetic overprint.
5. Introduce and discuss the application of novel quantitative methods, including mathematical petrophysical models and conceptual machine learning workflows, to support geological interpretations and provide a framework for future predictive reservoir modeling in this and similar carbonate systems. Figure 1.3 shows the analogy.

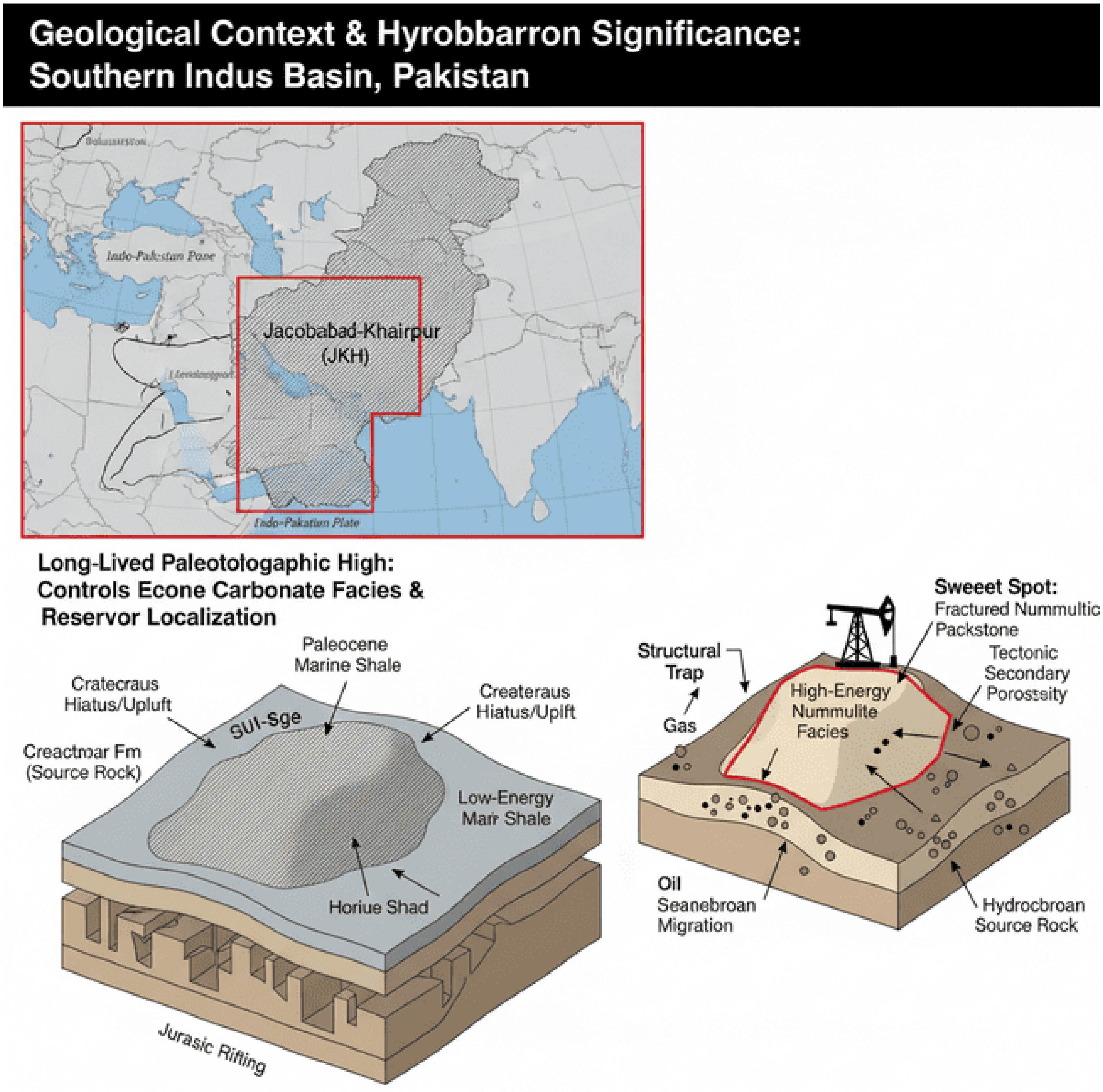

Figure 1.2: Geological Context and Hydrocarbons Significance Southern Indus Basin Pakistan, (Reference to JKH). illustrating the petroleum system of the Southern Indus Basin, Pakistan. It shows how an ancient paleotopographic high localized Eocene carbonate facies (reservoir rocks), which created structural traps for migrating oil and gas.

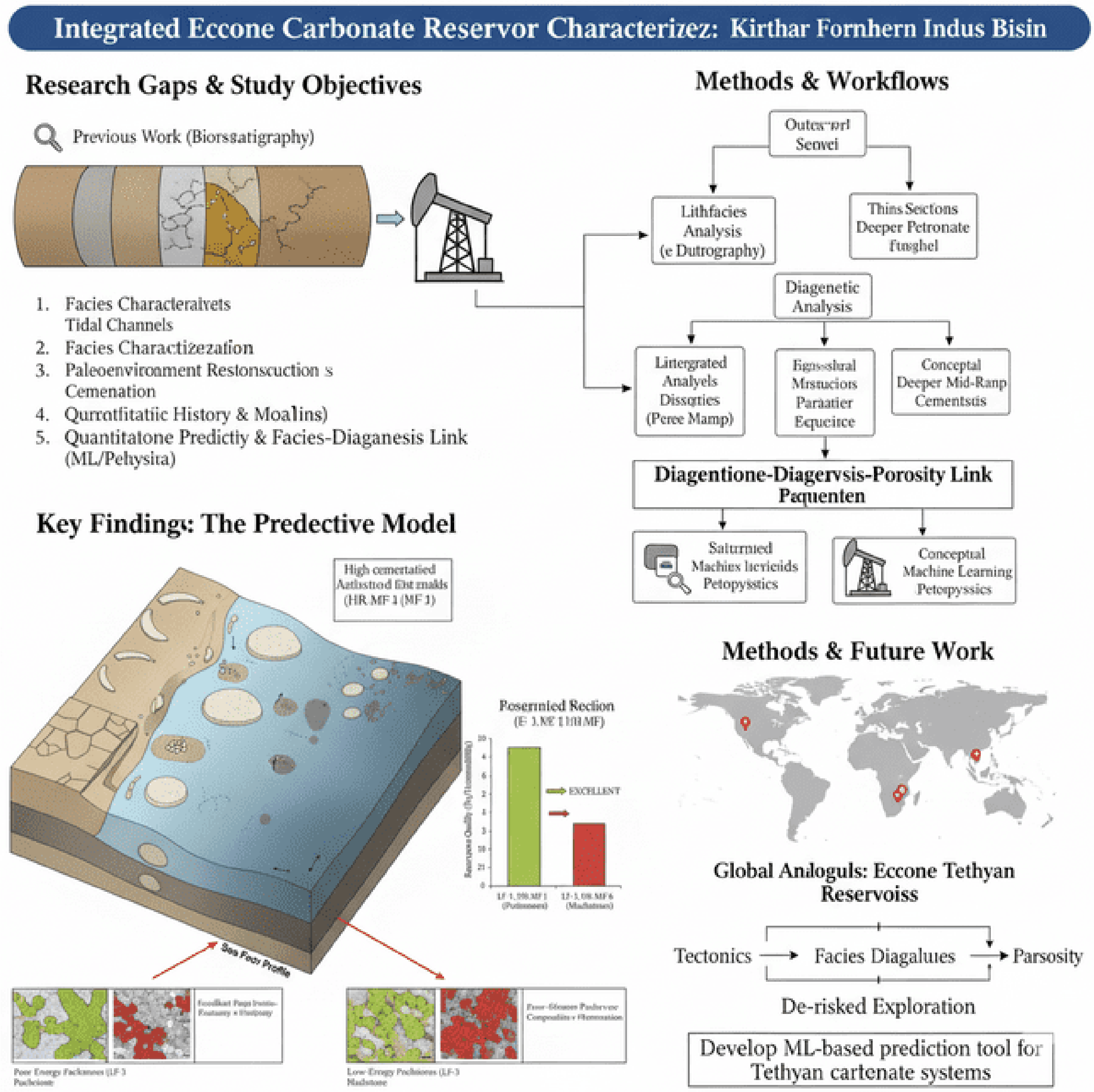

Figure 1.3: An integrated study for characterizing Eocene carbonate reservoirs in the Kirthar-Indus Basin. The workflow connects research gaps, methodologies (like facies and diagenetic analysis), and key findings to a predictive model for reservoir quality, with a future goal of developing a machine-learning tool for exploration.

2. GEOLOGICAL AND STRATIGRAPHIC FRAMEWORK

2.1. Tectonic Evolution of the Jacobabad-Khairpur High and the Sukkur Rift Zone

The study area is located on the Jacobabad-Khairpur High (JKH), a critical tectonic element that separates the Southern Indus Basin from the Middle Indus Basin. The JKH is a horst block structure trending NNW-SSE, forming part of the larger Sukkur Rift Zone, which also includes the Mari-Kandhkot High and the Pano Aqal Graben (11) (9). The genesis of this rift zone is linked to the Jurassic breakup of Gondwana, specifically the separation of the Indian Plate from the Australian-Antarctic Plate, which induced extensional tectonics and the formation of horst and graben structures (Figure 2.1). (9)

The JKH has acted as a persistent positive structural feature, or paleo-high, since its initial formation. Subsurface well data indicate that it remained uplifted and subject to subaerial exposure for significant periods, evidenced by the absence of the main Cretaceous source rock, the Sembar Formation, and in some areas, the entire Cretaceous succession, directly on the crest of the high. (11) This long-lived paleotopography fundamentally controlled the depositional architecture of overlying sequences. The high was subsequently submerged during the Paleocene, likely due to thermal subsidence as the Indian Plate passed over the Kerguelen Hotspot, becoming part of a broad carbonate shelf environment where the Paleocene Dunghan Formation and the subsequent Eocene successions, including the Kirthar Formation, were deposited. (11) The final structural expression of the high, including the exposure of Eocene rocks at the surface, is attributed to compressional forces and uplift during the Plio-Pleistocene Himalayan orogeny, related to the final collision of the Indian and Eurasian plates. (19) This tectonic history establishes the JKH not just as a structural boundary, but as a primary control on the specific shallow-water depositional environment in which the studied Kirthar Formation carbonates were deposited (Fig 2.3). The presence of coarse-grained, fossil-rich facies is a direct and predictable consequence of deposition atop this long-lived structural feature, where shallower water depths and higher hydraulic energy created favorable conditions for the proliferation of symbiont-bearing LBFs and associated fauna. (Figure 2.1) and (Figure 2.2) shows the detailed schematic structure.

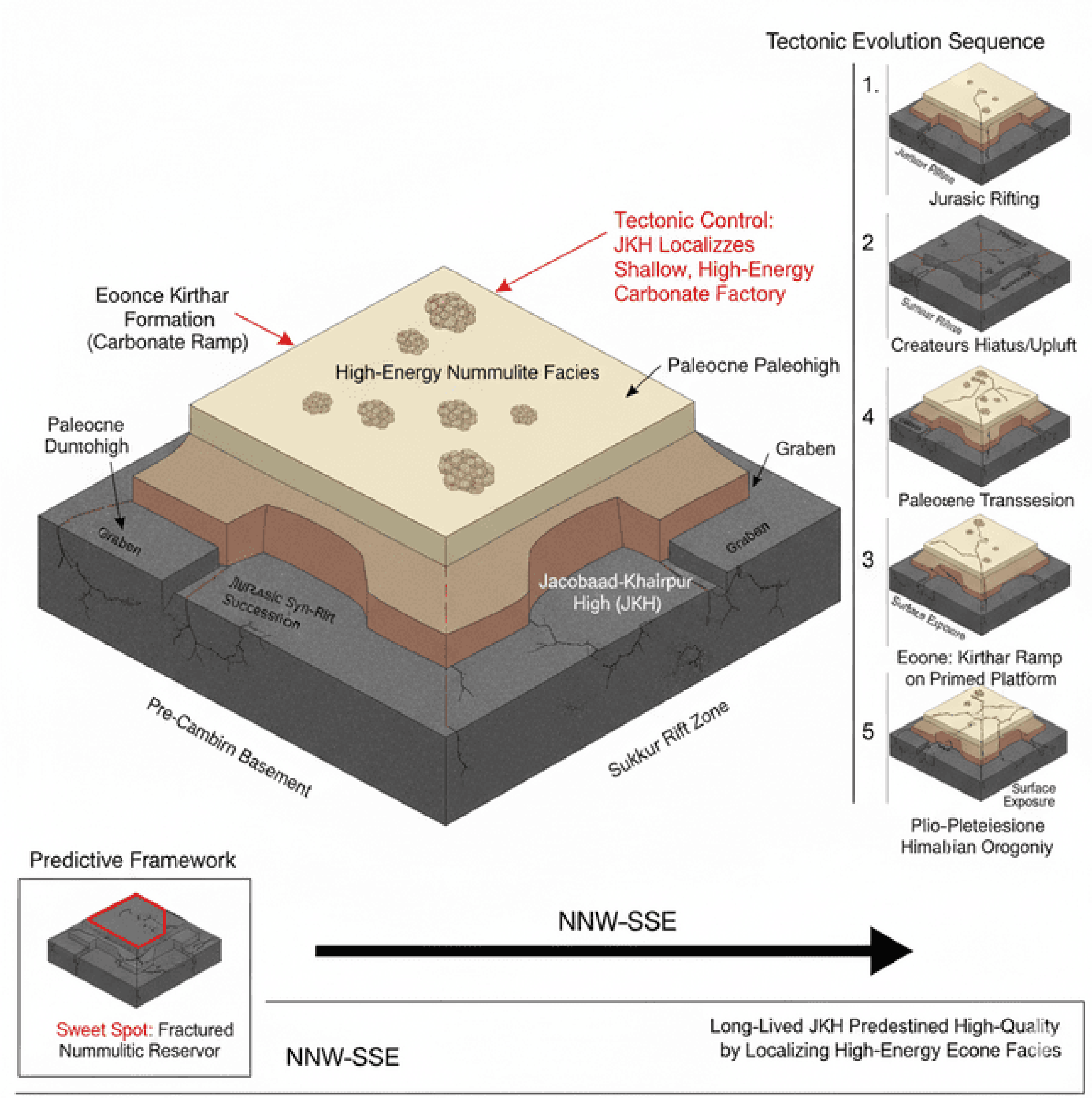

Figure 2.1: Tectonic Evolution of Jacobabad Khairpur Highs," showing how ancient (Pre-Cambrian) structures controlled the later deposition of Eocene-era carbonate reservoirs (High-Energy Nummulite Facies).

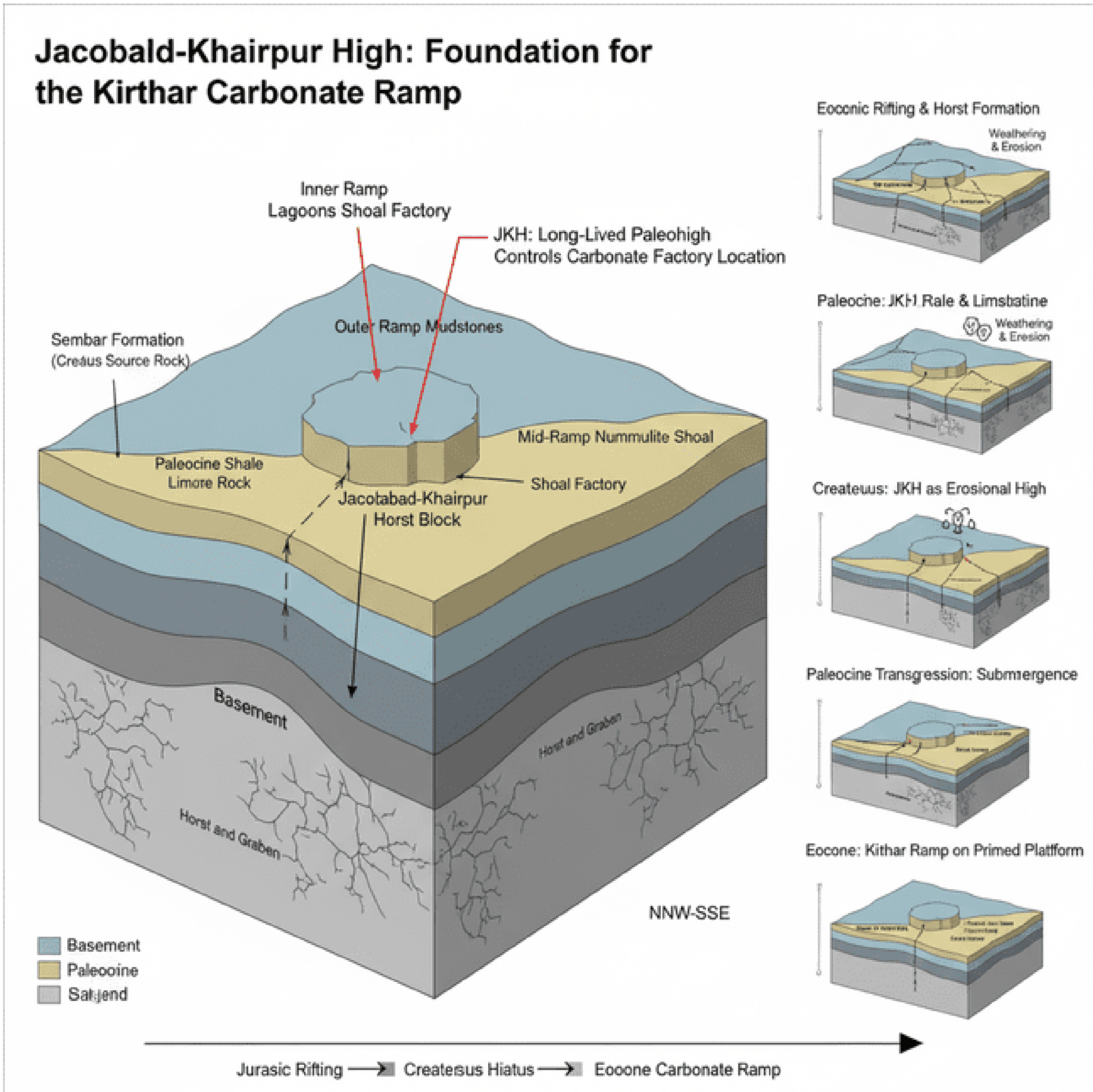

Figure 2.2: Jacobabad Khairpur High, a Foundation for Kirthar Carbonate Ramp. illustrating how the "Jacobald-Khairpur High," an ancient "Horst Block," provided a stable foundation (a "Long-Lived Paleohigh") for the development of the Kirthar Carbonate Ramp during the Eocene epoch. These steps show the area's progression from rifting and uplift ("Horst Formation") to submergence ("Transgression") and the final establishment of the carbonate ramp ("Kithar Ramp").

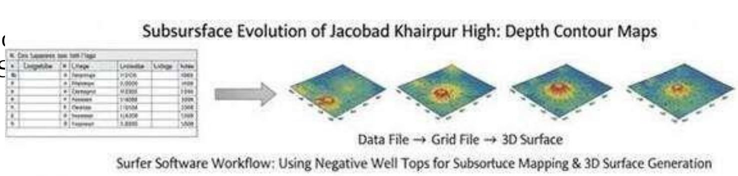

Figure 2.3. Structural Subsurface Evolution of Jacobabad Khairpur High at Different Time Periods, Modified after (9)**. The bulge in the picture is the uplift of the high which was the result of Himalayan Orogeny. A series of subsurface depth contour maps illustrating the geological evolution of the Jacobabad Khairpur High, showing its development as a persistent paleohigh from the Middle Jurassic through the Middle Eocene.**

2.2. Stratigraphy of the Southern Indus Basin with Emphasis on the Eocene Succession

The Southern Indus Basin contains a thick sedimentary sequence ranging from the Triassic to Recent alluvium. The generalized stratigraphic framework, summarized in Table 1, provides the context for the Eocene succession under investigation. The Mesozoic sequence includes the Triassic Wulgai Formation, the Jurassic Shirinab and Chiltan Formations, and a comprehensive Cretaceous package comprising the Sembar, Goru, Parh, and Pab Formations, among others. These units represent a complex history of marine deposition on a passive continental margin. (20)

A major unconformity often separates the Mesozoic and Cenozoic successions. The Paleocene is represented by the Ranikot Group, which is unconformably overlain by the Early Eocene Laki and Ghazij Formations. (13) The Kirthar Formation, the focus of this study, conformably and transitionally overlies the Ghazij Formation or its equivalent, the Laki Formation. It is predominantly a limestone unit with subordinate shale and marl interbeds. The upper contact of the Kirthar Formation is typically unconformable with the overlying Oligocene Nari Formation, marking a significant regional regression or period of uplift (Figure 2.1). Based on its rich foraminiferal assemblage, including diagnostic species such as *Nummulites striatus*, *N. fabiani*, and *Assilina dandotica*, the age of the Kirthar Formation in the study area is constrained to the Middle to Late Eocene (Bartonian to Priabonian) (Table 1) shows the stratigraphy of Southern Indus Basin. (23)

3. MATERIALS AND ADVANCED ANALYTICAL METHODS

3.1. Field Data Acquisition and Lithofacies Analysis

A comprehensive field investigation was conducted on an exposed section of the Kirthar Formation at Rohri (27° 40' 46'' N, 68° 54' 45'' E). The total thickness of the measured section is 28.8 m. The section was measured using the Jacob's Staff method and a measuring tape, with traverses oriented perpendicular to the strike of the beds to ensure accurate thickness measurements. Detailed lithological descriptions, including rock type, color, texture, bedding characteristics, fossil content, and sedimentary structures, were recorded at the outcrop. Based on these field observations, the section was subdivided into distinct lithofacies units (Figure 3.1). A total of 14 representative rock samples were collected from the base to the top of the section (Figure 3.2), ensuring that each identified lithofacies was sampled for subsequent laboratory analysis.

Table 1: Generalized Stratigraphy of the Southern Indus Basin (modified after Shah, 2009).

Era	Period/Epoch	Group	Formation	Lithology
Cenozoic	Pleistocene-Holocene		Alluvium/Lei Cong.	Alluvium, gravel, sand, silt, clay
	Miocene-Pliocene	Siwalik		Sandstone, shale, conglomerate
	Miocene		Gaj	Shale, sandstone, limestone
	Oligocene		Nari	Sandstone, shale, limestone
	Middle-Late Eocene		**Kirthar**	**Limestone, shale, marl**
	Early Eocene		Laki / Ghazij	Limestone, shale, sandstone
	Paleocene	Ranikot	Lakhra / Bara / Khadro	Limestone, sandstone, shale
Mesozoic	Late Cretaceous		Pab Sandstone	Sandstone
	Late Cretaceous		Fort Munro / Mughal Kot	Limestone, mudstone, shale
	Late Cretaceous		Parh Limestone	Limestone, marl

	Early-Late Cretaceous		Goru	Shale, limestone, siltstone
	Early Cretaceous		Sembar	Shale, siltstone, limestone
	Jurassic		Chiltan / Shirinab	Limestone, shale, sandstone
Paleozoic	Triassic		Wulgai	Shale, limestone

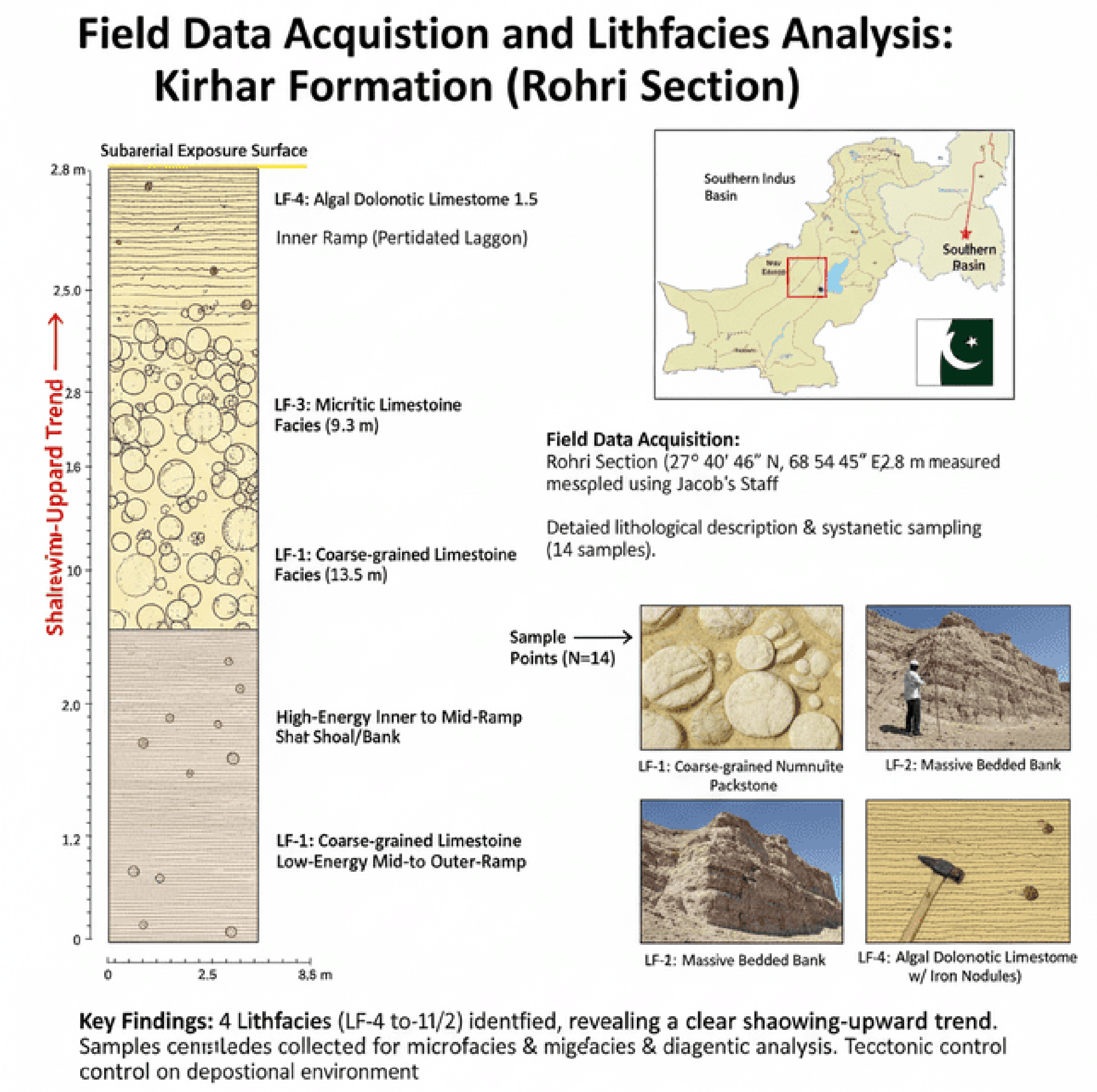

Figure 3.1: A detailed graphical representation of Field Data Collection. The main log on the left is a drawing of the rock layers studied. The most important discovery, shown by that big red arrow, is a clear "shallowing-upward trend." This just means the rocks at the bottom were formed in a deep sea, and as you move up the layers, the environment got progressively shallower—moving to a shoal, then a shallow lagoon, and finally becoming dry land. The photos on the right are what these ancient rocks actually look like in the field; the fossils in that "Nummulite Packstone".

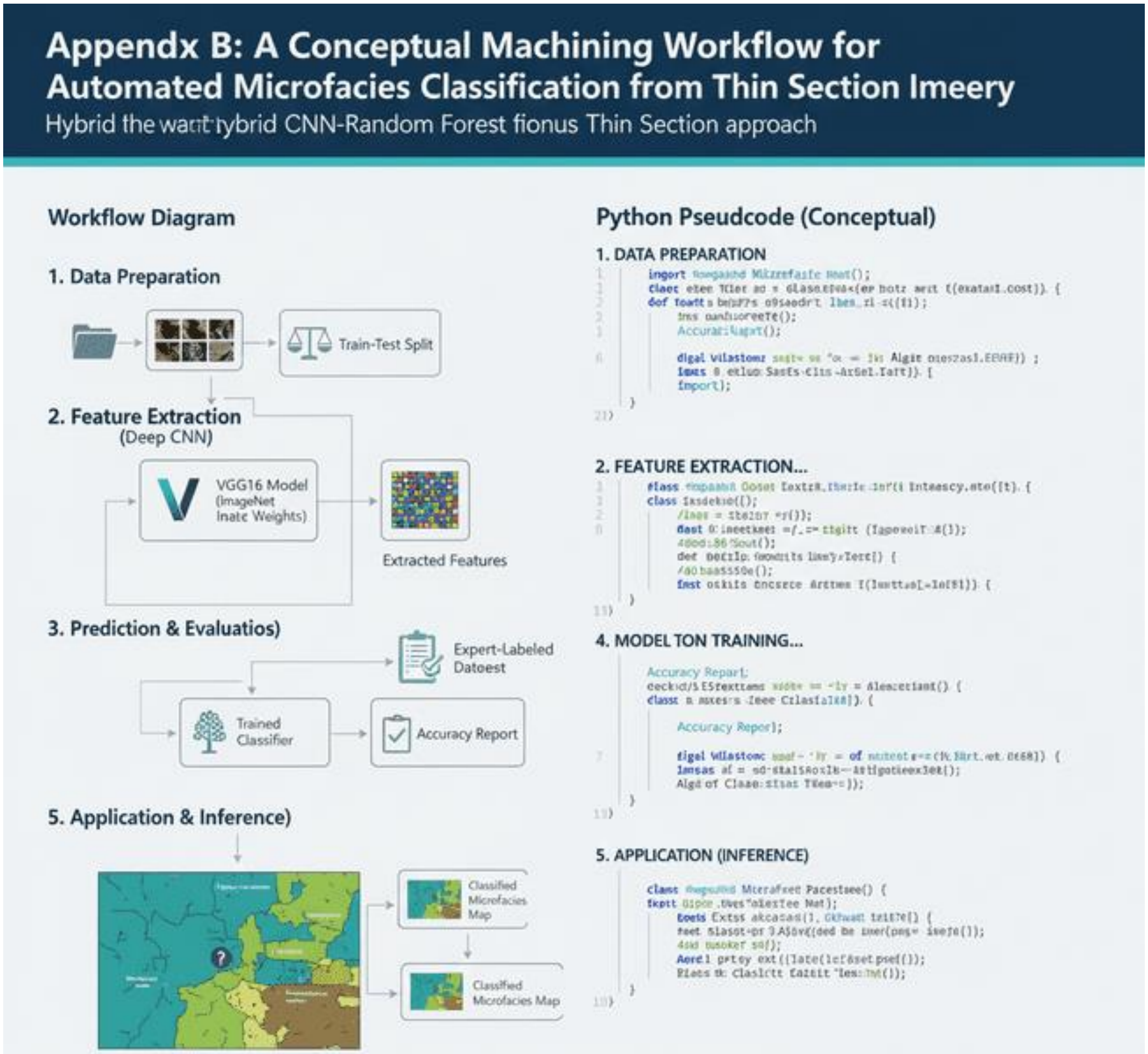

Figure 3.2: A detailed machine learning approach for the work using different networks and python scripts.

3.2. Petrographic Analysis

The 14 collected rock samples were processed to prepare standard thin sections (30 µm thickness) for detailed petrographic analysis. The thin sections were examined under a polarized light microscope to identify their mineralogical composition, textural characteristics, allochem types (skeletal grains, ooids, etc.), and diagenetic features. The carbonate rocks were classified based on their depositional texture using the schemes of Dunham (1962) and its modification by Embry and Klovan (1971). The compositional classification of Folk (1959) was used to categorize the limestones based on the relative proportions of allochems and micrite/sparite. The interpretation of microfacies and their paleoenvironmental significance was guided by the standardized microfacies types (SMF) and facies zones (FZ) proposed by Flügel (2004). (25) (Figure 3.3) shows the systematic approach allows for a robust reconstruction of the depositional environment and diagenetic history from the micro-scale evidence preserved in the rocks.

3.3. Quantitative Approaches to Reservoir Characterization

To augment the traditional geological interpretations and provide a forward-looking quantitative framework, this study conceptually incorporates advanced analytical methods. These approaches bridge the gap between qualitative petrographic description and quantitative reservoir property prediction.

3.3.1. Mathematical Modeling of Petrophysical Properties

The prediction of permeability from petrographic data in heterogeneous carbonates is a significant challenge. This study introduces the conceptual application of physics-based mathematical models, such as the Kozeny-Carman equation, which relates permeability to porosity and other geometric properties of the pore network. (26) In its modified form, the equation can incorporate parameters derived from thin section image analysis, such as average grain size (r_{grain}), tortuosity (T), and the fractal dimension (D) of the pore space. This approach provides a quantitative link between the observable rock fabric (texture and pore geometry) and its fluid-flow capacity, offering a powerful tool for predicting reservoir performance in areas with limited core data. (27) The theoretical basis for this model is detailed in Appendix A (Figure 3.4).

3.3.2. Machine Learning for Automated Facies Classification

Traditional petrographic analysis is time-consuming and can be subjective. Machine learning (ML) offers a pathway to rapid, objective, and automated classification of microfacies from digital thin section images. (31) This study proposes a conceptual workflow that leverages the power of deep learning for robust feature extraction and classification. The workflow involves using a pre-trained Convolutional Neural Network (CNN), such as VGG16 or ResNet, to extract complex textural and compositional features from image patches. These features are then fed into a classical machine learning classifier, like a Support Vector Machine (SVM) or Random Forest (RF), which is trained.

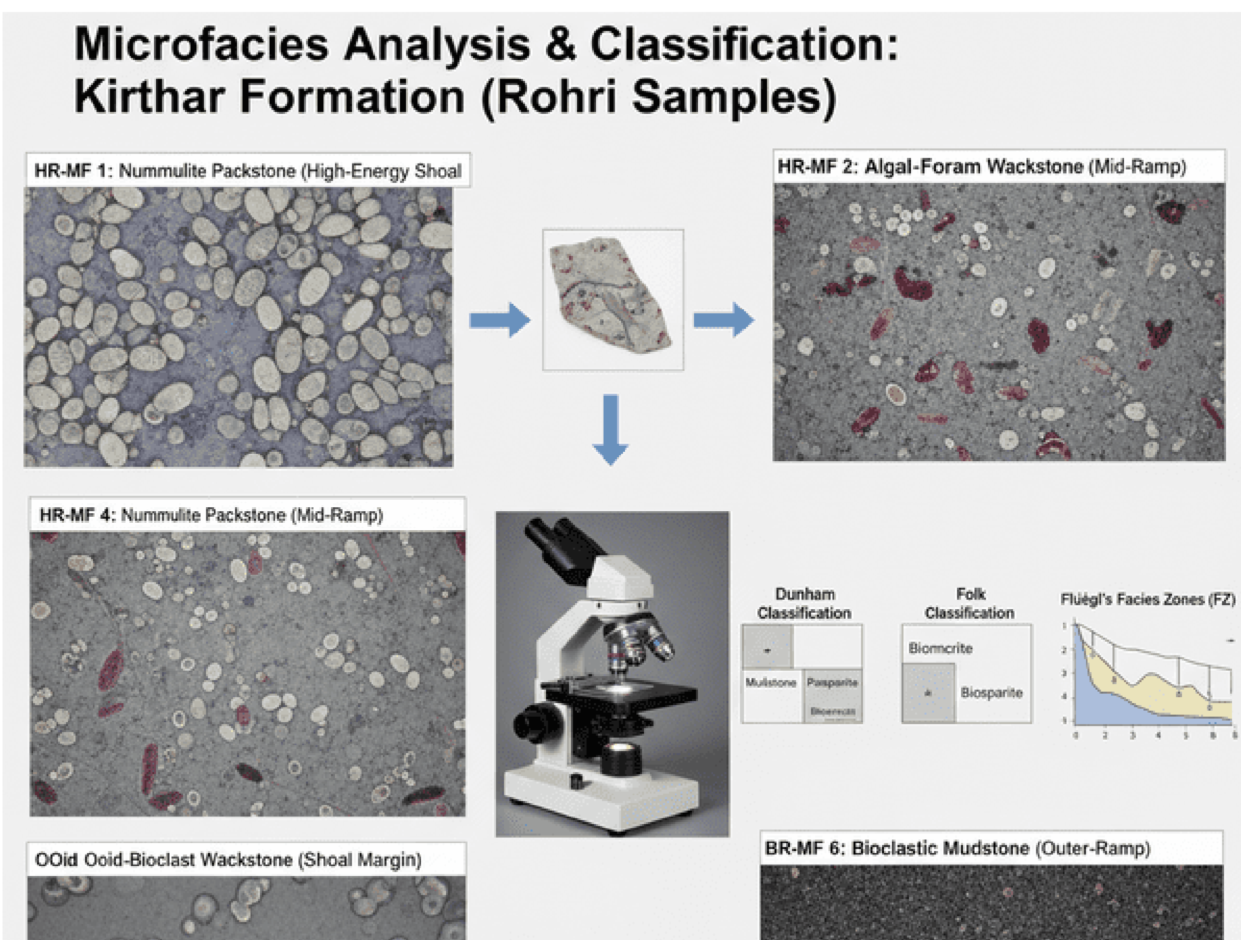

Figure 3.3: A systematic approach detail in a pictographic form from rock to thin section and under microscope using ML, All those different pictures are the 'micro-worlds' they find inside! Based on what they see—like a rock packed with fossils (a busy "High-Energy Shoal") or one that's mostly dark mud (a quiet "Outer-Ramp")—they can use classification charts to piece together the whole story of what that environment was like millions of years ago.

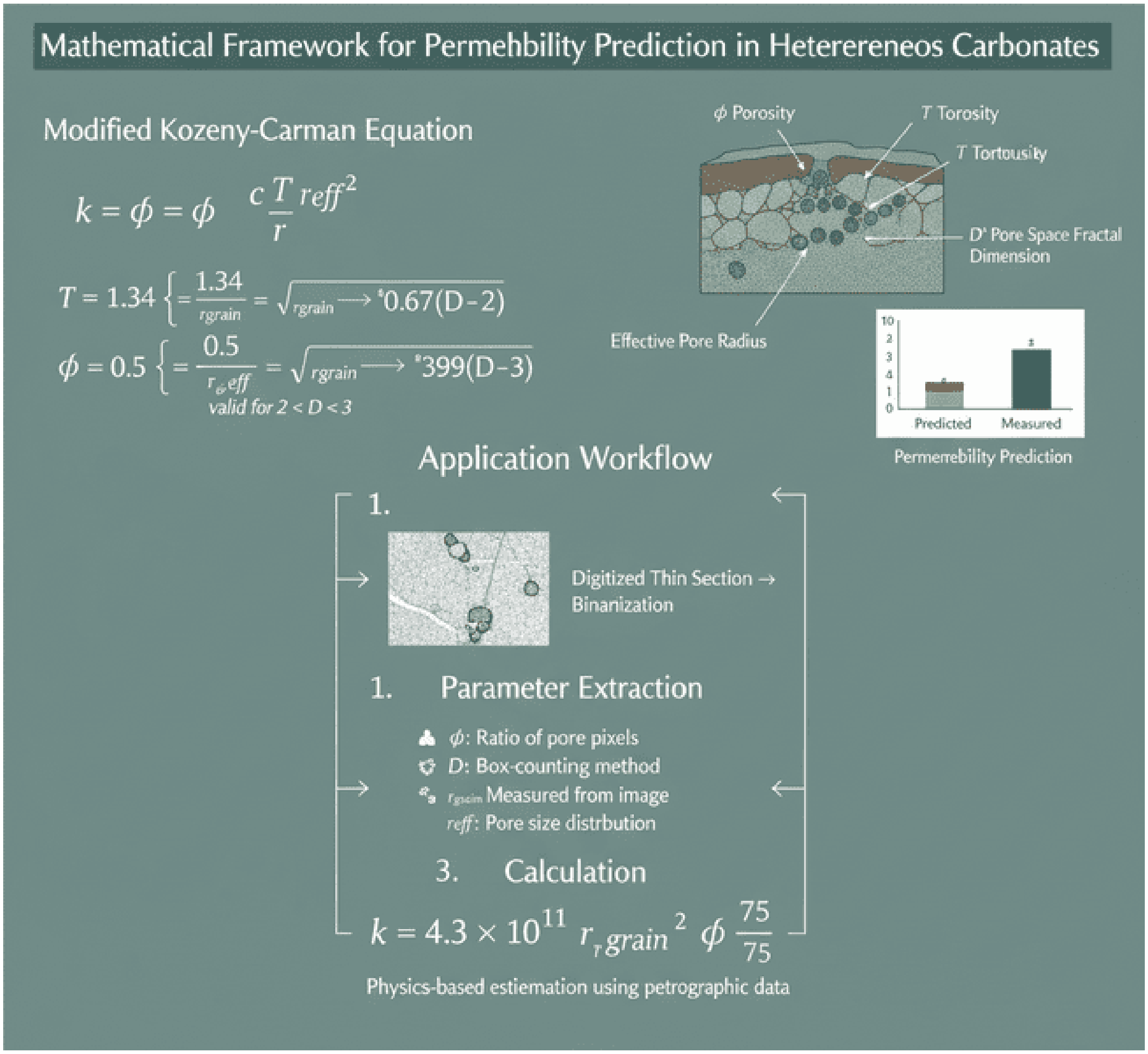

Figure 3.4: A mathematical approach using Machine Learning for Petrophysical work in Heterogenous Carbonates for Permeability calculations. Showing a method for predicting permeability (fluid flow) by analyzing microscopic rock images, extracting parameters like pore size, and using a modified Kozeny-Carman mathematical model to link the rock's micro-fabric to macro-scale flow.

on expert-labeled examples to classify new, unseen images. (34) This hybrid approach can significantly accelerate the characterization process, ensure consistency, and unlock quantitative data from vast archives of thin sections. A conceptual Python-based script outlining this workflow is provided in Appendix B and (Figure 3.5).

4. RESULTS: FROM OUTCROP TO MICRO-SCALE

4.1. Lithofacies of the Kirthar Formation

Based on outcrop observations of lithology, bedding style, texture, and faunal content, the 28.8 m measured section of the Kirthar Formation was subdivided into four distinct lithofacies (LF), described from base to top. The characteristics of these lithofacies are summarized in Table 2.

- **LF-1: Coarse-grained Limestone Facies:** This facies constitutes the thickest unit in the section (13.5 m) and is characterized by its whitish to yellowish color, coarse-grained texture, and thick to massive bedding. It is highly fossiliferous, dominated by abundant tests of LBF, including various species of *Nummulites* and *Assilina*. This facies represents the highest energy conditions observed at the outcrop (Figure 4.1a,b) and (4.2a).
- **LF-2: Massive Bedded Limestone Facies:** Overlying LF-1, this 4.5 m thick unit is distinguished by its maroonish-white color and massive, cliff-forming appearance. It remains rich in LBF, similar to the underlying facies, but exhibits a more homogenous, massive fabric (Figure 4.1).
- **LF-3: Micritic Limestone Facies:** This 9.3 m thick facies marks a shift to lower energy conditions. It is composed of yellowish, whitish, and maroonish micritic limestone (mudstone/wackestone). The abundance and size of fossils, particularly LBF, are noticeably reduced compared to the underlying facies (Figure 4.1a and b) and (Figure 4.2b).
- **LF-4: Algal Dolomitic Limestone Facies:** The uppermost unit of the measured section is a 1.5 m thick, yellowish-brown, laminated dolomitic limestone. (Figure 4.1a and b) This facies contains evidence of red algae, gastropods, and bioturbation (worm burrows). The presence of limonite, chert, and iron nodules suggests possible subaerial exposure or deposition in a very shallow, restricted, and evaporitic setting (Figure 4.2c).

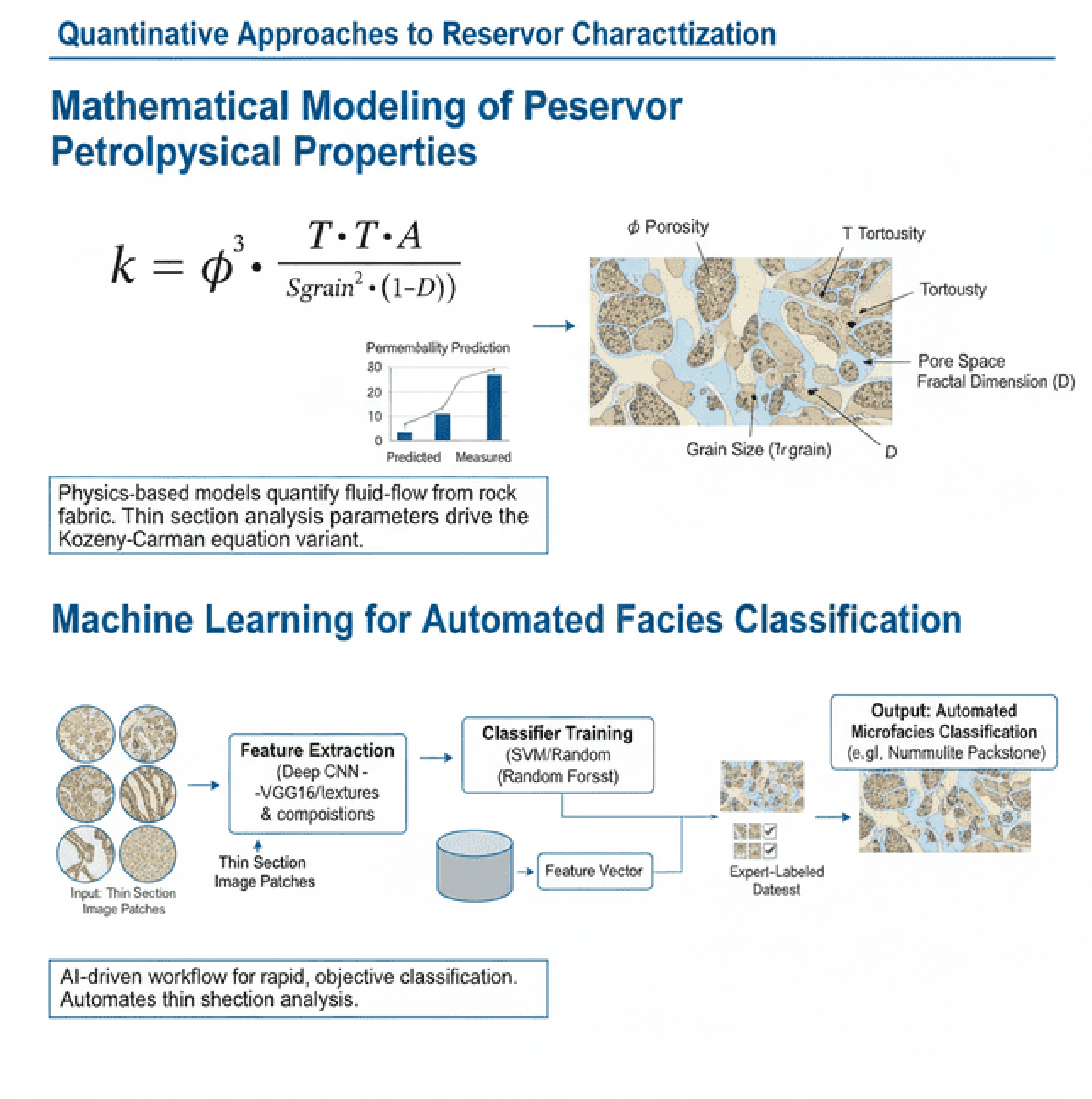

Figure 3.5: A Quantitative Approach for Reservoir Characterization and Facies Classification. First one shows a modified Kozeny-Carman equation used to predict permeability (k) based on petrophysical properties like porosity (ϕ), tortuosity (T), and grain size (S_{grain}), which are derived from thin section analysis. Second one shows details of an AI-driven workflow for automated facies classification, where thin section image patches are fed into a Deep CNN (like VGG16) for feature extraction, and then a classifier (like SVM or Random Forest) is trained on these features to automatically classify the rock type (e.g., "Nummulite Packstone").

Table 2: Summary of Lithofacies Characteristics of the Kirthar Formation at the Rohri Section.

Facies ID	**Lithology**	**Thickness (m)**	**Color**	**Key Characteristics**	**Sample Numbers**
LF-1	Coarse-grained Limestone	13.5	Whitish-Yellowish	Thick-bedded, highly fossiliferous with abundant *Nummulites* and *Assilina*.	HR-1 to HR-5, HR-12, HR-13
LF-2	Massive Bedded Limestone	4.5	Maroonish-Whitish	Massive, cliff-forming, rich in LBF.	HR-6, HR-7
LF-3	Micritic Limestone	9.3	Yellowish-Creamish	Fine-grained (micritic), reduced fossil content.	HR-8 to HR-11
LF-4	Algal Dolomitic Limestone	1.5	Yellowish-Brownish	Laminated, dolomitic, contains algae, gastropods, burrows, iron nodules, chert.	HR-14

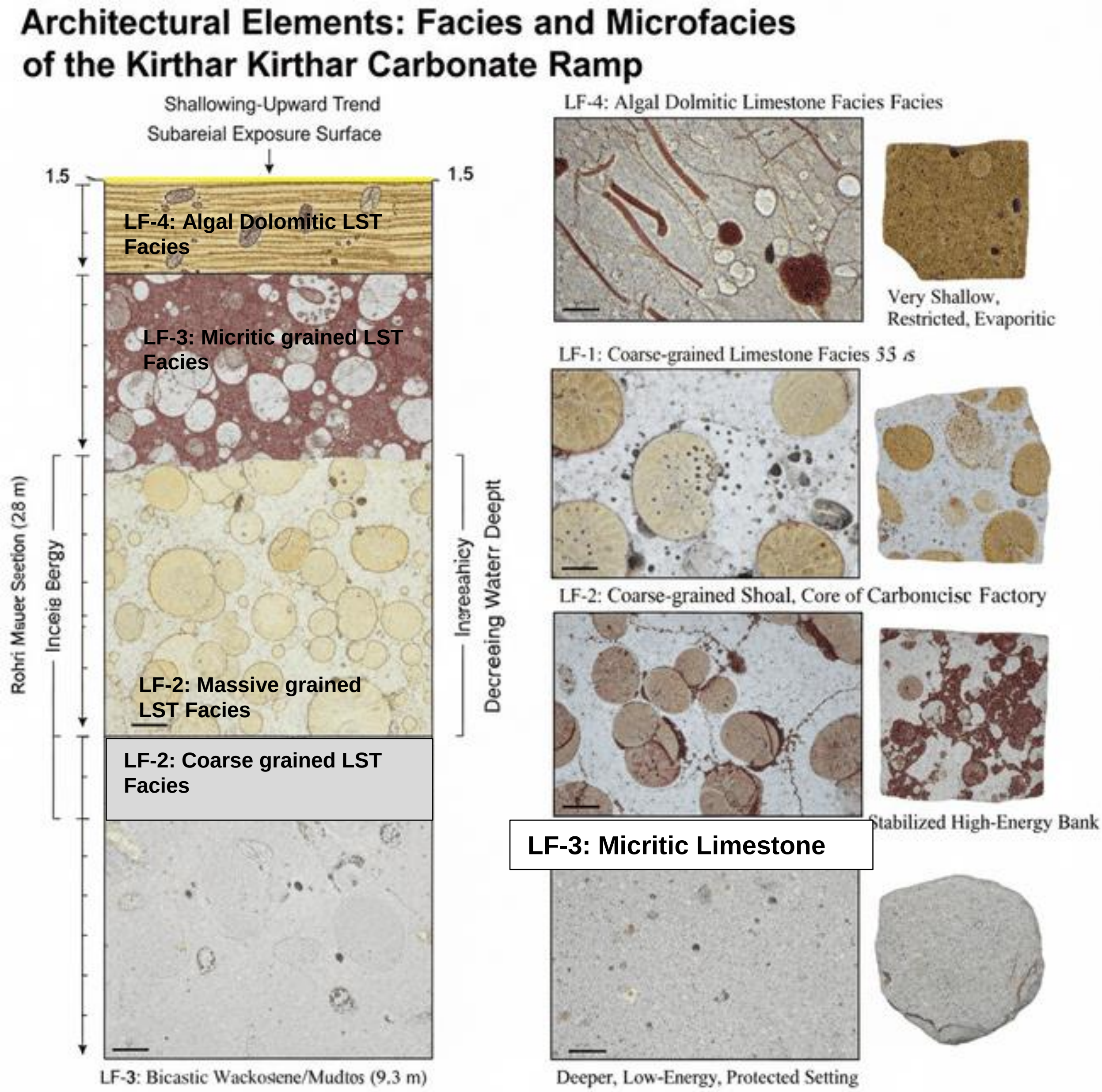

Figure 4.1a: presents a detailed litholog of the Kirthar Carbonate Ramp from the Rohri Section, analyzed using Machine Learning (ML). It illustrates the architectural elements by vertically stacking the different rock layers (lithofacies LF-1 to LF-4), showing a "Shallowing-Upward Trend" from deeper-water shales (LF-0) to a "Subaerial Exposure Surface." The diagram connects these large-scale facies to their corresponding microscopic (microfacies) images and interpreted depositional environments.

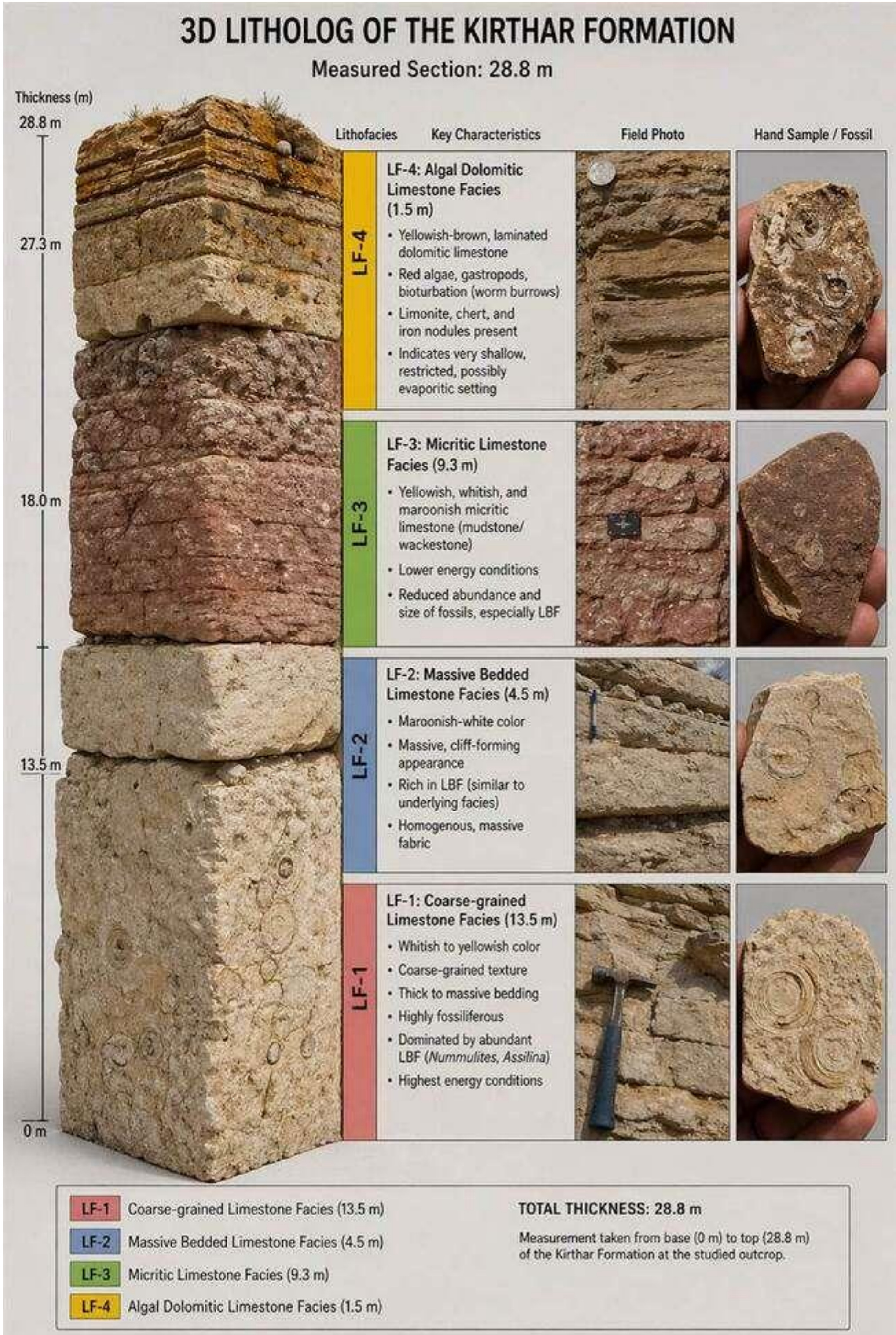

Figure 4.1b: Detailed Litholog based on Outcrop showing Lithofacies digitized using ML.

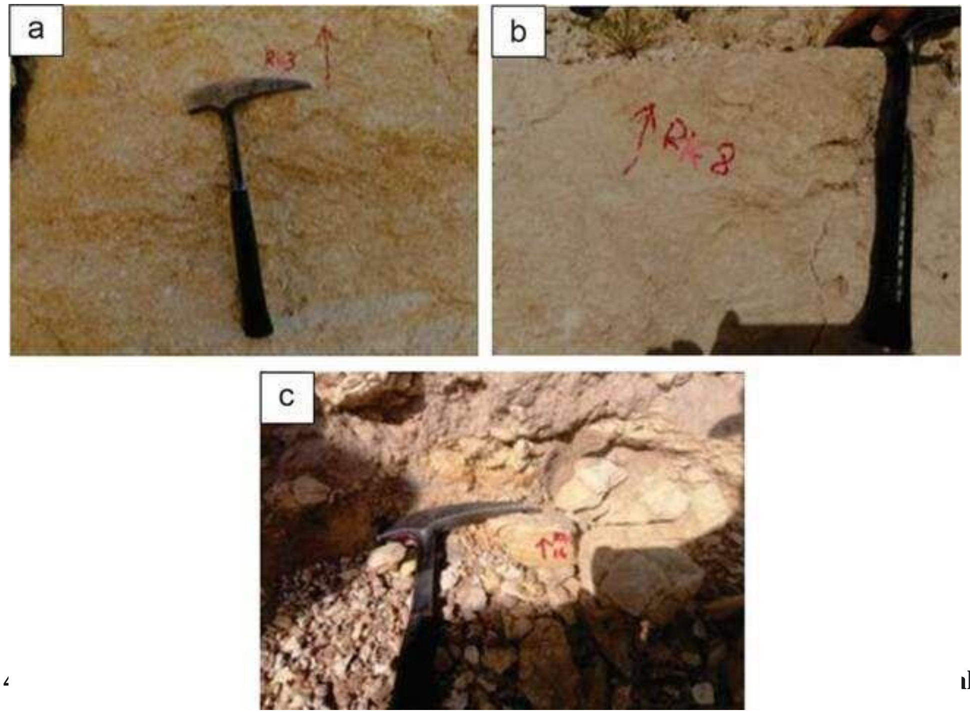

Figure ‹ ... ıl Dolomitic Limestone Facies.

4.2. Microfacies Analysis

Petrographic analysis of the 14 thin sections led to the identification of six recurring microfacies (HR-MF). These microfacies provide a detailed view of the depositional textures and biotic assemblages, allowing for a refined interpretation of the paleoenvironment. The characteristics of each microfacies are summarized in Table 3.

4.2.1. HR-MF 1: Benthonic Foraminiferal Nummulites Packstone

This microfacies is grain-supported and dominated by whole and fragmented tests of *Nummulites* and *Assilina*, with subordinate echinoderm fragments and smaller benthic foraminifera. The grains show signs of abrasion and sorting, and the matrix consists of micrite and microspar. This texture indicates deposition in a high-energy environment, such as a mobile carbonate sand shoal or bank, where wave and current action was sufficient to winnow away much of the mud. (2) (Figures 4.3a, 3b, 3c and 3d) illustrate the key features of this microfacies.

- The image (4.3 a-d) clearly shows a grain-supported texture where the larger bioclasts are touching and interlocked, with the spaces between filled by finer material (micrite and smaller grains).
- **Rock Name (Folk): Biomicrite/Biomicrosparite**. While predominantly micritic initially, the presence of microspar indicates some recrystallization of the original.

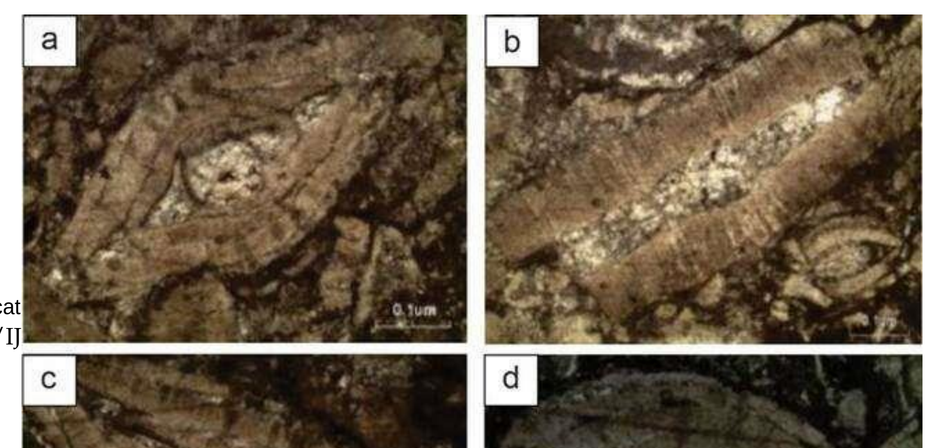

Figure 4.3. Photomicrographs (PPL) of Nummulites showing a) Oblique–equatorial Nummulites section with concentric lamellae in micrite. b) Longitudinal section showing aligned chamber partitions/septa. c) Tilted section with thickened septa and clear lamellar banding. d) Near-equatorial section with central plug and surrounding lamellae (0.1 mm).

micrite or filling of small pore spaces

- **Texture:** The rock is **grain-supported**. The large *Nummulitid* tests are in contact, forming the framework. This indicates a higher energy environment than the previous wackestone.
- **Allochems (Grains):**
  - **Dominant:** Large Benthic Foraminifera (LBFs), specifically **Nummulites** (large, coin-shaped, discoidal forms with internal coiling visible) and likely **Assilina** (similar but often flatter, though differentiation in thin section can be challenging without specific features). They are well-preserved but many show signs of fragmentation.
  - **Subordinate: Echinoderm fragments** (recognizable by their characteristic pseudouniaxial extinction if under crossed polars, but here appear as angular, lighter-colored grains) and **smaller benthic foraminifera** (tiny, often less organized shells in the interstitial spaces).
  - **Abrasion and Sorting:** The Nummulites tests are generally rounded to sub-rounded (Fig 4.3a-d) and many are fragmented, suggesting transport and agitation. While the sizes vary, there's a relative uniformity among the larger Nummulites, hinting at some degree of sorting by currents.
- **Matrix/Cement:** The spaces between the larger grains are filled with a mix of:
  - **Micrite:** Fine-grained carbonate mud. Its presence, even in a grain-supported rock, indicates some mud deposition or trapping.
  - **Microspar:** Slightly coarser crystalline calcite than micrite (usually 5-30 µm), often a product of recrystallization of micrite. Its presence suggests early diagenetic alteration. Would be discussed in detail in diagenesis section.
  - Some small intergranular pores might be present or filled by later sparitic cement (though not explicitly clear from the description or PPL image alone without crossed polars or higher magnification).
- **Diagenesis:** Signs of compaction are visible where grains are touching, and some grains are fractured. Recrystallization of micrite to microspar is also a diagenetic feature.

  Interpretation: This microfacies represents a **shallow, agitated, open-marine platform environment**, specifically a **high-energy carbonate shoal, bank, or tidal channel (Fig. 4.22)**, where robust bioclastic material (especially Nummulitids) accumulated. The winnowing of mud signifies deposition above or at the fair-weather wave base.

General Comparison Points (Assuming typical Nummulitid Facies Studies):

- **Consistency with Existing Facies Models:** This "Nummulites Packstone" microfacies is a very common and well-documented facies type in Paleogene carbonate sequences worldwide. Previous authors working on similar formations (e.g., Tethyan carbonates from the Eocene) would almost certainly describe very similar microfacies. It perfectly fits the model of "Nummulitic Limestones" representing shallow-water, high-energy bioclastic shoals (Fig 4.23).
- **Depositional Environment Consensus:** There would likely be strong agreement on the interpreted high-energy, shallow-marine shoal environment. Many authors have used such facies as indicators of platform-top environments, often associated with major sea-level lowstands or transgressive systems tracts where accommodations space is limited, leading to widespread shoal development.
- **Paleoenvironmental Zonation:** In many studies, Nummulites packstones are part of a broader "Nummulitic biofacies belt" that forms part of a larger-scale carbonate platform zonation (e.g., inner platform, middle platform, outer platform). This facies

would typically correspond to the middle to outer platform, near the platform margin, where wave energy is strongest (Fig 4.22).

- **Diagenetic Pathways:** Comparisons could be made regarding the diagenetic features observed (e.g., micrite to microspar recrystallization, compaction, early marine cementation if observable). Are the diagenetic processes similar to those described by others for equivalent rocks in the region (Fig 4.11-4.15)?
- **Biostratigraphic Correlation:** The presence of specific *Nummulites* and *Assilina* species would be crucial for precise biostratigraphic correlation with established biozonations (e.g., SBZ zones for larger benthic foraminifera) developed by authors like (Hottinger, 1993, Kiel, 1998), etc. This would confirm or refine the Paleogene age.
- **Sequence Stratigraphy:** This facies often marks specific parts of sequence stratigraphic cycles (e.g., transgressive systems tracts, highstand systems tracts) (Fig. 4.26-4.27).

4.2.2. HR-MF 2: Algal Foraminiferal Wackstone

This is a mud-supported microfacies where LBFs and abundant fragments of calcareous red algae (rhodophytes) "float" in a dense micritic matrix. The skeletal grains are generally well-preserved and show little evidence of transport. This microfacies represents a lower-energy setting, likely a mid-ramp environment below the fair-weather wave base, where both carbonate mud and skeletal material could accumulate (Fig 4.27). (2)

Rock Name (Dunham): Bioclastic Wackestone. The texture is explicitly **mud-supported**, with the grains (LBFs, red algae) "floating" in the matrix. If the grains are larger than 2 mm, this could also be termed a "**Floatstone**".

Rock Name (Folk): Biomicrite. The rock is composed of biological grains (*bio-*) set within a fine-grained carbonate mud matrix (*micrite*) (4.4a-c).

Allochems (Grains): The grain assemblage is a classic "foralgal" association:

1. **Large Benthic Foraminifera (LBFs):** These could include *Nummulites*, *Assilina*, *Discocyclina*, or *Alveolina*, depending on the precise age and setting.
2. **Calcareous Red Algae (Rhodophytes):** These are abundant fragments of (most likely) coralline algae.

Matrix: A dense, fine-grained carbonate mud (micrite).

Texture & Preservation: The grains are **well-preserved** and show **little evidence of transport** (i.e., they are not abraded or highly fragmented). This indicates they are *autochthonous* (preserved in place) or *parautochthonous* (minimal transport) (Fig. 4.4 a-c).

In the standard carbonate ramp models (e.g., **Burchette & Wright, 1992**; **Flügel, 2010**), the mid-ramp is characterized by the transition from grain-dominated inner-ramp facies to mud-dominated outer-ramp facies. It is the zone dominated by *in-situ* production of bioclasts in a low-energy setting, often corresponding to **bioclastic wackestones and packstones**.

The "Foralgal" Assemblage: This specific association of LBFs and (coralline) red algae is a hallmark of the Cenozoic, often termed the **"foralgal" facies**. This assemblage is widely documented as colonizing the mid-ramp and deeper parts of the inner ramp (Fig 4.22).

LBFs in Low-Energy Settings: Racey (2001) and **Buxton & Pedley (1989)**, in their key works on *Nummulites* accumulations (the dominant Eocene LBF), specifically note that *autochthonous* (in-place) deposits are often **wackestones to packstones** associated with **red algae, echinoderms, and bryozoans**. They explicitly interpret these as forming in moderately **low-energy environments located between the fair-weather and storm wave bases**—the exact definition of the mid-ramp (4.24-4.27).

Regional Pakistan Geology (Sakesar Limestone): Studies on the Eocene **Sakesar Limestone** in the Potwar Plateau and Salt Range (e.g., **Afzal et al., 2011; 2017**) frequently identify a "foraminiferal-algal wacke-packstone" microfacies. This facies, containing LBFs like *Nummulites* and *Alveolina* along with algal fragments in a micrite matrix, is consistently interpreted as having been deposited in a **low-energy inner- to mid-ramp** environment.

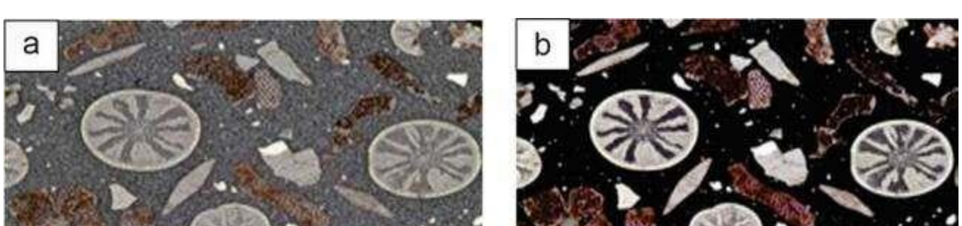

Figure 4.4. Photomicrographs show a) Oblique section of a nummulite test in micritic matrix. b) Cross Polarized light Axial/equatorial section showing internal septa/lamella showing Nummulites and Red Algae. c) Nummulitic packstone–grainstone with densely packed discoidal tests.

4.2.3. HR-MF 3: Foraminiferal Nummulites Wackstone-Packstone

This microfacies represent a transitional texture between mud-supported and grain-supported fabrics (4.5 a-c). It contains a high abundance of LBFs, but not enough to form a continuous grain-supported framework. This suggests deposition in an environment with fluctuating energy levels, such as a mid-ramp setting periodically affected by storm events that transported and concentrated skeletal grains. (38)

The thin section is overwhelmingly dominated by large, discoidal (coin-shaped) benthic foraminifera, clearly identifiable as **Nummulites**. They exhibit characteristic internal septa radiating from a central point (Fig 4.5b).

- Various sizes of Nummulites are present, ranging from larger, more prominent tests to smaller ones.
- Many Nummulites appear well-preserved, with clear internal structures. Some show minor fragmentation or abrasion, particularly the smaller grains.

The rock exhibits a **transitional texture** between mud-supported (wackstone) and grain-supported (packstone).

- There are numerous areas where Nummulites are in direct contact, forming a partial framework.
- However, significant amounts of fine-grained carbonate mud (micrite) fill the interstitial spaces, often surrounding individual Nummulites or clusters of them.
- This "floating" appearance of some Nummulites within the micrite, alongside areas of grain-to-grain contact, visually confirms the wackstone-packstone nature.
- Smaller bioclastic debris (fragments of other organisms, smaller foraminifera) are also dispersed within the micritic matrix.
- The wackstone-packstone texture is the key indicator. It signifies an environment with **fluctuating energy levels**. It's not consistently high enough to winnow all the mud (like a grainstone shoal), nor is it consistently low enough to allow mud to dominate completely and bury all grains without any contact (like a pure wackstone/mudstone in a very deep or restricted setting) (Fig 4.22).
- **Mid-Ramp Setting:** This is the most appropriate interpretation. The mid-ramp lies between the constantly agitated inner ramp (above fair-weather wave base) and the consistently calm outer ramp (below storm wave base) (Fig 4.27).
- **Storm Influence:** The presence of both mud and concentrated Nummulite grains strongly suggests that storm events (or other

episodic high-energy events) periodically swept and concentrated the larger skeletal material, intermixing it with or layering it within the ambient fine mud deposits of a generally lower-energy setting. The Nummulites themselves are large, robust, and often transported during such events.

- **Photic Zone:** As discussed previously, *Nummulites* are Large Benthic Foraminifera (LBFs) that housed symbiotic algae and thus required sunlight. Therefore, this mid-ramp setting was still within the **photic zone**, allowing for the proliferation of these organisms (Fig 4.21).
- The wackstone-packstone texture is the key indicator. It signifies an environment with **fluctuating energy levels**. It's not consistently high enough to winnow all the mud (like a grainstone shoal), nor is it consistently low enough to allow mud to dominate completely and bury all grains without any contact (like a pure wackstone/mudstone in a very deep or restricted setting) (Fig. 4.22).

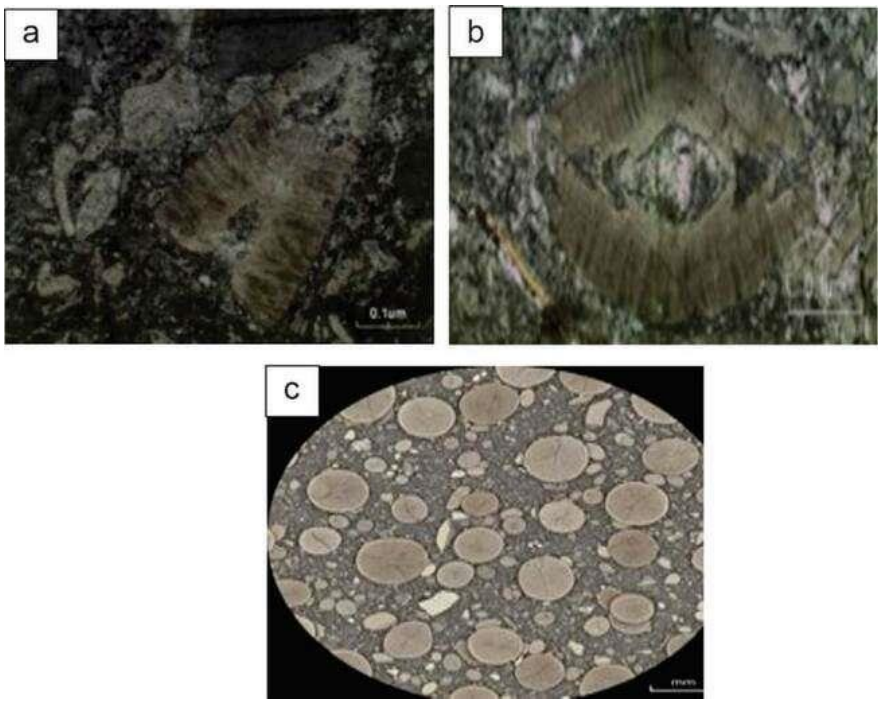

Figure 4.5. Photomicrographs shows views of nummulitic facies: a) oblique section of a nummulite in micrite; b) axial/equatorial section showing internal lamellae; c) densely packed nummulitic packstone–grainstone.

4.2.4. HR-MF 4: Benthonic Foraminiferal Wackstone/Oo-Biomicrite

This mud-supported microfacies is characterized by the presence of scattered LBFs, bioclasts, and, significantly, sparse ooids within a micritic matrix. The presence of ooids, even in small quantities, is a strong indicator of shallow, agitated, and carbonate-saturated marine waters, typical of an inner-ramp shoal margin or tidal channel environment (Fig 4.22).

- **Texture (Dunham Classification): Mud-supported wackstone**. The image clearly shows grains "floating" in a dominant, fine-grained matrix. There is no continuous grain-to-grain contact between the larger allochems (4.6 a-e).
- **Rock Name (Folk Classification): Oo-Biomicrite**. This reflects the presence of ooids and bioclasts within a micritic matrix.
- **Matrix:** The pervasive matrix is dark and fine-grained, consistent with **micrite** (carbonate mud). It constitutes the bulk of the rock, confirming the mud-supported nature.
- **Allochems (Grains):** The sparse grains are diverse and scattered throughout the micritic matrix:
  - **Large Benthic Foraminifera (LBFs):** Scattered, often discoidal or elongate, with visible internal structures. These are relatively large compared to other non-ooidal grains.
  - **Bioclasts:** Various fragments of skeletal material are present, appearing as irregular or elongate light-colored grains. Their detailed identification (e.g., mollusk fragments, echinoderms) would require XPL and higher magnification, but

ISSN 2250-3153

their presence is clear.

- **Ooids:** This is the diagnostic component. Small, spherical to sub-spherical grains exhibiting distinct concentric laminae (layers) around a nucleus are clearly visible. They are sparse, meaning they are present but not abundant enough to form a significant part of the rock framework, nor are they the dominant grain type.

- **Grain Preservation and Transport:** The grains generally appear sub-angular to sub-rounded. While some fragmentation is evident among the bioclasts, the ooids and LBFs seem relatively intact, suggesting either limited transport or deposition in an environment where breakdown wasn't severe despite agitation. The mud-supported nature, however, implies that the depositional *setting* was not one of constant, strong agitation.

The combination of features in this microfacies provides a nuanced interpretation of the depositional environment:

- **Primary Contradiction/Reconciliation:** The most striking aspect is the co-occurrence of **ooids** (typically high-energy indicators) with a **mud-supported texture** (low-energy indicator). This apparent contradiction necessitates a specific interpretation.
- **Ooid Formation:** Ooids form in very specific conditions: shallow water, high agitation (waves/currents), and supersaturated marine water, typically found in **shoals, tidal channels, or agitated inner-ramp settings** (Fig 4.22).
- **Mud Accumulation:** The dominant micritic matrix (wackstone texture) indicates that the *overall* accumulation site was a **low-energy environment** where fine mud could settle and persist. This is below the influence of consistent strong waves and currents.
- **Proposed Reconciliation: Transport from High-Energy to Low-Energy:** The most logical interpretation is that the sparse ooids were formed in a nearby **high-energy ooid shoal or agitated inner-ramp margin**, and then **transported** (likely by episodic events like storms, tidal currents, or gentle background currents) into an adjacent, quieter, **lower-energy setting** where carbonate mud was accumulating (Fig 4.21)
- **Specific Environment: Inner-Ramp Shoal Margin / Back-Shoal / Protected Inner Ramp:** This microfacies likely represent:
  - The **downcurrent or leeward side of an ooid shoal**, where ooids are swept off the shoal into quieter waters.
  - A **protected lagoonal or back-shoal environment** that occasionally received ooids from nearby agitated areas.
  - A **sheltered part of an inner ramp**, possibly a localized depression or a more quiescent zone immediately adjacent to an ooid-forming area (Fig 4.22).
- **Water Depth & Light:** The presence of LBFs and the requirement for ooid formation point to a **shallow-marine, photic zone** environment.

4.2.5. HR-MF 5: Planktonic Foraminiferal Nummulites Packstone

This grain-supported microfacies is distinguished by a mixed faunal assemblage. It is dominated by benthic foraminifera (*Nummulites*) but also contains a significant proportion of smaller planktonic foraminifera within the matrix (Fig 4.7 a-d). This mixing suggests a depositional setting with open-marine influence, such as a distal shoal or outer-ramp environment, where transported benthic material from shallower areas was mixed with the continuous "rain" of pelagic organisms from the overlying water column (Fig 4.22).

Texture: The rock is **grain-supported**. The large fossil grains are abundant and in contact with each other, forming a framework. The space between these larger grains is filled with a dense, dark, fine-grained carbonate mud (**micrite**) and smaller bioclastic debris.

Allochems (Grains): The grains are dominated by a mixed assemblage of **Large Benthic Foraminifera (LBFs)**. Specifically:

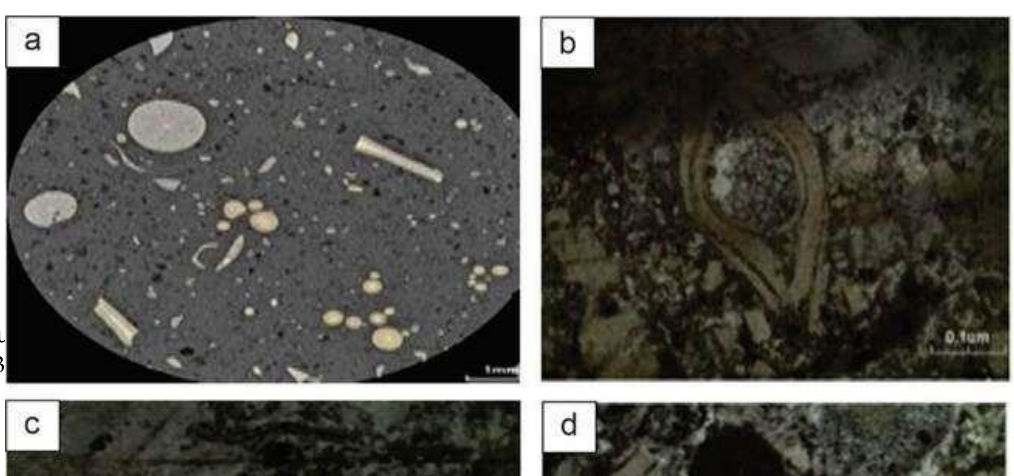

Figure 4.6. Photomicrographs (plane-polarized light) showing carbonate facies and textures. a) Nummulitic–foraminiferal packstone with abundant larger benthic foraminifera, peloids, and bioclasts in a micritic matrix. b–d) Close-ups of larger benthic foraminifera with micritized walls and spar-filled chambers. e) Micritic mudstone–wackstone with dispersed foraminiferal fragments and low interparticle porosity.

- **Nummulitids (e.g., *Nummulites* or *Assilina*):** The top-left image shows a perfect equatorial section of a large, discoidal (coin-shaped) foraminifera with complex internal chambers. Another oblique section is visible in the bottom-right image.
- ***Alveolina*:** The other images (bottom-left, bottom-right, and bottom-most) show prominent axial, sub-axial, and oblique sections of elongate, fusiform (cigar-shaped) foraminifera.

Diagenesis: The center of the *Nummulite* in the top-left image has been dissolved (creating moldic porosity) and later filled with a coarse, clear **sparry calcite cement** (Fig 4.8b).

This microfacies provide two critical clues for interpreting the depositional environment:

1. **The Biotic Assemblage (Age and Setting):** The co-occurrence of abundant *Nummulites* and *Alveolina* is a classic "index fossil" assemblage. This definitively places the rock in the **Eocene Epoch** (part of the Paleogene Period). Both of these LBFs hosted symbiotic algae, which required them to live in the **photic zone** (shallow, warm, clear, sunlit marine waters).
2. **The Texture (Energy Level):** The rock is a **Packstone**.
    - The **grain-supported** nature indicates a very high rate of skeletal production (a "foraminiferal factory") or some concentration by currents.
    - The presence of abundant **micrite** in the matrix proves that the environment was **low-to-moderate energy**. It was not a high-energy shoal or beach, as strong waves would have washed away all the fine mud.

Interpretation: The combination of a photic-zone assemblage with a low-to-moderate energy, mud-rich packstone texture points to a **protected, shallow-marine environment**.

This is best interpreted as a **protected inner ramp** or a **shallow middle ramp**, below the zone of constant wave action but well within the range of sunlight. The high concentration of fossils suggests a highly productive foraminiferal "meadow" or "biostrome" where the organisms lived and died *in-situ* or were only gently reworked by occasional storms.

This interpretation is strongly supported by a vast body of established sedimentological research, both globally and regionally.

- **Global Facies Models:** In the standard microfacies models of **Flügel (2010)** and **Wilson (1975)**, facies dominated by LBFs (like *Alveolina* and *Nummulites*) in a mud-rich matrix (wackstone/packstone) are classic indicators of **shallow, protected inner-ramp or lagoonal settings** (e.g., Standard Microfacies Belt 8).
- **LBF Paleoecology:** The work of **Hottinger (1983, 1997)** established the paleo ecological preferences for these LBFs. *Alveolina* (fusiform shape) is strongly associated with protected, shallow-water inner-ramp and lagoonal environments. *Nummulites* (lenticular/discoidal shape) are common in a range of inner- to mid-ramp settings. The *mixing* of these two dominant groups in a packstone texture is a hallmark of these highly productive, shallow, low-energy Eocene platform environments.
- **Regional Geology (Sakesar Limestone):** This microfacies is a textbook example of the **Eocene Sakesar Limestone** found in the Salt Range and Potwar Plateau of Pakistan. Numerous authors (e.g., **Afzal et al., 2011; 2017**) have described this exact "Alveolinid-Nummulitid Packstone" facies. These studies *consistently* interpret it as representing deposition in a **low-energy, shallow marine, inner- to middle-ramp** or **protected lagoonal** environment.

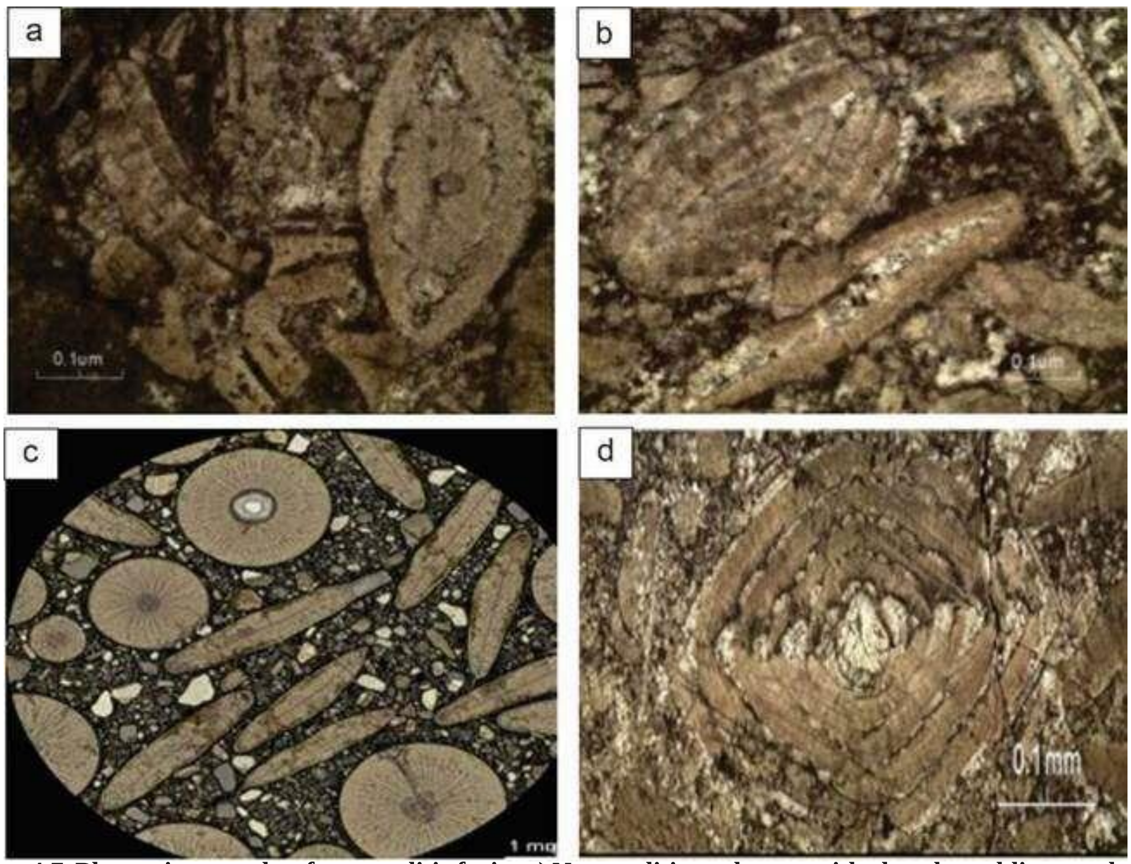

Figure 4.7. Photomicrographs of nummulitic facies a) Nummulitic packstone with abundant oblique and axial sections in micrite. b) Fragmented Nummulites showing micritized walls and internal lamellae. c) Overview: mixed equatorial discs and elongated axial tests in a packstone–grainstone framework. d) Close-up equatorial section with concentric lamellae and chamber infill; minor cross-cutting fracture (0.1 mm).

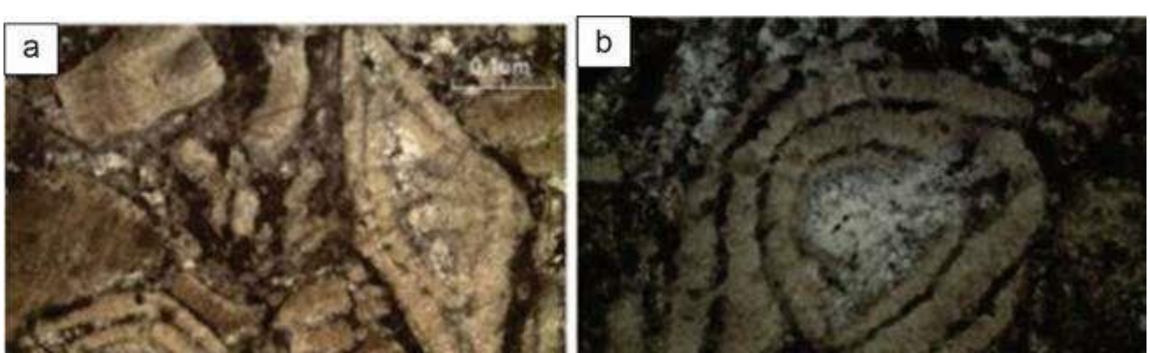

Figure 4.8. Photomicrographs of Nummulites a) Packstone with multiple oblique sections; micritized walls and sparry chamber fills. b) Near-equatorial section showing concentric lamellae around a central plug. c) Tilted section with stepped lamellae and partial dissolution along septa. d) Longitudinal/axial section displaying parallel lamellae and chamber partitions.

4.2.6. HR-MF 6: Bioclastic Carbonate Mudstone

This microfacies is dominated by a dense micritic matrix (>90%) with only sparse, fine-grained, and often unidentifiable bioclasts (Fig 4.9 a-d). It represents the lowest-energy depositional environment in the succession, corresponding to a protected, low-energy lagoonal setting or a deeper outer-ramp environment, well below the influence of storm waves (Fig 4.21).

Texture: The rock is overwhelmingly **mud-dominated**. The vast majority of the view (well over 90%) consists of a dense, dark, fine-grained carbonate mud matrix (**micrite**).

Allochems (Grains): The grains are very **sparse** (<10%), fine-grained, and appear to be "floating" in the micrite. They consist of:

- Small, unidentifiable bioclastic debris.
- A few small benthic foraminifera or ostracods (visible as small circular shapes, especially in the top-right and bottom-right images).

Diagenesis: The images show significant diagenetic alteration. The bottom-left image shows a patch where the original micrite has recrystallized into coarser-grained **microspar** (neomorphism). The top-right image shows a large, clear rhombic crystal of **sparry calcite**, which has likely replaced a pre-existing grain or filled a small vug.

The interpretation of this facies is straightforward and based on one primary piece of evidence: the overwhelming abundance of carbonate mud.

- **Energy Level:** A mud-dominated rock indicates deposition in a **very low-energy environment**. The water column was calm and quiet, with little to no wave or current energy. This allowed the finest mud particles (micrite) to settle out of suspension and be preserved.
- **Environmental Setting:** This facies represents the lowest-energy setting in the depositional system. This points to one of two possibilities:
    1. **A Protected, Low-Energy Lagoon (Inner Ramp):** A shallow-water area on the inner ramp that was completely

sheltered from open-marine wave action by a barrier (such as an ooid shoal, a Nummulite bank, or an algal reef).

2. **A Deeper Outer-Ramp Environment:** A deeper-water setting located *below* the storm wave base. At this depth, even major storms could not agitate the seafloor, allowing only fine mud and the remains of pelagic or sparse benthic organisms to accumulate (Fig 4.22).

Given its context within a shallowing-upward Eocene succession (implied by the other facies), both interpretations are plausible. It represents the quietest conditions, either in a protected shallow lagoon or in the deepest part of the ramp.

- **Global Facies Models:** In the standard carbonate facies models of **Wilson (1975)** and **Flügel (2010)**, micrite-dominated rocks (Carbonate Mudstones) with sparse, fine-grained bioclasts are characteristic of the lowest-energy settings. They correspond to **Standard Microfacies (SMF) 9 (Bioclastic Mudstone)**, which is typically placed in either a **restricted, low-energy lagoon (Facies Belt 8)** or a **deep-water outer ramp/basin (Facies Belt 1)**.
- **Energy and Texture:** Authors like **Bathurst (1975)** established that the preservation of carbonate mud is the single most important indicator of deposition below the level of effective wave agitation.
- **Regional Pakistan Geology:** Studies of the Eocene **Sakesar Limestone** in the Potwar Plateau and Salt Range (e.g., **Afzal et al., 2011; 2017**) frequently identify "Bioclastic Mudstone" and "Bioclastic Wackstone" as the lowest-energy facies in the sequence. These authors consistently interpret these mud-rich facies as representing deposition in either a **protected lagoonal (inner-ramp)** environment or a **deeper, low-energy outer-ramp** setting.

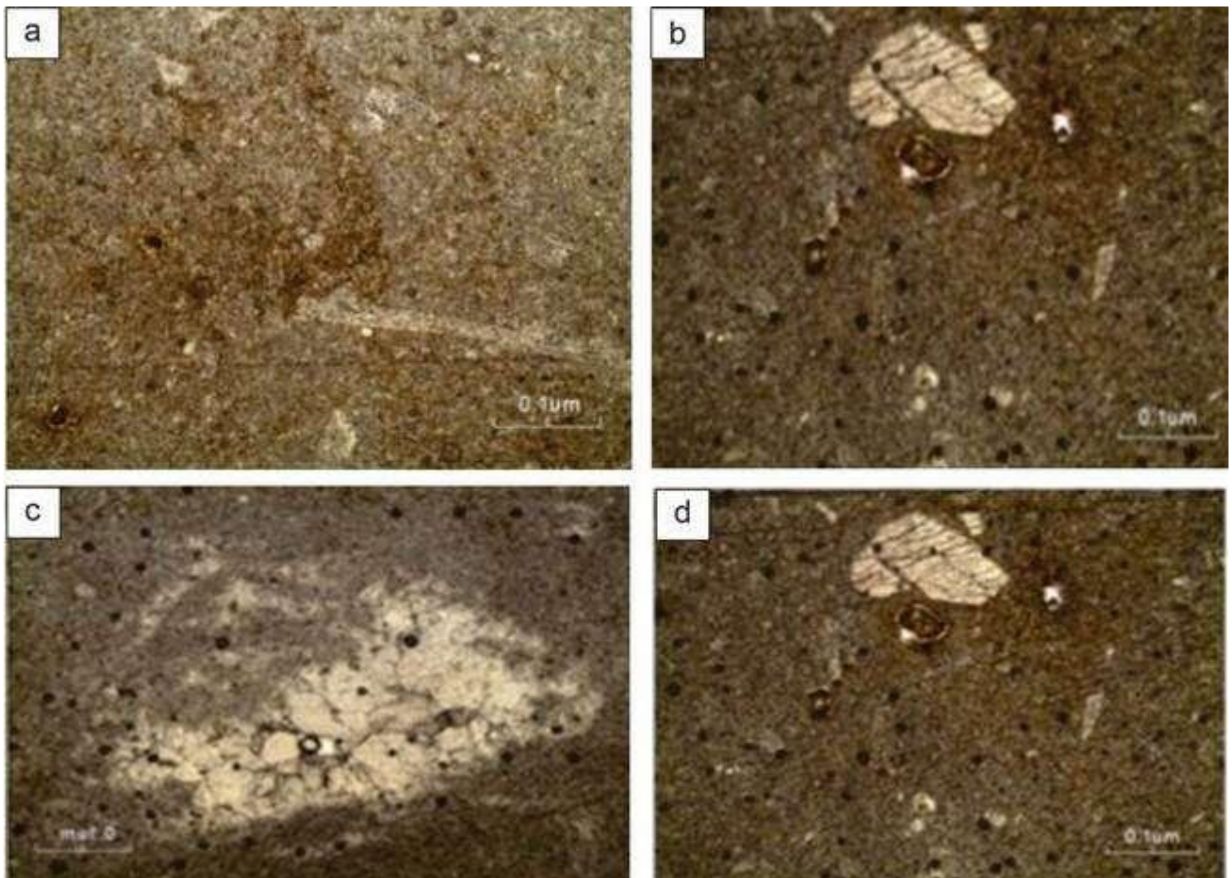

Figure 4.9. Photomicrographs of micritic facies a) Laminated/mottled micrite with subtle burrow or micro-bedding. b) Micrite with sparse skeletal grains/peloids; isolated small foraminifer. c) Clotted/aggregate micrite patch within a mud-rich matrix. d) Micrite with dispersed bioclasts and peloids; very low interparticle porosity.

Table 3: Detailed Microfacies Descriptions, Classifications, and Environmental Interpretations for the Kirthar Formation.

Microfacies ID	Description (Allochems, Matrix, Texture)	Dunham Classification	Folk Classification	Flügel Interpretation	Depositional Environment
HR-MF 1	Dominated by whole/fragmented *Nummulites* & *Assilina*; echinoderms. Grain-supported, sorted, abraded grains. Micrite matrix.	Packstone	Biomicrite	SMF 18 / FZ 7	High-energy inner-ramp shoal/bank
HR-MF 2	Floating LBFs and abundant red algal fragments in a dense micrite matrix. Mud-supported, well-preserved grains.	Wackstone	Biomicrite	SMF 9 / FZ 3	Low-energy mid-ramp (below FWWB*)
HR-MF 3	Abundant LBFs in a micrite matrix; transitional between mud- and grain-supported.	Wackstone-Packstone	Biomicrite	SMF 9 / FZ 3	Mid-ramp (storm-influenced)
HR-MF 4	Scattered LBFs, bioclasts, and sparse ooids in a micrite	Wackstone	Oo-Biomicrite	SMF 15 / FZ 8	Inner-ramp shoal margin/tidal channel

	matrix. Mud-supported.				
HR-MF 5	Grain-supported fabric of benthic *Nummulites* with abundant planktonic foraminifera in the matrix.	Packstone	Biomicrite	SMF 3 / FZ 2	Outer-ramp / distal shoal (open marine)
HR-MF 6	Dominated by dense micrite matrix (>90%) with sparse, fine-grained bioclasts. Mud-supported.	Mudstone	Micrite	SMF 3 / FZ 1	Low-energy outer-ramp / protected lagoon

**FWWB: Fair-Weather Wave Base*

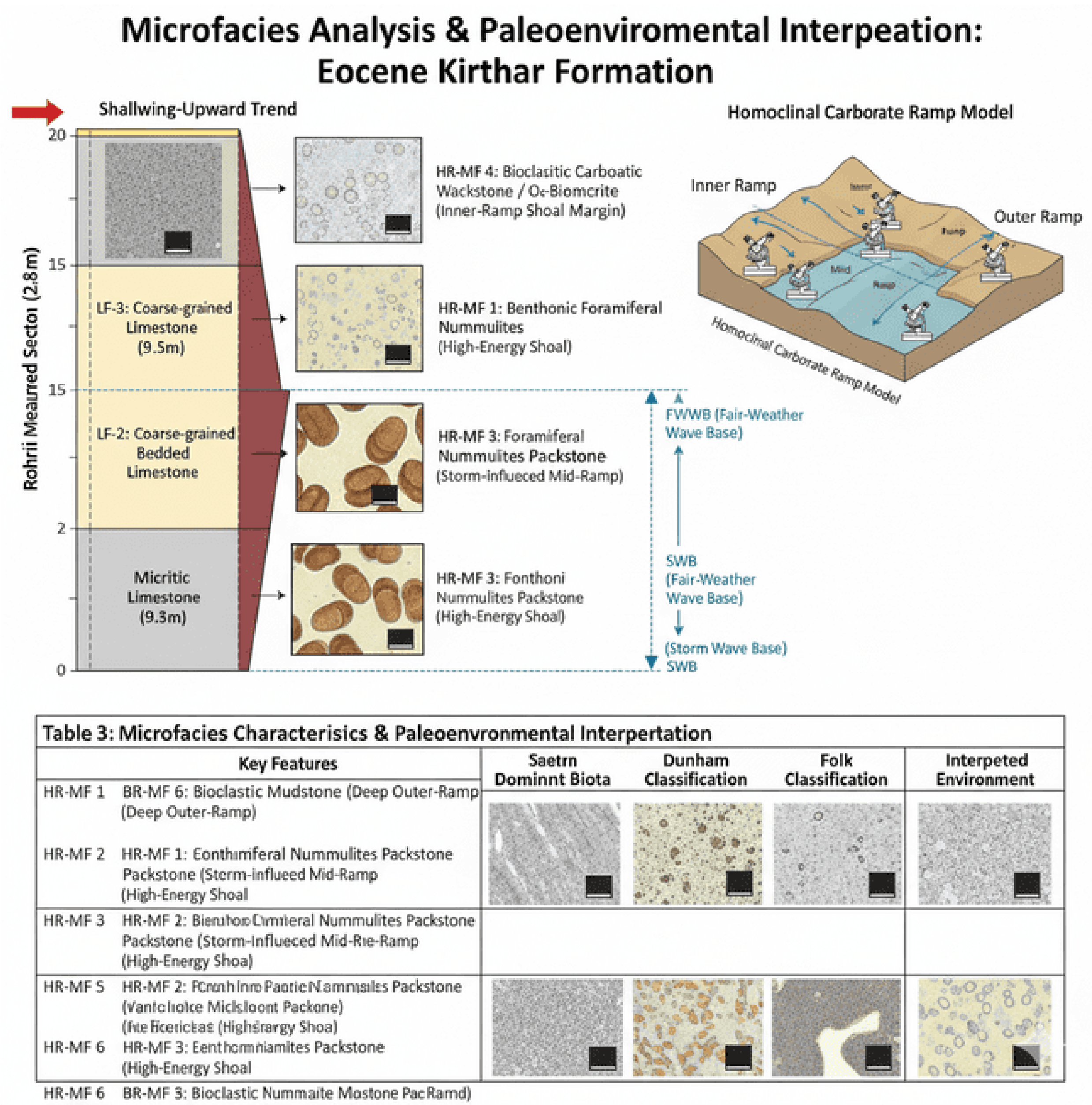

Figure 4.10. Summarizes a microfacies analysis of the Eocene Kirthar Formation. It links a "shallowing-upward" stratigraphic column from the Rohri Section to its corresponding microscopic rock fabrics, using this data to create a "Homoclinal Carbonate Ramp Model" that reconstructs the ancient depositional environment.

4.3. Diagenetic History and Paragenesis

The Kirthar Formation limestones have been subjected to a complex series of post-depositional diagenetic alterations that have significantly modified their original fabric and pore system. These processes occurred in three main diagenetic realms: the early, near-surface marine and meteoric environments (eogenesis) (Fig 4.12); the deep, subsurface burial environment (mesogenesis) (Fig 4.14); and the late-stage, uplift-related meteoric environment (telogenesis) (Fig 4.15). The relative timing of these events has been established through petrographic analysis of cross-cutting relationships and is summarized in the paragenetic sequence (Table 4) or (Fig 4.19).

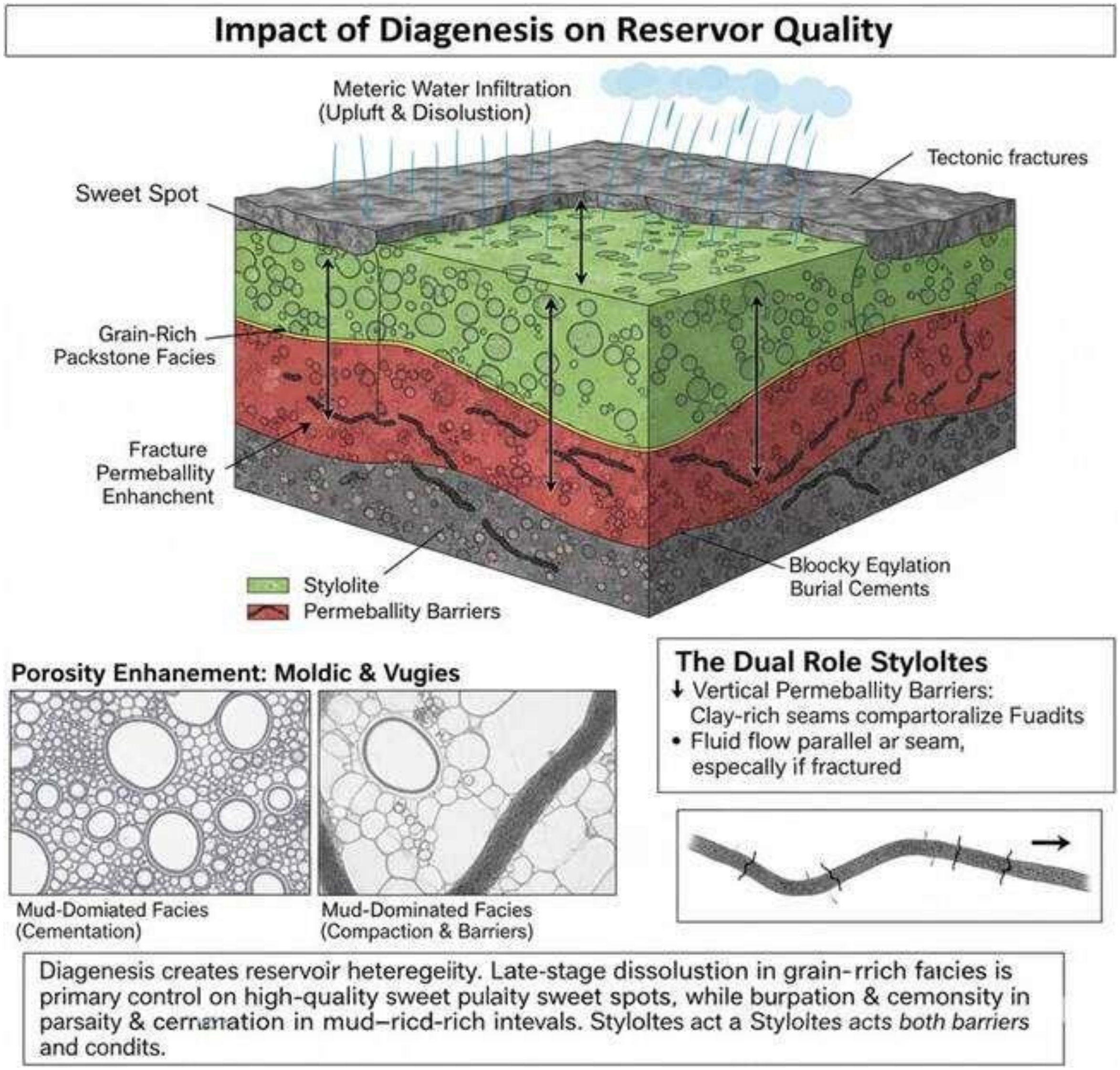

Figure 4.11. Shows the "Impact of Diagenesis on Reservoir Quality," showing how late-stage uplift and "Meteoric Water Infiltration" cause dissolution to create "sweet spots" in "Grain-Rich Packstone Facies." This process enhances porosity by forming "Tectonic Fractures" and "Moldic & Vugies." The image contrasts this with porosity destruction in "Mud-Dominated Facies" via "Burial Cements." It also explains the "Dual Role of Stylolites," which act as vertical "Permeability Barriers" but can also become horizontal fluid conduits when fractured.

Table 4: Paragenetic Sequence of Diagenetic Events in the Kirthar Formation.

Diagenetic Realm	Timing	Process	Description	Effect on Porosity

Eogenesis	Syndepositional/Early Burial	Micritization	Formation of micrite envelopes around grains by microbes.	Neutral / Minor Decrease
(Marine)	Early Burial	Early Marine Cementation	Precipitation of isopachous fibrous calcite cements in pores.	Decrease
Mesogenesis	Early to Deep Burial	Mechanical Compaction	Grain rearrangement, fracturing, and deformation under overburden.	Decrease
(Burial)	Moderate to Deep Burial	Chemical Compaction (Stylolites)	Pressure dissolution at grain contacts and formation of stylolites.	Decrease
	Moderate to Deep Burial	Neomorphism	Recrystallization of micrite; inversion of aragonite to calcite.	Neutral / Minor Redistribution
	Moderate to Deep Burial	Burial Cementation (Calcite)	Precipitation of blocky, drusy, and syntaxial calcite cements.	Major Decrease
	Deep Burial	Dolomitization / Saddle Dolomite	Replacement of limestone by dolomite; precipitation of saddle dolomite cement.	Variable (Increase/Decrease)
	Deep Burial	Late Cementation (Ferroan Calcite)	Precipitation of iron-rich calcite in remaining pores	Decrease

			and fractures.	
Telogenesis	Uplift	Dissolution	Leaching of unstable grains and cements by meteoric fluids.	**Major Increase**
(Meteoric)	Uplift	Fracturing	Tectonic fracturing related to regional uplift.	Increase
	Uplift	Late Vein-Fill Calcite	Precipitation of coarse calcite cement within fractures.	Decrease

4.3.1. Eogenesis (Early Diagenesis)

- **Micritization:** The earliest observed diagenetic feature is the formation of micrite envelopes around skeletal grains. This process, mediated by boring endolithic microbes (algae, fungi) (Fig. 4.12) in the marine-phreatic zone, partially or completely obliterated the original grain margins. (39)
- **Early Marine Cementation:** Isopachous fibrous calcite cements are observed lining some primary interparticle and intraparticle pores. This cement morphology is characteristic of precipitation in the marine-phreatic environment, where pore waters are saturated with respect to calcium carbonate. (40)

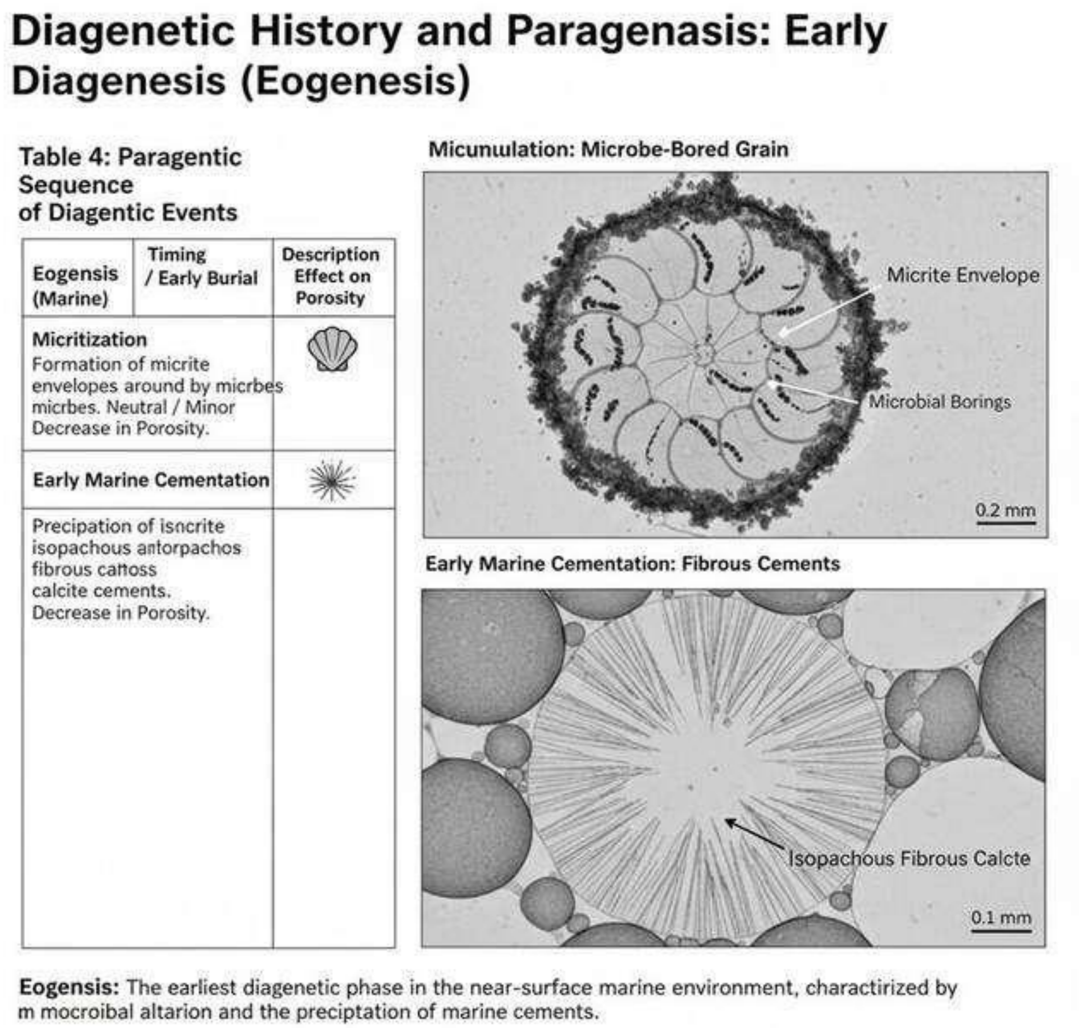

Fi ... Diagenesis (Eogenesis), de ... lists Micritization and Early Marine Cementation as key processes, both of which decrease porosity. These events are visualized with corresponding micrographs showing a microbe-bored grain and isopachous fibrous calcite cements.

4.3.2. Mesogenesis (Burial Diagenesis)

As sediments were buried, they were subjected to increasing temperature, pressure, and evolving pore fluid chemistry, leading to a suite of significant alterations.

- **Compaction:** Both mechanical and chemical compaction are pervasive. Mechanical compaction is evidenced by grain reorientation, fracturing of brittle bioclasts (e.g., *Nummulites* tests), and plastic deformation of softer grains. (41) Chemical compaction (pressure dissolution) is prominently displayed by the formation of stylolites and solution seams. These stylolites are often filled with a dark residue of insoluble materials (Fig 4.14), including clays and organic matter, and act as significant barriers to vertical fluid flow. (42)

- **Cementation:** Burial cementation is the primary cause of primary porosity occlusion. The most common cement types include:
    - **Blocky and Drusy Mosaic Calcite:** Coarsely crystalline, equant to elongate calcite crystals that fill remaining interparticle and secondary dissolution pores. These cements precipitate from pore fluids during moderate to deep burial.[45]
    - **Syntaxial Overgrowths:** Calcite cements that grow in optical continuity on single-crystal echinoderm fragments, a common process during burial diagenesis (Fig 4.14).
    - **Ferroan Calcite and Saddle Dolomite:** Late-stage, iron-rich calcite and coarsely crystalline dolomite with curved crystal faces and sweeping extinction are observed filling fractures and vugs. Their presence indicates precipitation from hot, saline, and reducing brines during deep burial (Fig 4.13). (46)
- **Neomorphism:** This process involves the in-situ transformation of carbonate minerals. It is observed as the aggrading recrystallization of fine micrite matrix into coarser microspar and the inversion of original aragonitic skeletal components (e.g., gastropods, corals) to the more stable mineral, low-magnesium calcite (Fig 4.14). (48)
- **Dolomitization:** Dolomite occurs as a replacement of the original limestone fabric, particularly noted in the algal limestone facies (LF-4). This can range from fabric-preserving mimetic replacement to fabric-destructive, coarsely crystalline mosaics. The presence of saddle dolomite cements suggests at least one phase of dolomitization was related to hot fluids during burial (Fig 4.14).

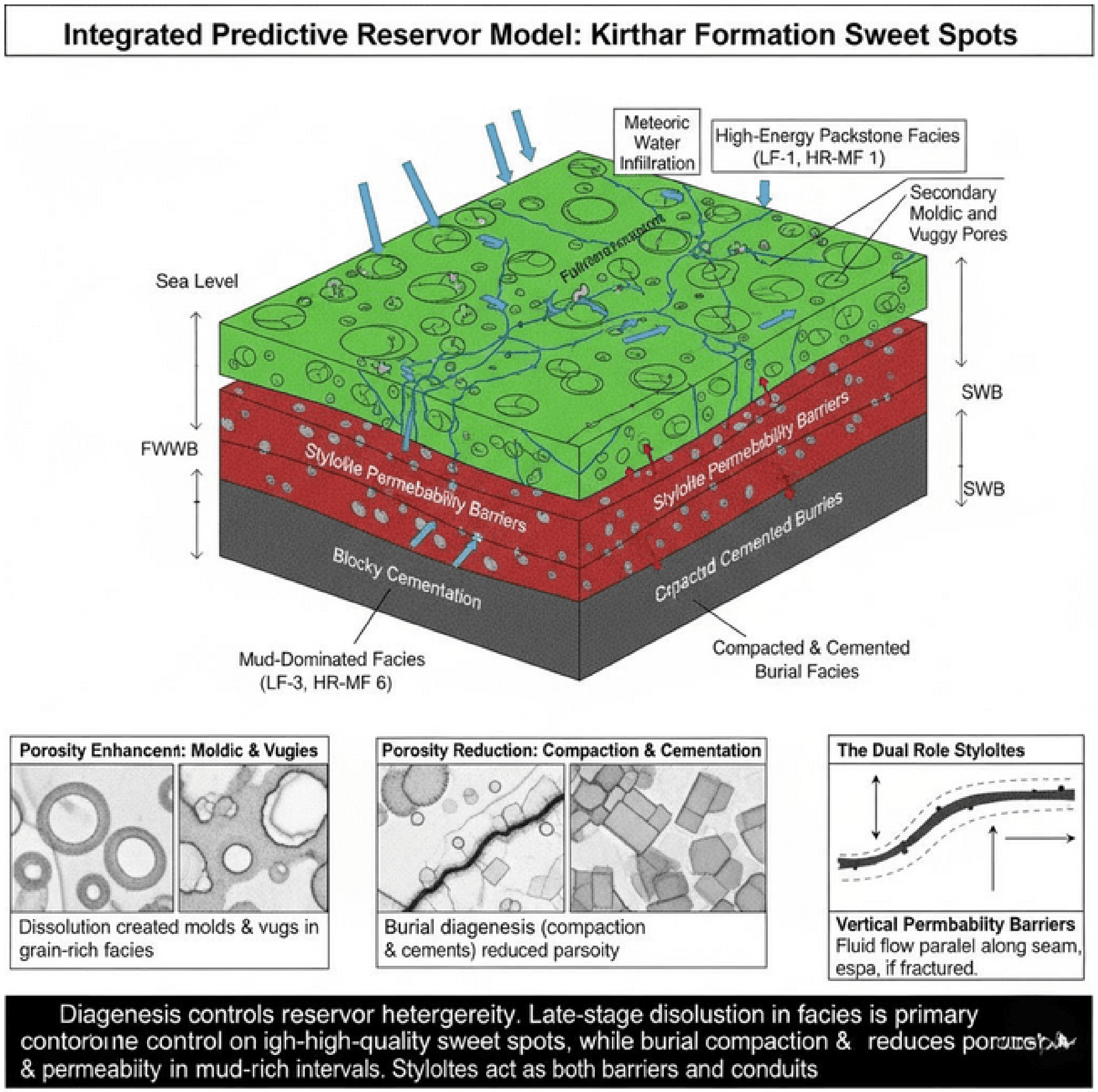

Figure 4.13. Stylolite-Controlled Diagenetic Influence on Reservoir Architecture. an "Integrated Predictive Reservoir Model" for Kirthar Formation "sweet spots." It shows how diagenesis (geological alteration) controls reservoir quality: late-stage "Meteoric Water Infiltration" causes dissolution, creating "Secondary Moldic and Vuggy Pores" (porosity enhancement) in the upper "High-Energy Packstone Facies." In contrast, the lower "Mud-Dominated Facies" experiences "Porosity Reduction" through "Compaction & Cementation." The model also details the "Dual Role of Stylolites" as both vertical barriers and potential horizontal fluid conduits.

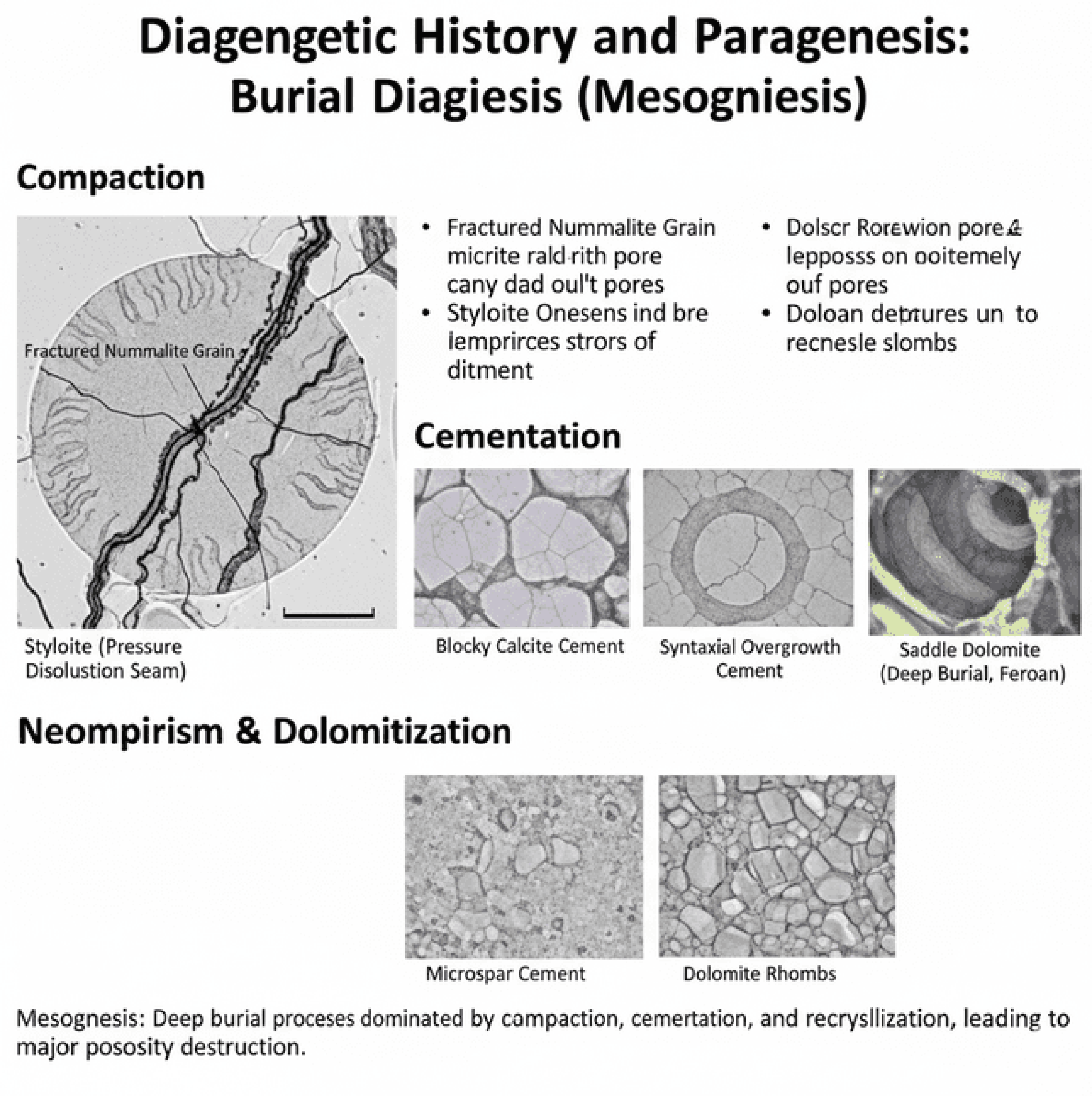

Figure 4.14. Shows the details of the processes of Burial Diagenesis (Mesogenesis), showing how it leads to "major porosity destruction." It breaks the process into three categories with microscopic examples: 1. Compaction, illustrated by a "Fractured Nummulite Grain" and "Stylolite (Pressure Dissolution Seam)"; 2. Cementation, showing "Blocky Calcite Cement," "Syntaxial Overgrowth Cement," and "Saddle Dolomite"; and 3. Neomorphism & Dolomitization, exemplified by "Microspar Cement" and "Dolomite Rhombs."

4.3.3. Telogenesis (Late-Stage Diagenesis)

Following tectonic uplift and exhumation, the Kirthar Formation was exposed to meteoric fluids, leading to late-stage alterations.

- **Dissolution:** This is a critical process for secondary porosity enhancement. The circulation of undersaturated meteoric fluids led to the partial or complete dissolution of chemically unstable components, such as aragonitic fossils and some calcite cements (Fig 4.15). This created significant moldic porosity (dissolution of a grain, leaving its shape) and vuggy porosity (larger, fabric-cutting pores). (47)
- **Fracturing:** Tectonically induced fractures and veins are common, related to the compressional stresses of the Himalayan orogeny that uplifted the region (Fig 4.15). These fractures cut across all earlier fabrics and are often filled with very late-stage, coarsely crystalline calcite cements. (48)

4.4. Reservoir Characterization

The hydrocarbon reservoir potential of the Kirthar Formation is a direct function of its pore system, which is the product of the original depositional fabric modified by the complex diagenetic history described above (Fig 4.16).

4.4.1. Porosity Types and Distribution

Both primary and secondary porosity are observed in the Kirthar Formation limestones, though secondary porosity is volumetrically more significant for creating effective reservoir intervals.

- **Primary Porosity:**
  - *Interparticle Porosity:* The space between grains, which was likely high initially in the grain-dominated packstone facies (HR-MF 1) but has been largely occluded by burial cements (Fig 4.17).
  - *Intraparticle Porosity:* The internal chambers within foraminiferal tests, particularly *Nummulites*. This is a key porosity type in many Eocene carbonate reservoirs and can be preserved if not filled by cement. (2)
- **Secondary Porosity:**
  - *Moldic and Vuggy Porosity:* These are the most important porosity types for reservoir quality. They were created by the dissolution of unstable skeletal grains (molds) and cements/matrix (vugs) during meteoric diagenesis. (50) This type of porosity is best developed in the initially grain-rich facies (HR-MF 1, HR-MF 5) (Fig 4.17).
  - *Fracture Porosity:* Tectonically induced fractures create significant permeability pathways, especially in the more brittle, well-cemented limestone beds. While the fracture volume itself may be low, they are critical for connecting otherwise isolated pores. (48)
  - *Intercrystalline Porosity:* The pore space between dolomite crystals, which can form excellent, well-connected pore networks in dolomitized intervals. (48)

ISSN 2250-3153

Figure 4.15. Late-Stage Diagenesis (Telogenesis), an uplift-related process where meteoric water infiltration enhances reservoir quality. It details the two primary mechanisms: 1) Dissolution, where "undersaturated meteoric fluids" leach unstable grains to create "Secondary Moldic & Vuggy Pores," and 2) Fracturing, which forms "Tectonic Fractures" that act as fluid pathways and significantly enhance permeability.

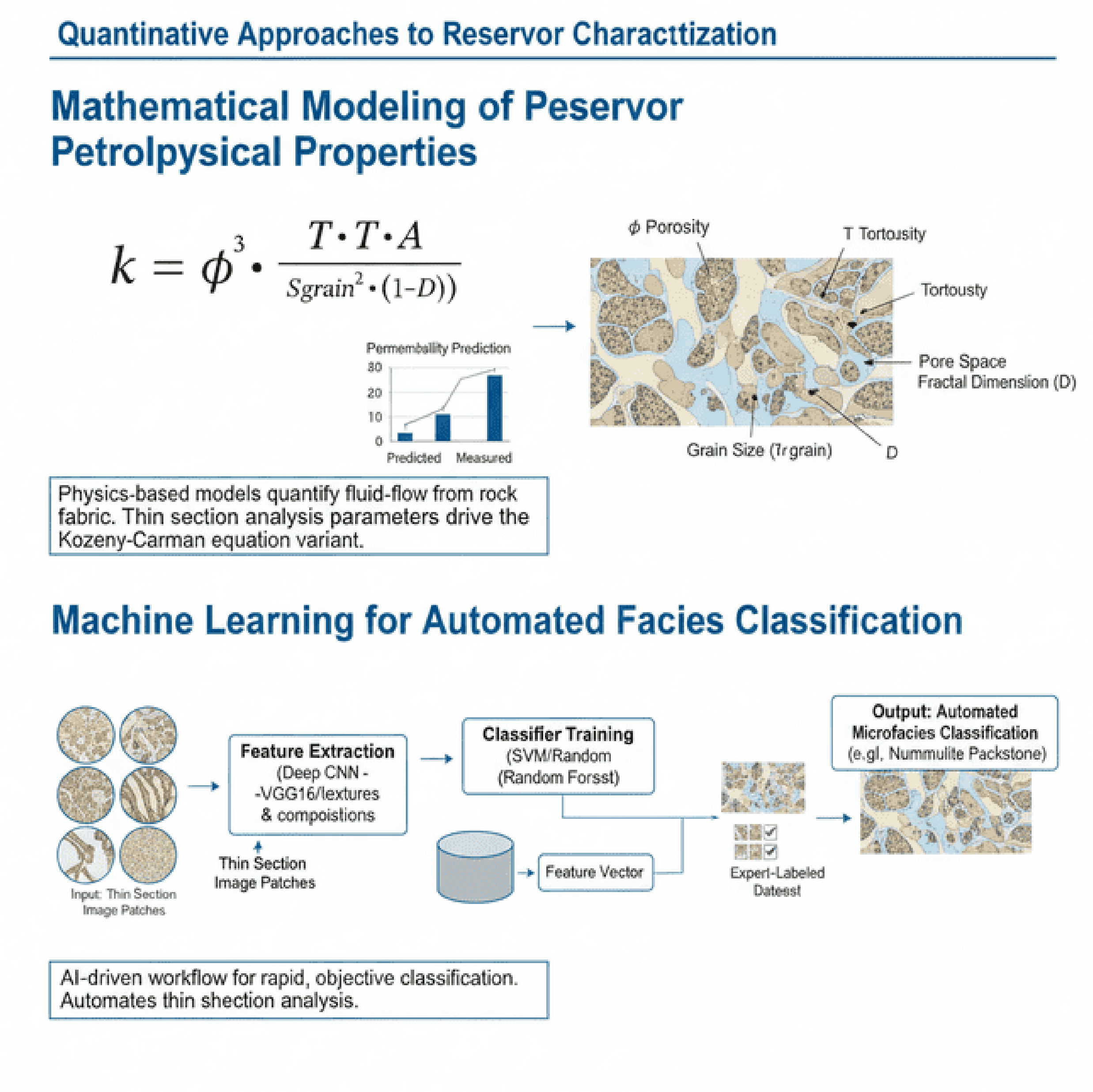

Figure 4.16. Quantitative approaches to reservoir characterization.

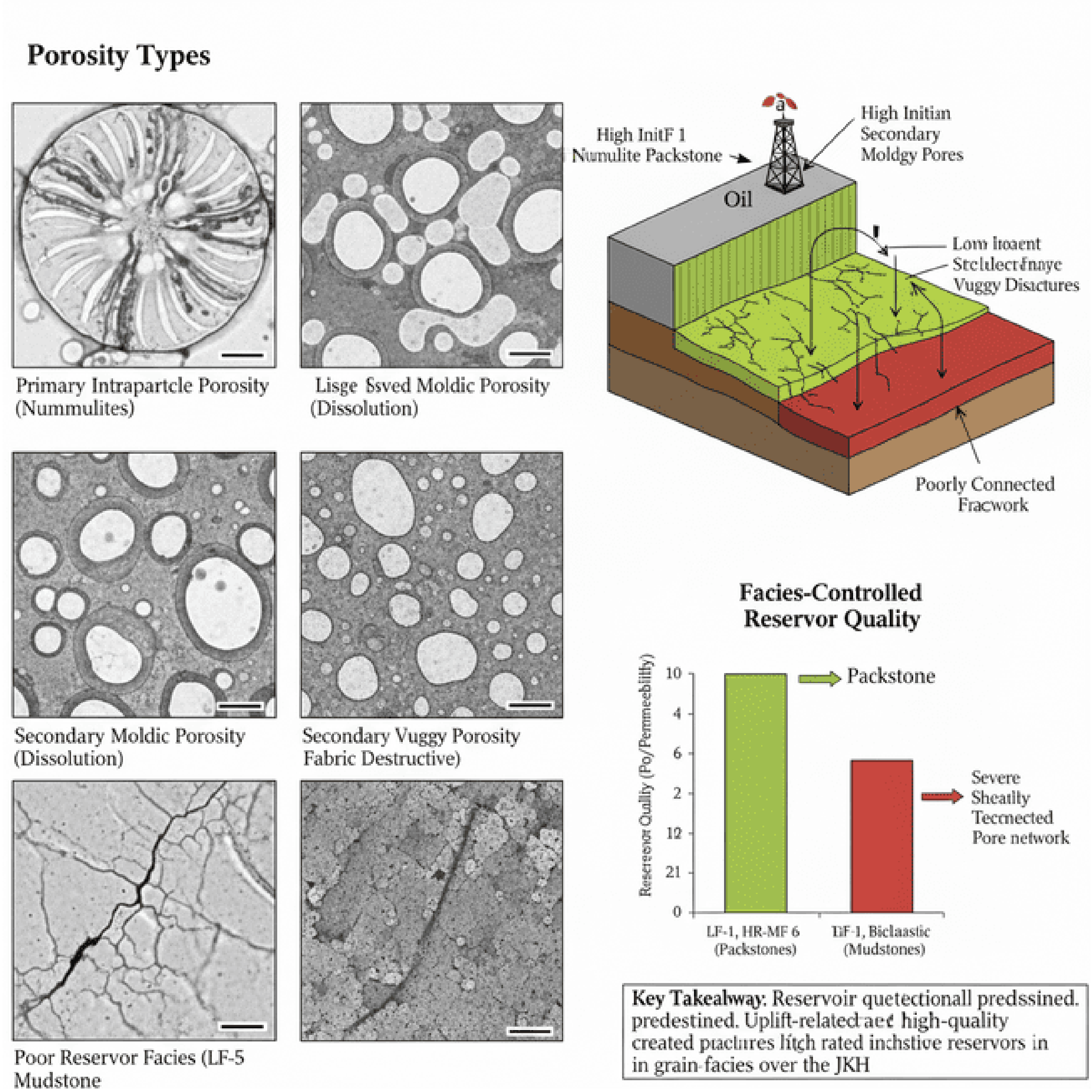

○

Figure 4.17. illustrates "Porosity Types" and "Facies-Controlled Reservoir Quality." It uses a series of micrographs to compare different porosity types, including good-quality primary intraparticle (Nummulites), secondary moldic, and vuggy porosity, with a "Poor Reservoir Facies" (Mudstone). A 3D block diagram and a bar chart demonstrate how this works in a reservoir, showing that the "High-Energy Nummulite Packstone" (LF-1) forms a high-quality "sweet spot" for oil, while the mudstone facies has poor reservoir quality.

4.4.2. Impact of Diagenesis on Reservoir Quality

The diagenetic processes have had a dichotomous impact on the reservoir quality of the Kirthar Formation.

- **Porosity Enhancement:** The single most important process for creating viable reservoir rock was late-stage dissolution associated with meteoric water influx during uplift. This process created extensive secondary porosity, particularly in the grainstone/packstone facies that contained abundant chemically unstable aragonitic bioclasts. (54) Dolomitization also has the potential to enhance porosity and permeability by creating a new intercrystalline pore network (55) (Fig 4.18).
- **Porosity Reduction:** Burial diagenesis was largely destructive to reservoir quality. Mechanical and chemical compaction

significantly reduced the bulk volume and pore space. The subsequent precipitation of extensive blocky calcite and late-stage ferroan calcite cements occluded most of the remaining primary interparticle porosity (48) (Fig 4.18).

- **The Dual Role of Stylolites:** Stylolites introduce significant heterogeneity and anisotropy. Their clay-rich seams act as effective vertical permeability barriers, potentially compartmentalizing the reservoir. However, these same stylolite surfaces can act as high-permeability conduits for fluid flow parallel to the seam, especially if they are associated with fractures or have not been completely cemented. (56) This dual behavior means that stylolites can both trap hydrocarbons and facilitate their migration, depending on the orientation and connectivity of the stylolite network relative to fluid flow paths (Fig 4.11).

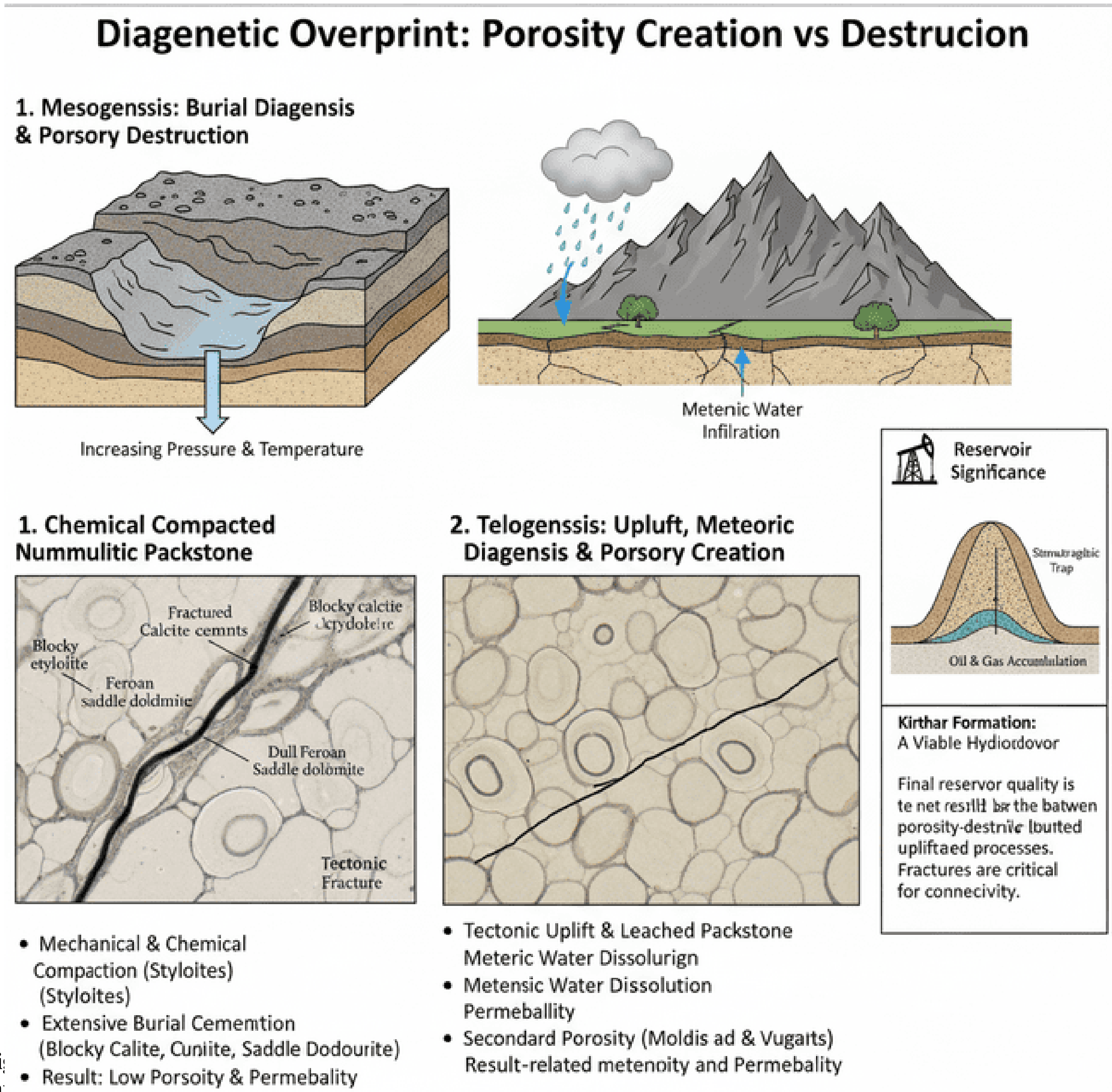

Fi[illegible] porosity th[illegible], and 2) Telogenesis (Uplift Diagenesis), which creates secondary porosity (molds and vugs) through meteoric water dissolution and fracturing. The final "Reservoir Significance" of the Kirthar Formation is shown to be the net result of this porosity creation vs. destruction, with fractures being critical for hydrocarbon accumulation.

International Journal of Scientific and Research Publications, Volume 16, Issue 8, August 2026 124
ISSN 2250-3153

Table 2: Paragenetic Sequence of Diageotic Events in in the Kirthar Formation

Diagenetic (Marine)		Process Description Burinial	Effect on Poreer (Dεrrblusty)
Eogrine Cementation	Syndpostion Early Burial	Formation of micrite envelope envelopes of wiplees around by aroınd grains by mbrben do cements.	Neutral / Minor
Econgėrasion	Early to Deep Burial	Precıpatal Compachus fibrus calcte deformation.	Decrease
Mechanical Comptation	Moderate Deep Burial	Early to Deep Burial Grain araangenent, fracturing tnrnem contacts at grain aragonite as to along seams. Precipation disolustion at grain contacts of aragonite to calctte.	Decrease Resbrifidution
Neeonization (Sy]dotis)		Burial Cementation (Calcite) Precipation of blocky. micrite; inversion of synttarsy, and syntastion of cıniction of remaining to calcite.	Neutral / Leaching unaisr-dements by increase/Decrase)
Dolomization	Darly Burial	Dolomization / Saddle Dolomite preciictation saddle dommuite dolomuie.	Major Decrease
Froposis	Upluift	Replaccation iron-rich fmıech-calcite in töcreise/tæıldgrase) Decrease	Moldic posich Dolomite)
Late Vein-Fill Calcite	Tectonic fracturing relaid	Deep Upluft	Variable Major Increase.
Telogessis	regional uphift	Precipation of co:ır.calcrte cements by metieon froccurs.	Tecteatic calcite within a flutids.

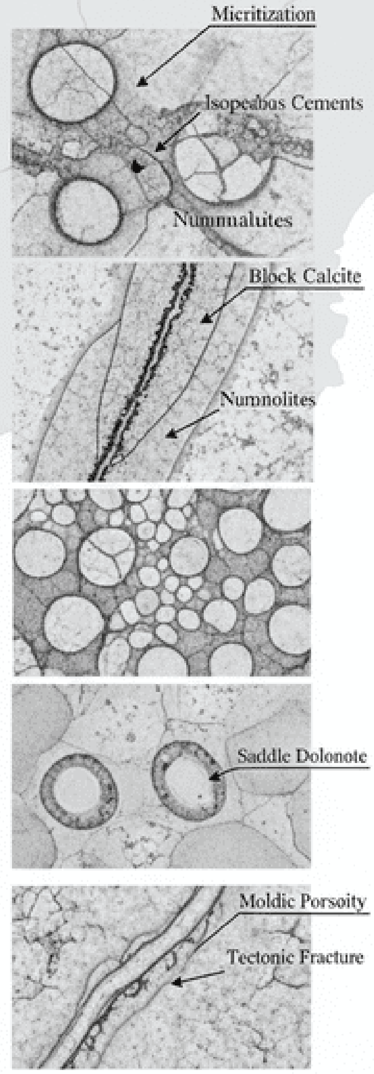

Figure 4.19. Paragenetic sequence of diagenetic events in the Kirthar Formation. detailing the complete geological history from early marine (Eogenesis) and burial (Mesogenesis) diagenesis to late-stage uplift (Telogenesis). It outlines each process (e.g., Cementation, Compaction, Dolomitization), its timing, and its ultimate effect on porosity. The sequence is illustrated with a corresponding set of micrographs showing key diagenetic features like Isopachous Cements, Block Calcite, Saddle Dolomite, Moldic Porosity, and Tectonic Fractures.

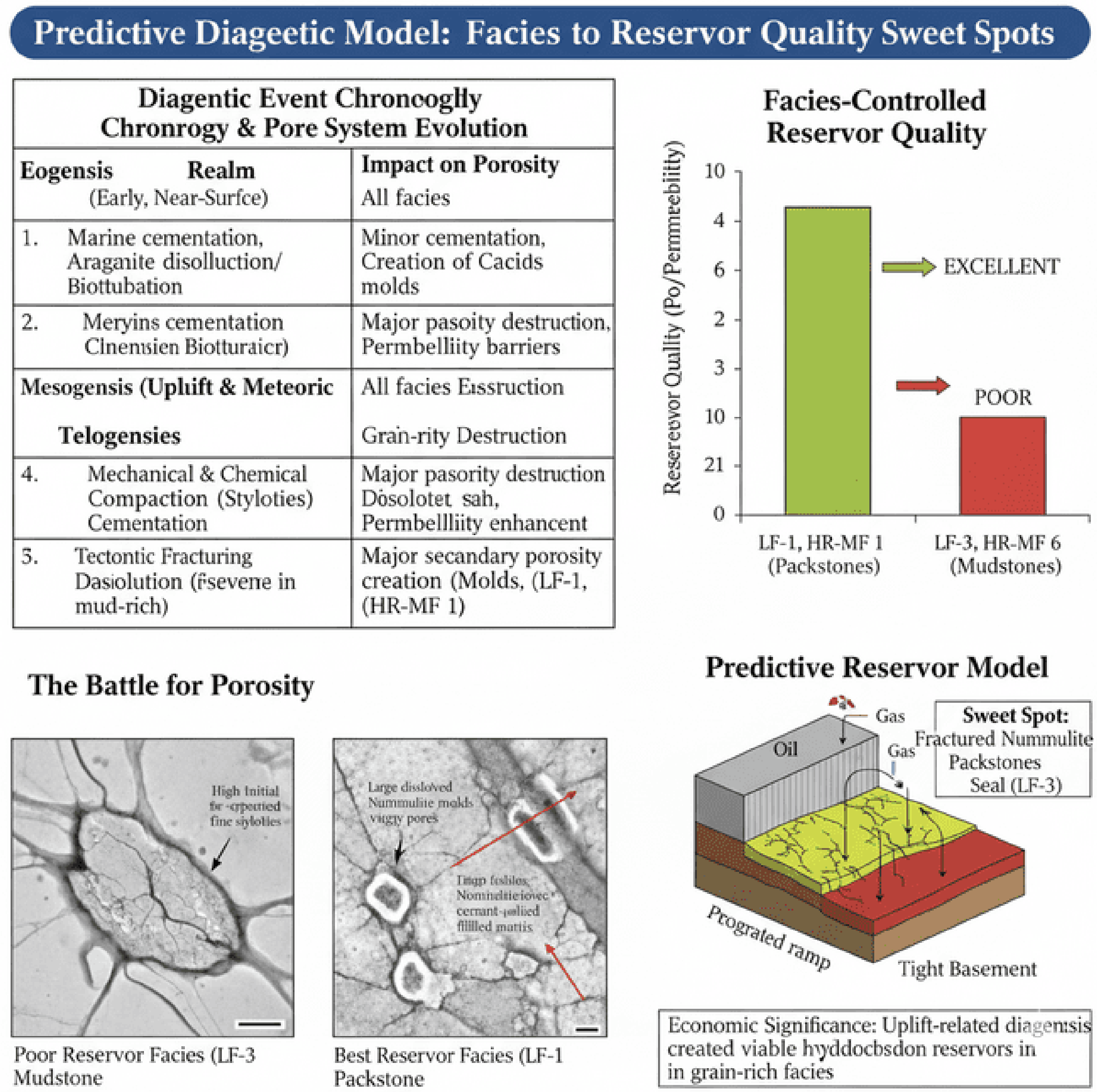

Figure 4.20. Predictive diagenetic model linking facies to reservoir-quality sweet spots. It gives the details of the diagenetic chronology—from Eogenesis (early) to Mesogenesis (burial) and Telogenesis (uplift)—and its impact on porosity. A bar chart and micrographs show that facies-controlled reservoir quality is "Excellent" in "Packstones" (LF-1) due to dissolution (creating vuggy pores), but "Poor" in "Mudstones" (LF-3) due to compaction. A final 3D model shows oil and gas trapped in this high-quality, fractured packstone "Sweet Spot."

5. DISCUSSION

5.1. Depositional Environment and Platform Model

The collective evidence from the lithofacies and microfacies analysis strongly indicates that the Kirthar Formation in the Rohri area was deposited on a homoclinal carbonate ramp (Fig 4.22). A ramp is a gently sloping platform without a continuous, high-relief marginal reef or shoal complex separating it from the deeper basin. (1) The identified facies represent a classic transect across such a ramp environment, developed on the paleotopographic high of the JKH (Fig 1.2).

- The **inner ramp** is represented by the algal dolomitic limestone (LF-4) and the oolitic wackstone (HR-MF 4). This zone was characterized by very shallow, restricted to high-energy, agitated waters, likely within the photic zone, allowing for algal growth and ooid formation. The evidence of iron nodules and dolomitization in LF-4 suggests periodic subaerial exposure or deposition in peritidal to sabkha-like conditions at the landward extent of the ramp (Fig 4.21, 4.22 and 4.23).
- The **mid-ramp** was the most extensive environment, characterized by moderate to high energy. It was dominated by vast shoals and banks of LBFs (*Nummulites*, *Assilina*), represented by the coarse-grained packstone and wackstone-packstone facies (LF-1, LF-2, HR-MF 1, HR-MF 3). The hydrodynamic behavior of Nummulites tests, which are easily transported by currents, was a key factor in the formation of these accumulations. (2) The presence of both well-preserved (autochthonous) and abraded/fragmented (allochthonous) tests indicates that these shoals were dynamic features, with LBFs living in situ but also being constantly reworked and concentrated by wave and storm currents. (2) The algal foraminiferal wackstones (HR-MF 2) likely represent slightly deeper or more protected areas on the mid-ramp, below the constant agitation of fair-weather waves (Fig 4.21, 4.22 and 4.23).
- The **outer ramp** is indicated by the microfacies containing planktonic foraminifera (HR-MF 5) and the bioclastic mudstone (HR-MF 6) as shown in (Fig 4.21-4.23). These facies represent deeper water settings below the storm wave base, with increasing influence from the open ocean. The mixing of transported benthic material with pelagic fauna in HR-MF 5 is characteristic of the transition from the mid- to outer-ramp (3).

This ramp model, with LBF shoals dominating the mid-ramp, is consistent with established models for many Eocene Tethyan carbonate platforms as shown in (Fig 4.21-4.23). (1) As noted by Racey (2001), large flat *Nummulites* tend to be associated with deeper, outer ramp settings, while smaller, more robust lenticular forms are found in shallower, inner ramp settings, with large banks occupying the intermediate space, which aligns with the facies distribution observed in this study. (62)

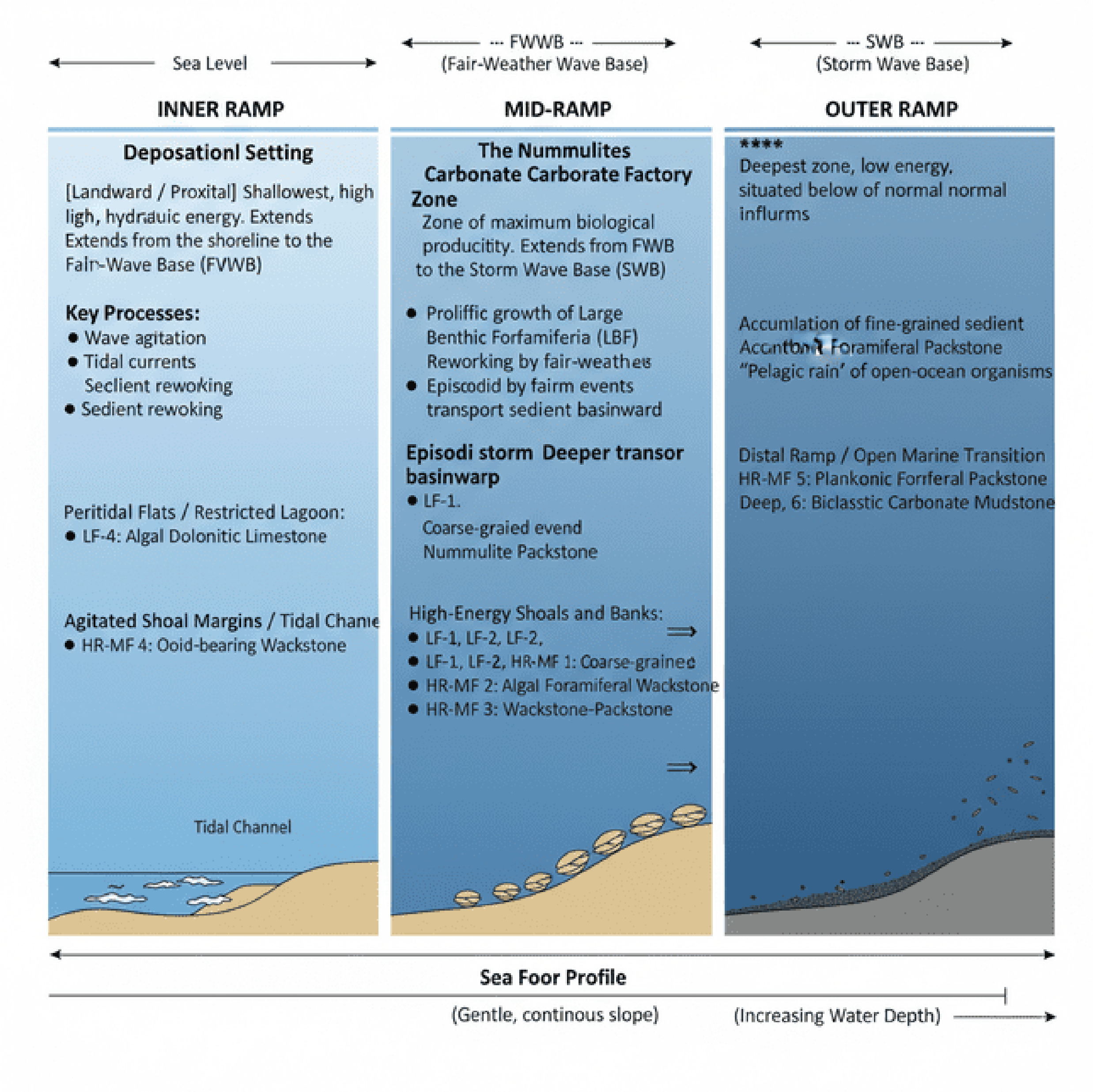

Figure 4.21. Carbonate ramp depositional framework and facies distribution. Comparison based on the facies, environment of deposition in details with facies. A new approach and proposed model showing a "Forced Regressive System Tract," combining 3D block diagrams of the "Rohri Section" with a 2D time-distance graph. The 3D blocks on the left show the vertical depositional sequence at Time 1 (Early Stage), Time 3: Main Stage, and Time 3: Late Stage. The 2D graph on the right explains this sequence by plotting the basinward migration of sedimentary environments (e.g., "Outer Ramp Shoal" to "Inner Ramp Lagoon") over time, culminating in a final "Exposure Surface" that matches the late-stage block.

ISSN 2250-3153

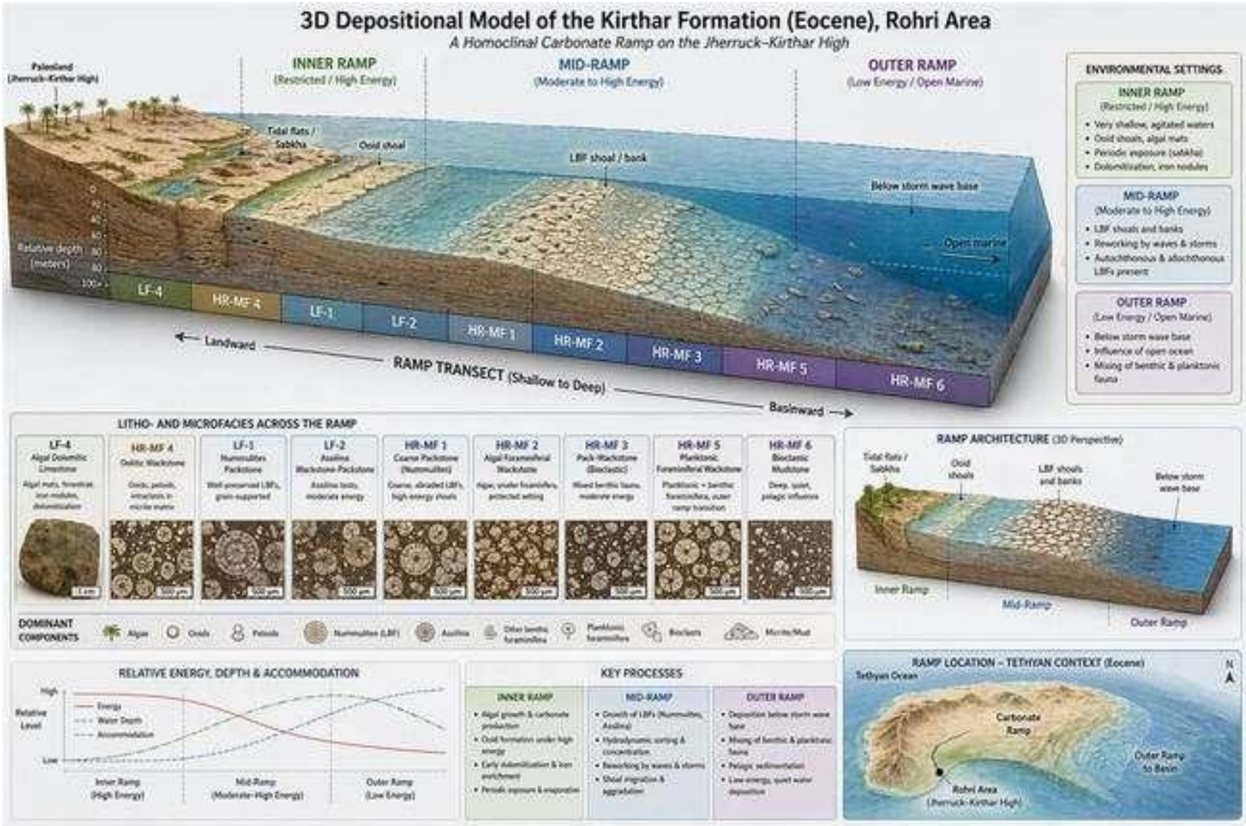

Figure 4.22. A new model proposed carbonate ramp depositional model, showing the lateral distribution of sedimentary facies controlled by increasing water depth. The model transitions from landward "Peritidal Mudflats" to a high-energy "Inner Ramp" dominated by a "Coarse-grained Nummulite Packstone" shoal (LF-1, LF-2). As water depth increases "Basinward," the facies grade through various ooid-bearing, algal, and plankton-rich wackestones and packstones into a low-energy "Outer Ramp Distal" environment, characterized by "Bioclastic Carbonate Mudstone" (HR-MF 6).

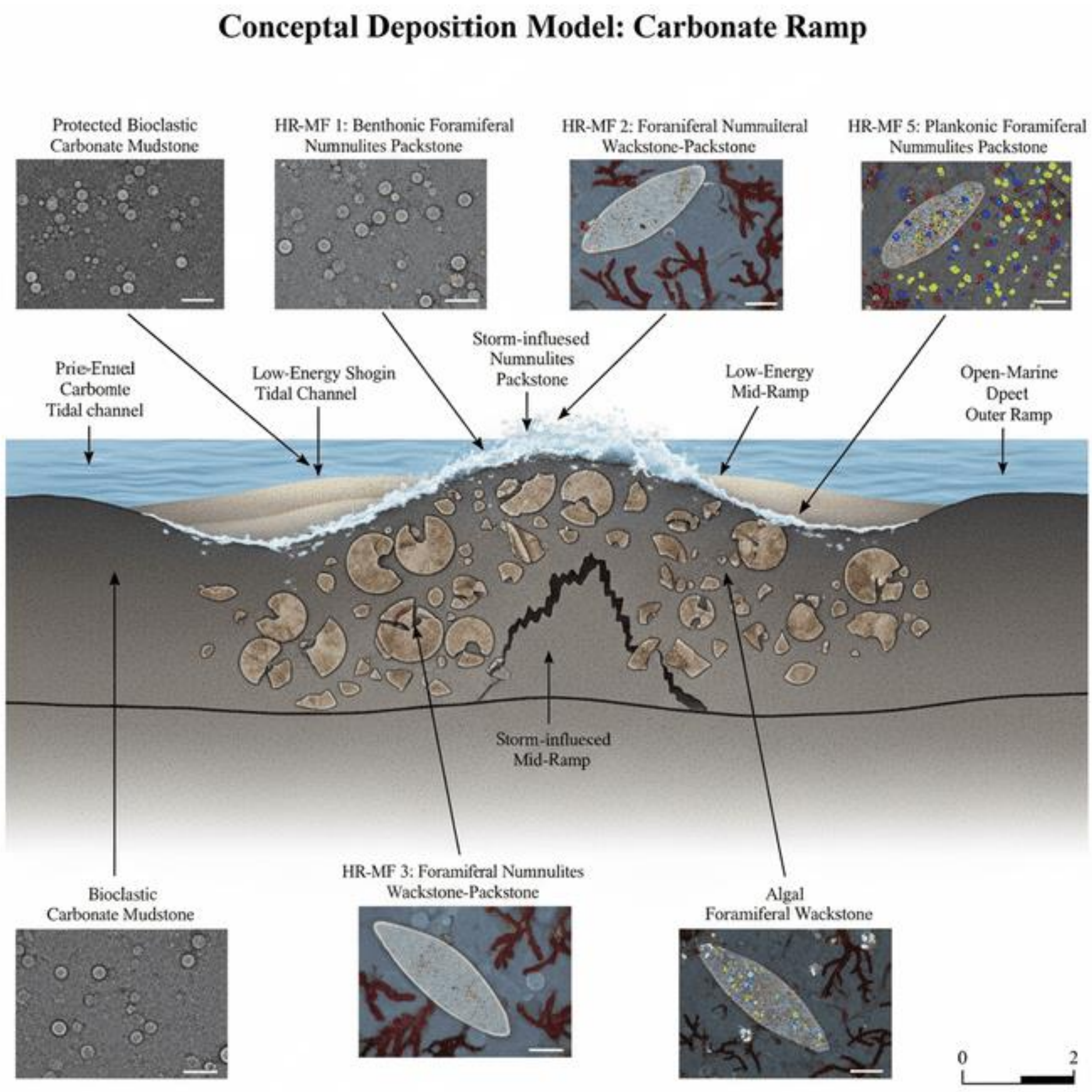

Figure 4.23. Conceptual depositional model linking facies to ramp energy zones; thin-section textures illustrate protected muds, algal and foraminiferal wacke/packstones, and storm-influenced nummulite deposits. A detailed pictogram model by using new approach by ML.

5.2. Sequence Stratigraphic Framework

The vertical succession of facies in the measured section provides insights into the relative sea-level changes during the deposition of the Kirthar Formation (Fig 4.29). The overall stacking pattern is progradational, or coarsening-upward, transitioning from lower-energy micritic limestones (LF-3) at the base of the main succession to higher-energy coarse-grained limestones (LF-1, LF-2) towards the top, capped by peritidal deposits (LF-4). This progradational pattern is characteristic of a Highstand Systems Tract (HST) or, more likely given the evidence of exposure at the top, a Forced Regressive Systems Tract (FRST) (Fig 4.24- 4.28). (25)

This observed third-order regression occurred within a broader, second-order sea-level rise (Transgressive Systems Tract) that characterized much of the Eocene.The driver for this third-order regression could be eustatic (global sea-level fall) or tectonic. Given the location on the tectonically active JKH (Fig 4.27), it is plausible that localized uplift of the high could have forced the shoreline to prograde seaward, creating the observed shallowing-upward sequence independent of global sea-level changes. (65) This interpretation effectively links the basin's tectonic evolution directly to its sequence stratigraphic architecture. (Fig 4.27).

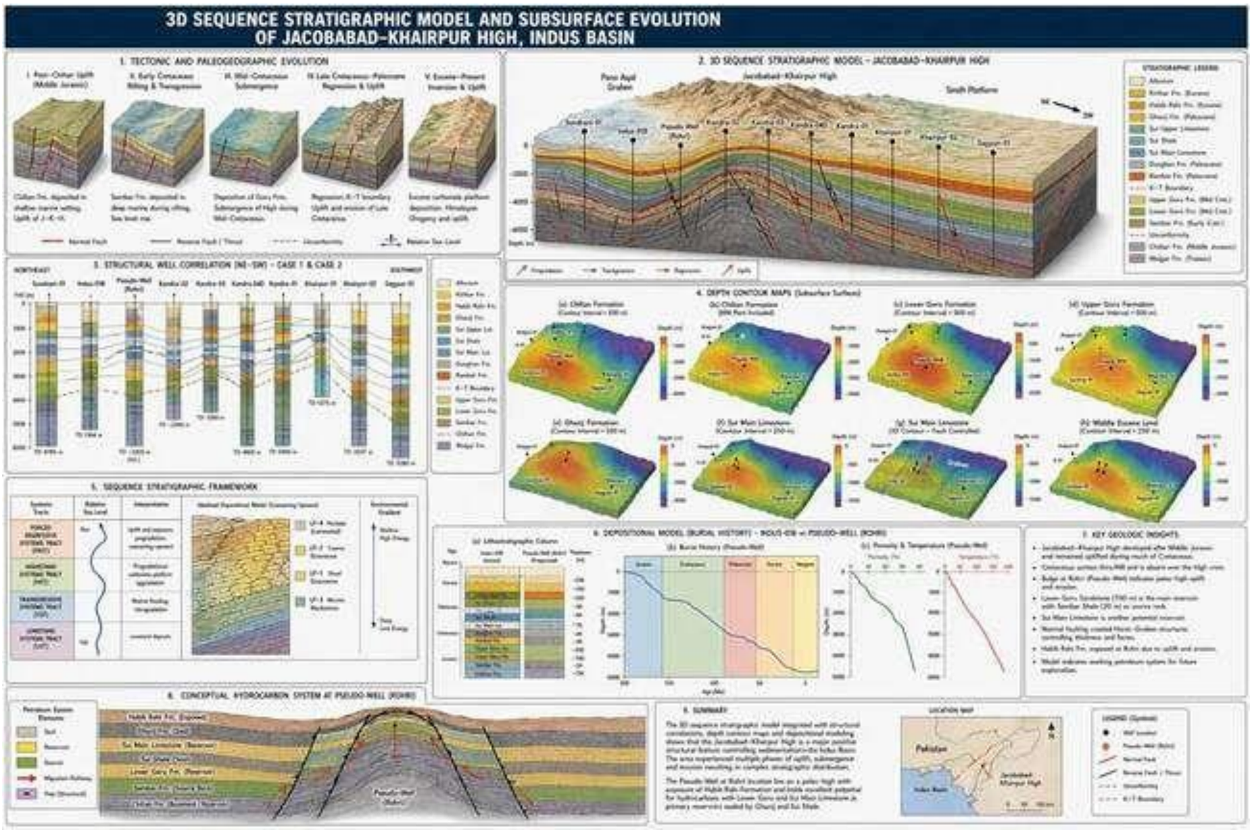

Figure 4.24. Sequence Stratigraphy of the Kirthar Formation," linking tectonic activity to sea-level change. It connects the "Rohri Measured Section," a shallowing-upward sequence identified as a "Forced Regressive Systems Tract" (FRST), to its causal mechanisms: a "Relative Sea-Level Curve" (a rapid, third-order fall superimposed on a long-term, second-order rise) and the "Tectonic Driver" of localized "JKH Uplift," which forced progradation and exposure,

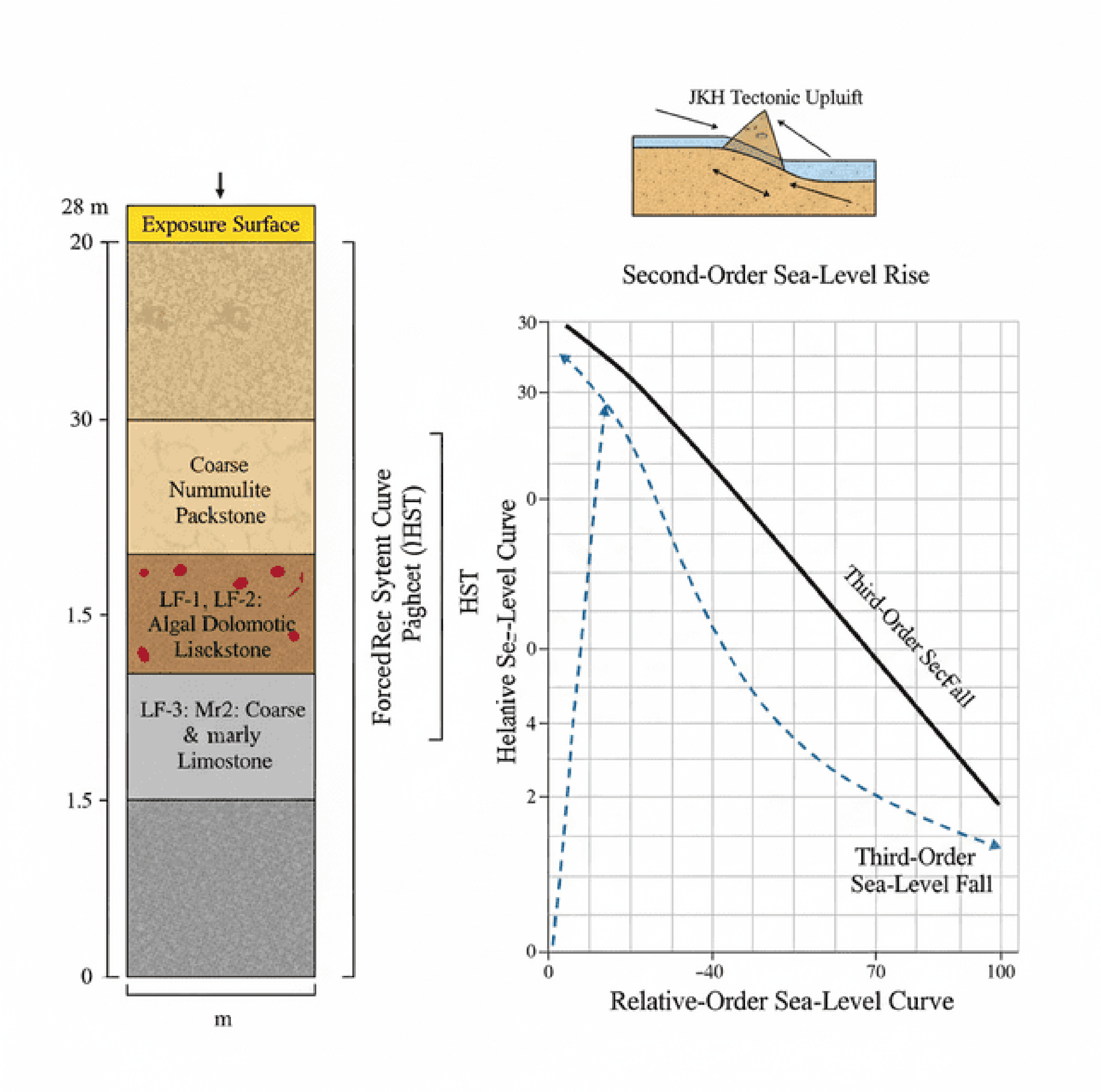

Figure 4.25. links a stratigraphic column that culminates in an "Exposure Surface" to its cause: a "Forced Regressive System Tract." This event was driven by "JKH Tectonic Uplift" and a rapid "Third-Order Sea-Level Fall," which together overpowered the long-term "Second-Order Sea-Level Rise," forcing the sea to retreat and expose the seabed.

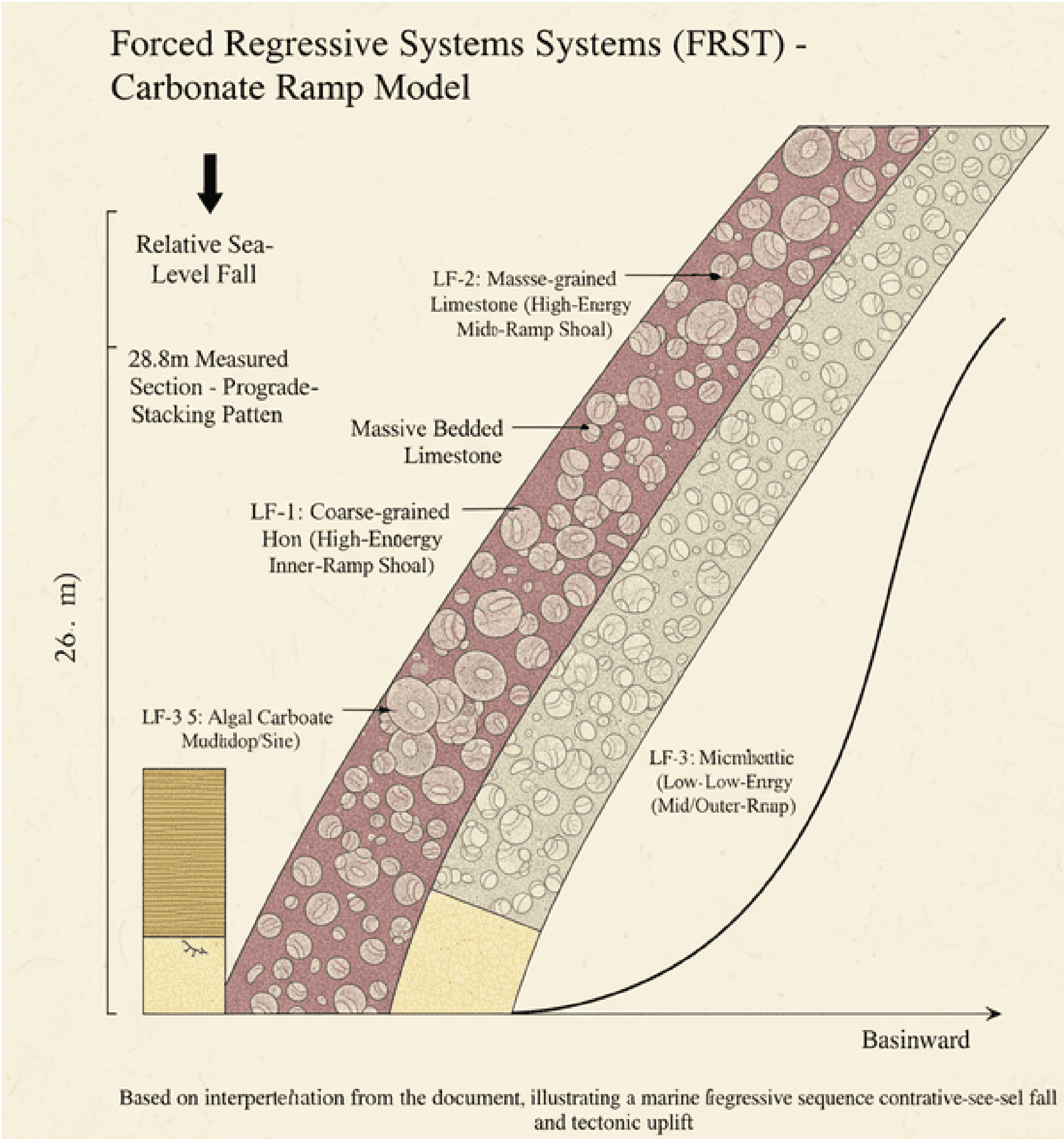

Figure 4.26. a "Forced Regressive Systems Tract (FRST)" carbonate ramp model, driven by a relative sea-level fall and tectonic uplift. It uses a time-distance plot to show a "Prograde-Stacking Pattern" where shallower, high-energy facies build out "Basinward" over time. The sequence shows low-energy mid/outer-ramp deposits (LF-3) being progressively overlain by high-energy inner-ramp shoals (LF-1) and mid-ramp shoals (LF-2). This model corresponds to the observed "28.8m Measured Section" shown on the left.

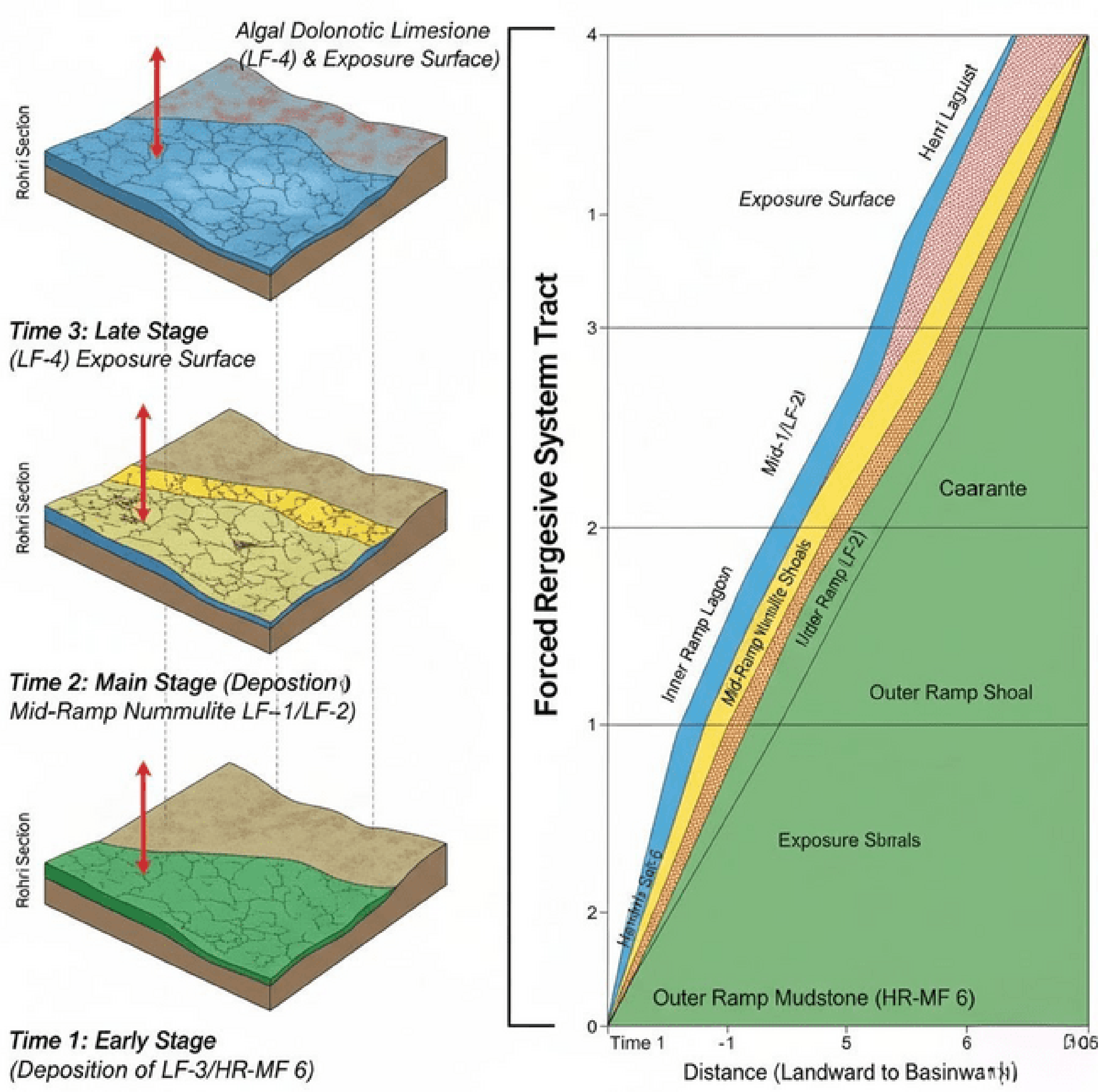

Figure 4.27. FRST evolution through time. Early stage deposits outer-ramp mudstone (LF-3/HR-MF6); main stage builds mid-ramp nummulitic shoals (LF-1/LF-2); late stage forms algal dolostone (LF-4) and exposure. Right panel shows landward-to-basinward facies belts and migrating exposure surfaces.

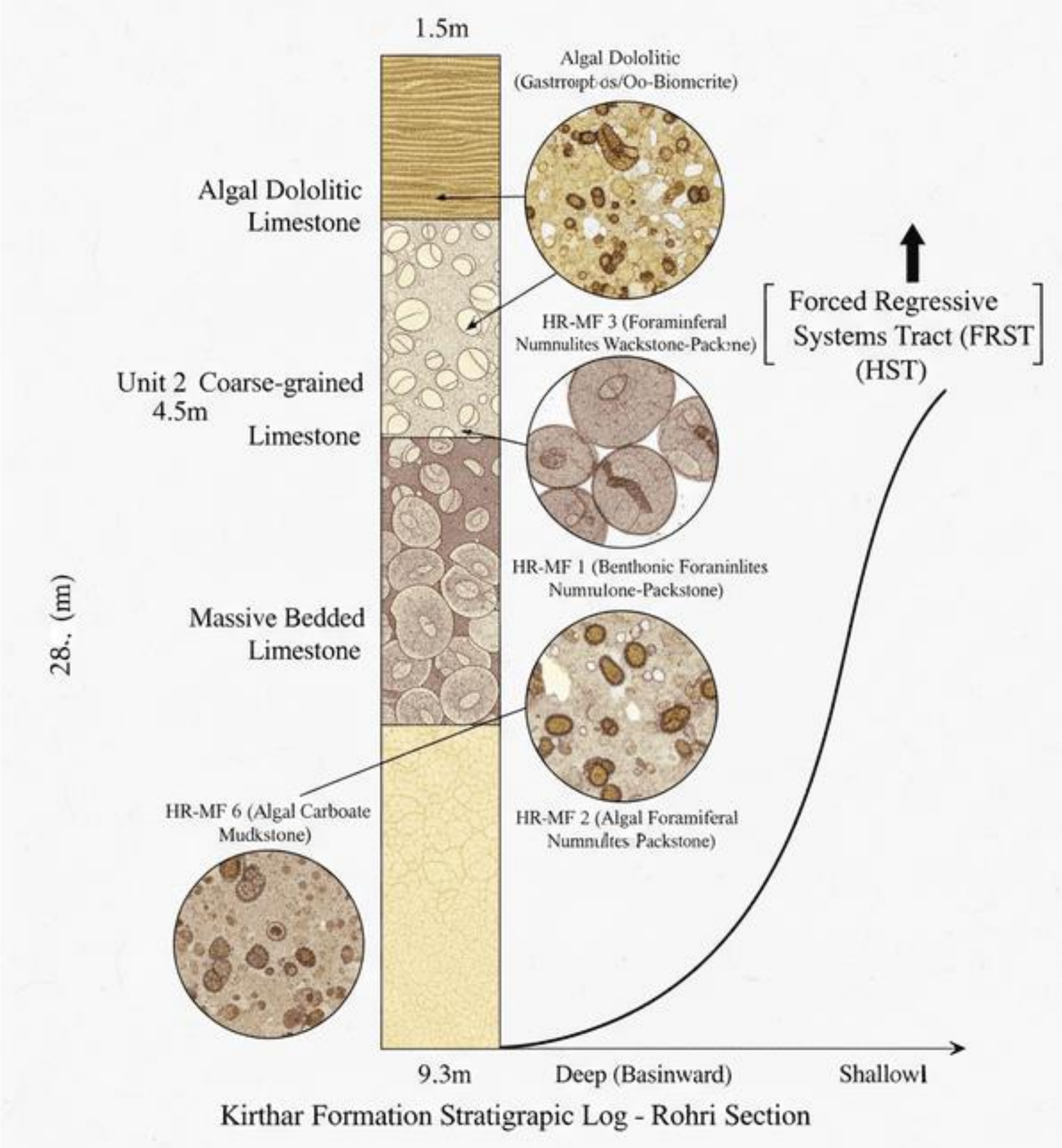

Figure 4.28. Kirthar Formation stratigraphic log (Rohri). A 28 m, upward-shoaling FRST from algal carbonate mudstone to massive and coarse nummulitic packstones, capped by algal dolomitic limestone; thin-section inserts show corresponding HR-MF facies.

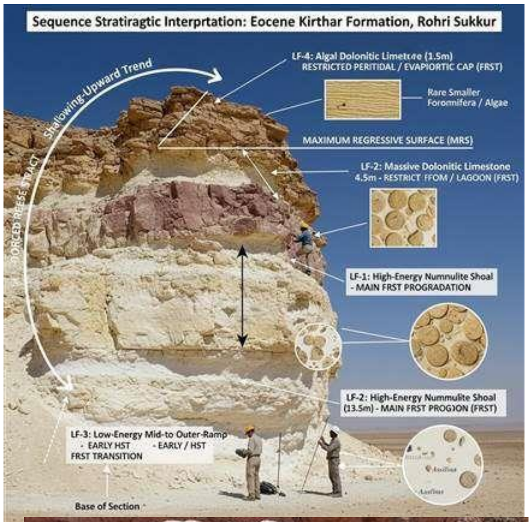

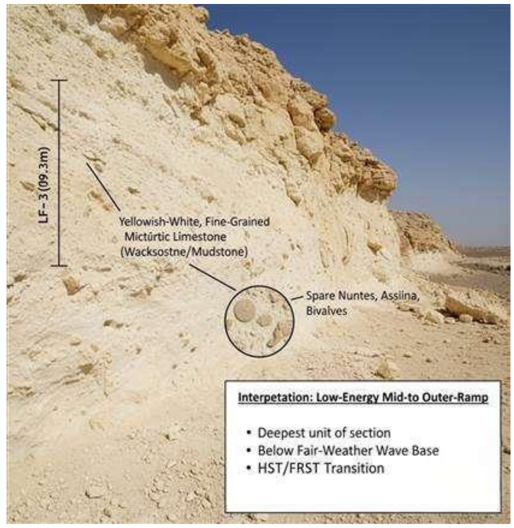

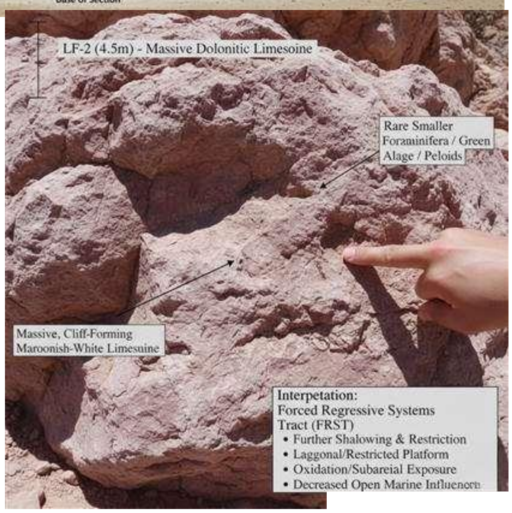

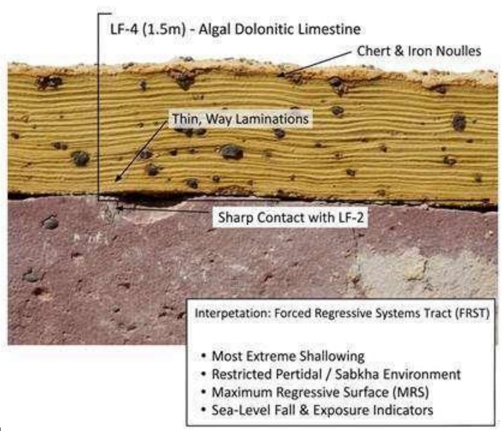

Figure 4.29: Shows the seque a) complete outcrop picture with all the sequences labeled from the base to the Top. b) micritic limestone bed, c) mehroonish massive dolomitic limestone LF, d) massive bedded limestone facie, e) Algal dolomitic limestone facie with a sharp contact.

5.3. Controls on Reservoir Quality: An Integrated Model

The final reservoir quality of the Kirthar Formation is not a random attribute but is the predictable outcome of the interplay between the primary depositional environment and the subsequent diagenetic overprint (Fig 5.1). This relationship allows for the development of a predictive model for reservoir "sweet spots."

The primary control is the depositional facies, which dictates the initial porosity, permeability, and mineralogical composition. High-energy, grain-dominated facies, such as the Nummulite Packstones (HR-MF 1) (Fig 4.3 a-d), started with the highest potential. They possessed significant primary interparticle porosity and permeability, and their skeletal grains (many originally aragonitic) were susceptible to later dissolution. (66) In contrast, low-energy, mud-dominated facies, like the Wackestones and Mudstones (HR-MF 2, HR-MF 6) (Fig 4.4 a-c) and (Fig 4.9 a-d), had low initial permeability and were composed of fine-grained calcite mud (micrite), which is prone to severe compaction. (66)

The secondary control is the diagenetic pathway each facies experienced. This pathway was itself influenced by the primary fabric.

- The **grain-dominated facies** acted as initial high-permeability conduits, focusing the flow of diagenetic fluids. While this made them susceptible to pore-occluding cements during burial, it also made them prime targets for dissolution by undersaturated meteoric fluids during later uplift, leading to the creation of excellent secondary moldic and vuggy porosity. (39)

- The **mud-dominated facies**, with their low initial permeability, were more prone to developing overpressure during burial, leading to intense chemical compaction and the formation of stylolitic barriers that further reduced permeability. (42) However, these fine-grained precursors are also more susceptible to pervasive dolomitization, which, if it occurs, can transform a non-reservoir rock into an excellent reservoir with high intercrystalline porosity. (53)Therefore, the best reservoir quality in the Kirthar Formation is predicted to occur in the thick-bedded, coarse-grained Nummulite packstone facies (LF-1, HR-MF 1) that were positioned favorably to be flushed by meteoric fluids during telogenesis, leading to significant secondary dissolution while escaping complete cementation during burial (Fig 5.1). The poorest quality is expected in the heavily compacted and cemented micritic limestone facies (LF-3, HR-MF 6). This integrated model provides a powerful predictive tool: by mapping the distribution of depositional facies, which can potentially be identified on seismic data, one can infer the likely diagenetic overprint and thereby predict the distribution of the most promising reservoir intervals.

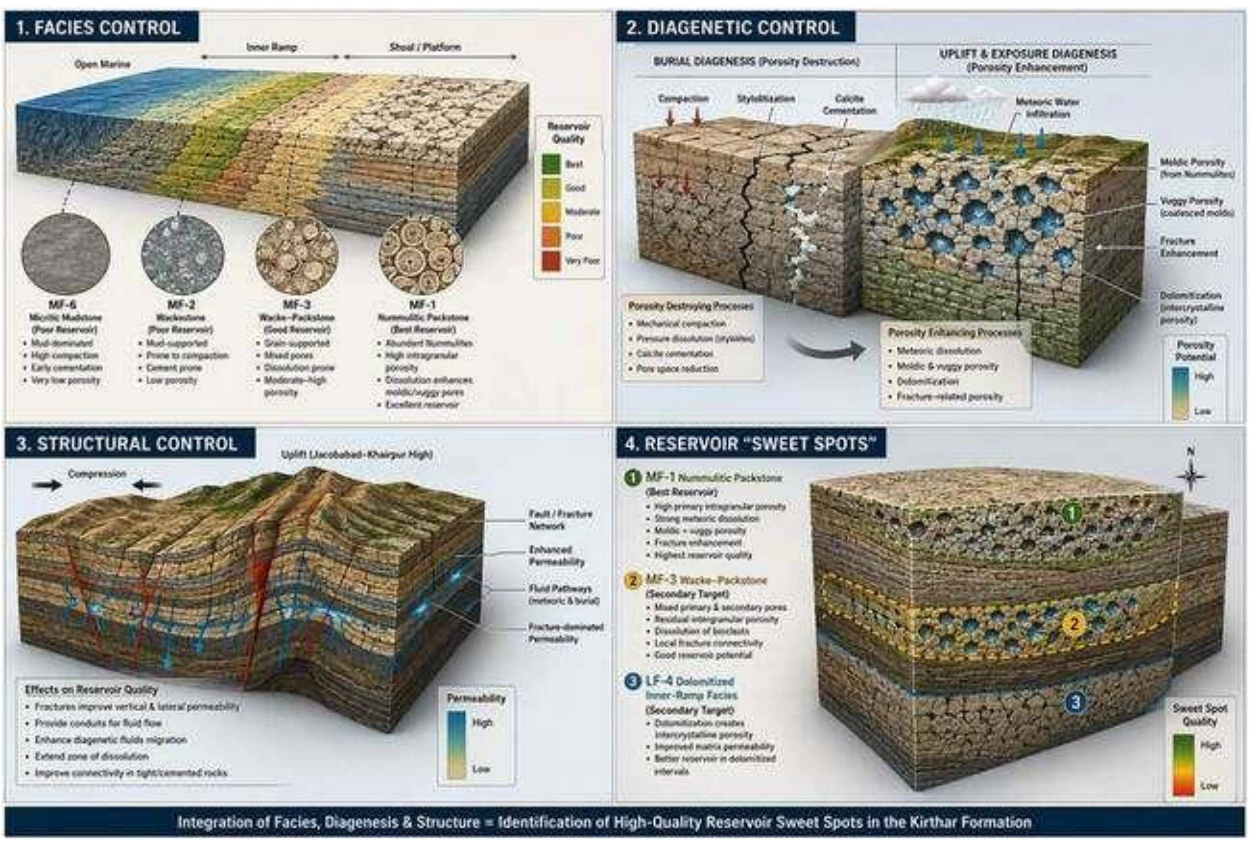

Figure 5.1. Tectonic control on reservoir quality. Uplift of the Jacobabad–Khairpur High focuses wave/current energy and winnowing, creating high-porosity nummulitic packstone shoals, whereas low-energy ramp mudstones remain tight; predictive framework highlights sweet spots near fractured shoals.

5.4. Regional Context and Comparison

The depositional and diagenetic characteristics of the Kirthar Formation at Rohri show strong similarities to other Eocene carbonate successions in Pakistan and across the former Tethyan margin (Fig 5.2). The facies associations are comparable to those described for the Sakesar Limestone in the Potwar Basin and the Margala Hill Limestone near Islamabad, which also represent deposition on carbonate ramps or shelves dominated by LBFs. (66) For instance, the study by Jamil et al. (2022) on the Sakesar Limestone identified six microfacies ranging from mud-dominated outer ramp to grain-dominated inner ramp settings, a zonation that closely mirrors the findings of this study (66)

Similarly, the Eocene Nisai Formation of the Pishin Belt contains rich assemblages of *Nummulites*, *Assilina*, *Discocyclina*, and algae, which have been interpreted to represent a spectrum of inner to outer ramp environments. (20) This direct parallel in both faunal content and environmental interpretation suggests that the processes governing carbonate deposition were consistent across different sub-basins on the northwestern margin of the Indo-Pakistan Plate during the Eocene. The diagenetic processes observed—including compaction, multi-phase cementation, dissolution, and dolomitization—are common themes in the diagenetic evolution of these Eocene carbonates, highlighting the regional importance of burial and subsequent meteoric diagenesis in controlling reservoir quality. (69)

Furthermore, the Kirthar Formation serves as an excellent analogue for the highly productive Nummulitic reservoirs of North Africa and the Middle East, such as the El Garia Formation in offshore Tunisia. (3) These reservoirs, as detailed by Racey (2001), are also characterized by accumulations of reworked LBFs in shoal and bank settings, and their quality is similarly controlled by the balance between cementation and secondary dissolution. (24) The insights gained from the Kirthar Formation on the JKH can thus be applied to exploration models in other basins along the Tethyan belt where similar depositional and tectonic settings exist (Fig 5.2 a-c).

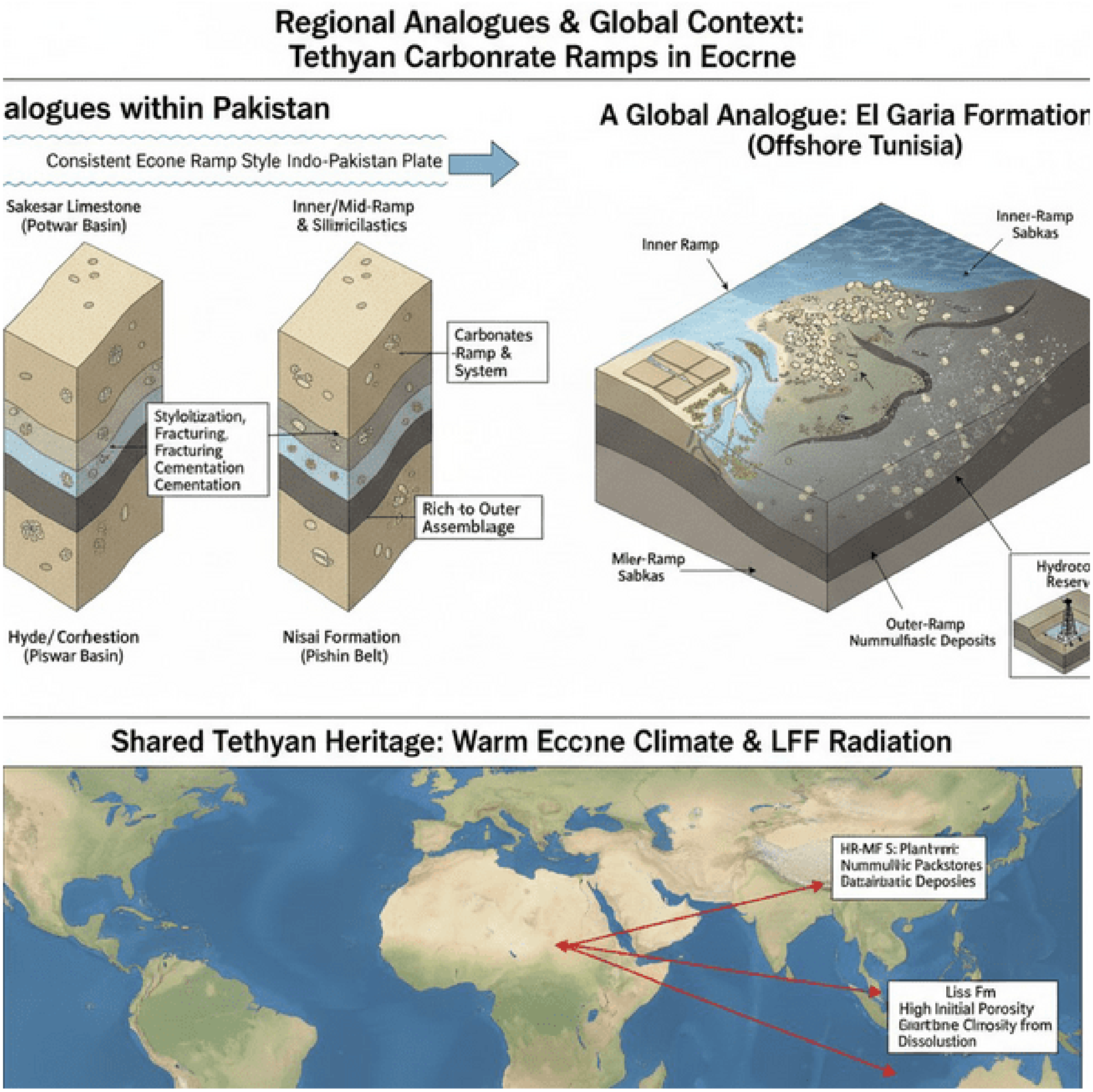

Figure 5.2. Eocene Tethyan carbonate-ramp analogs from Pakistan to El Garia (Tunisia) show inner–mid–outer ramp belts with nummulitic shoals and proven charge; target fractured nummulitic packstones as reservoir sweet spots. A predictive model for global exploration.

5.5. Implications of Quantitative Modeling

The conceptual introduction of mathematical and machine learning models in this study points toward the future of carbonate reservoir characterization. While traditional petrography remains the foundation, its time-consuming and subjective nature can create bottlenecks in reservoir evaluation. These quantitative techniques offer a powerful means to enhance efficiency, reduce subjectivity, and extract predictive, quantitative information from the same datasets.

- **Permeability Prediction:** Physics-based models like the Kozeny-Carman equation, when calibrated with petrographic data from thin sections (such as pore fractal dimensions and grain radii), can provide rapid, first-order estimates of permeability. As demonstrated in the workflow (Appendix A), this provides a direct, physics-based link between the observable rock fabric and its fluid-flow capacity. This is invaluable for populating reservoir models in areas between cored wells, significantly reducing uncertainty in fluid flow simulations.(Fig 3.4 and 3.5). (26)

- Automated Petrography: The proposed hybrid machine learning workflow (using a CNN like VGG16 for feature extraction and a Random Forest for classification) is designed to automate the labor-intensive task of microfacies classification. Such systems can process thousands of images in the time it takes a petrographer to analyze a few, providing consistent, objective, and quantitative data on facies proportions and distributions (Fig 5.3). This high-throughput analysis can identify subtle textural trends that might be missed in manual studies and can be used to rapidly screen large sample sets, identifying key intervals for more detailed investigation. (Fig 5.4) (71).

Integrating these data-driven approaches into standard geological workflows is not merely a novelty; it is a critical step for de-risking exploration and optimizing the development of complex, heterogeneous carbonate reservoirs like the Kirthar Formation. This study provides a conceptual blueprint for how to bridge the gap from qualitative observation to quantitative prediction

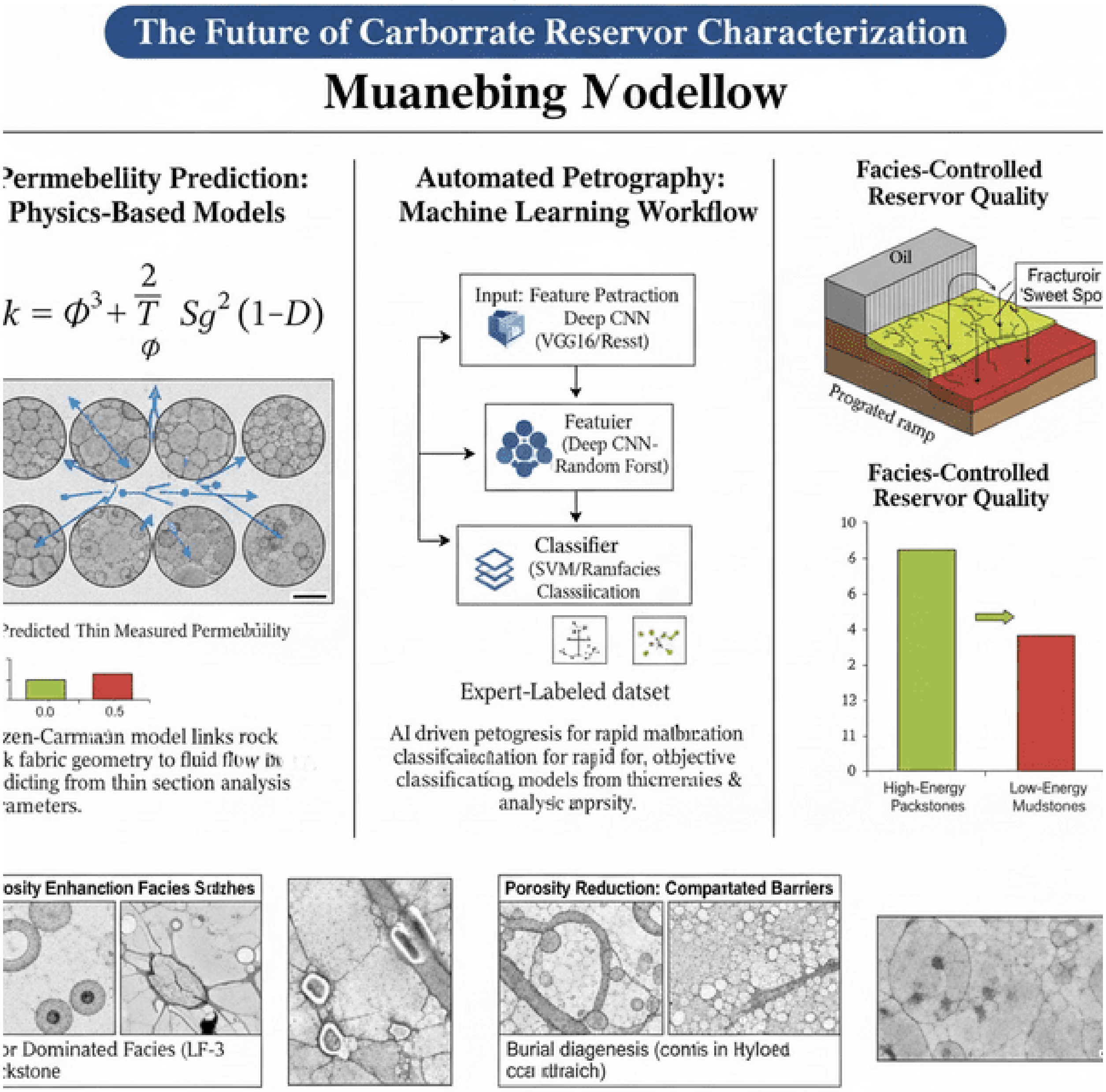

Figure 5.3. Combine physics-based permeability models with ML-driven petrography for fast, objective facies mapping; reservoir quality is highest in packstones and lowest in mud-rich facies, modulated by diagenesis. A hybrid approach to modeling carbonate reservoirs. It argues that the "future" is to combine traditional physics-based permeability models (left) with faster, more objective machine learning workflows (center) that can automatically classify rock types from images. The ultimate goal

is to create more accurate predictive models of reservoir quality (right), which is controlled by the original depositional facies (e.g., high-energy packstones) and subsequent diagenetic changes (porosity creation vs. destruction).

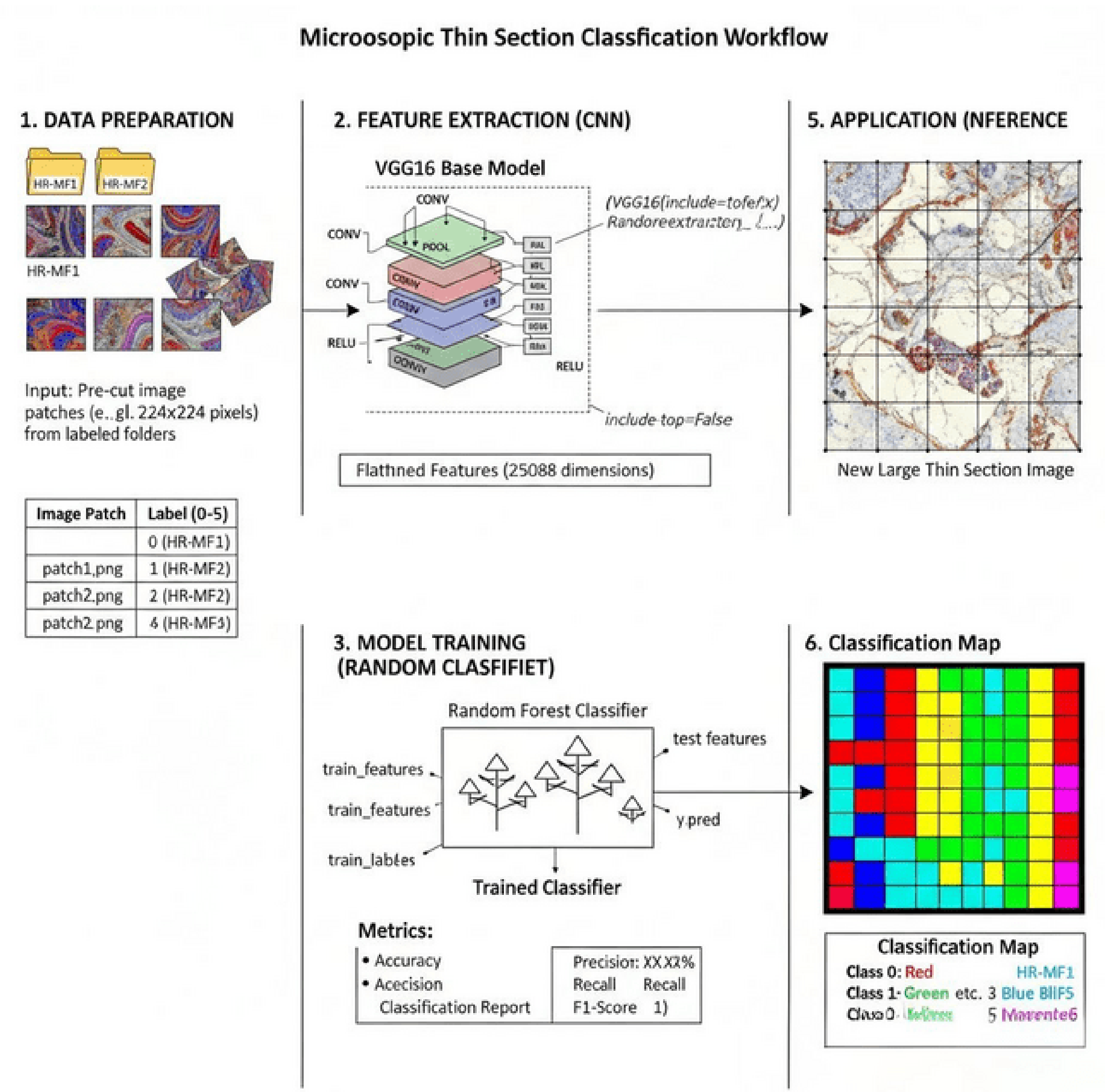

Fig 5.4. ML codes and script: shows a machine learning workflow for automatically classifying geological thin sections. First, a training dataset is made from labeled image patches. A VGG16 (CNN) model extracts numerical features from these patches, and a Random Forest model is then trained to link these features to the correct rock type. Finally, this trained system can analyze a new, large image and produce a "Classification Map" that shows where each different rock type is located.

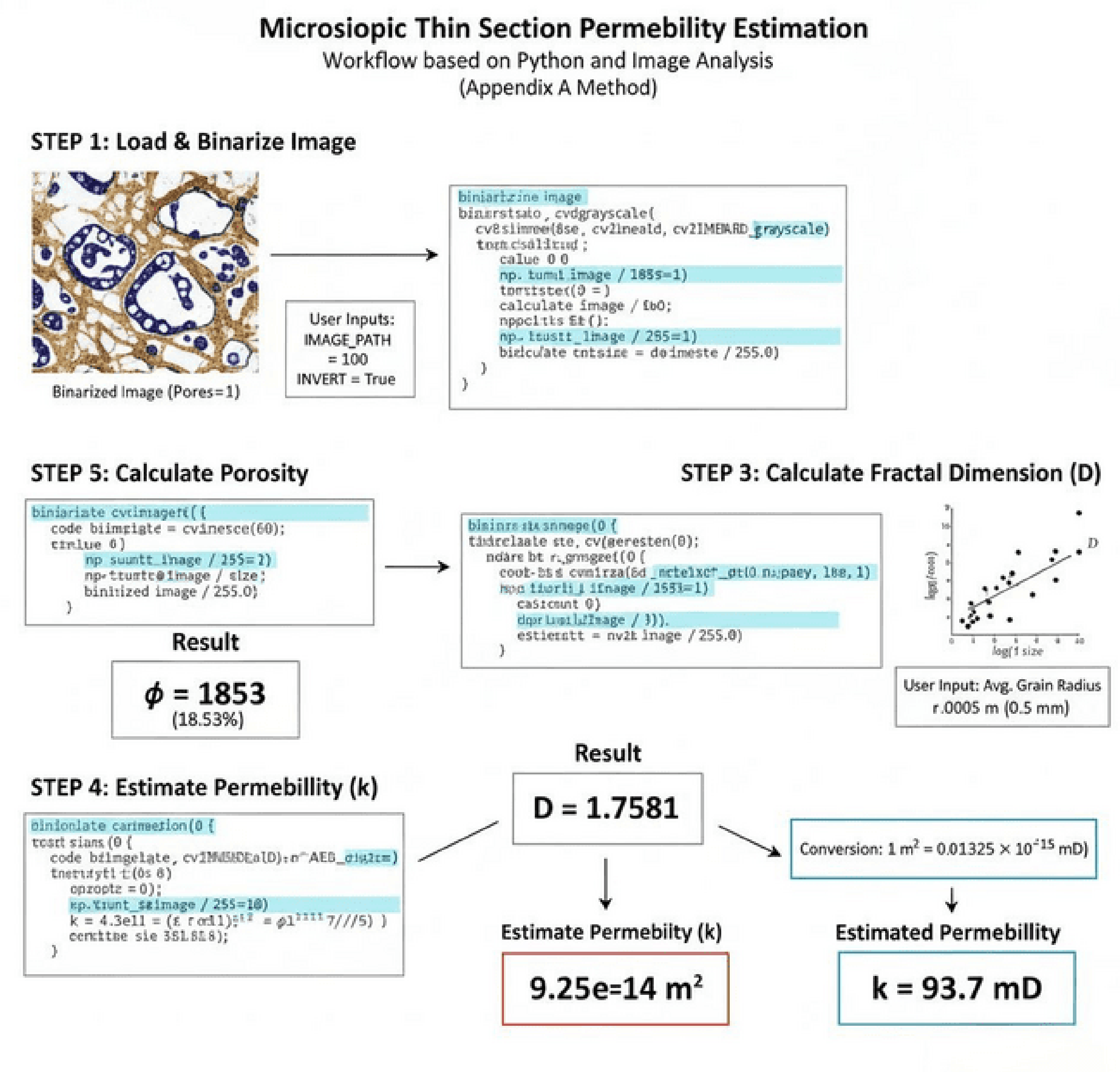

Figure 5.5: ML algorithms to calculate and estimate porosity and permeability. A new approach.
illustrates a step-by-step computational method to estimate rock permeability from a microscope image. First, the image is binarized to create a simple map of the pore spaces. This map is then analyzed to calculate two key parameters: porosity (phi), which is 18.53%, and the fractal dimension (D), which is 1.7581. Finally, these two values are put into a formula to calculate the permeability, yielding a final result of 93.7 md.
:

6. CONCLUSIONS

This integrated analysis of the Kirthar Formation confirms that its reservoir potential is the predictable outcome of a two-part story: the primary depositional fabric and its subsequent diagenetic overprint. The tectonically active Jacobabad-Khairpur High was the fundamental architectural control, creating a paleotopographic high that localized a high-energy "Nummulites factory" on a homoclinal ramp. This process created the coarse, grain-dominated packstones that form the foundation for reservoir "sweet spots". However, this potential was only unlocked by a complex diagenetic history. The most critical reservoir-enhancing process was late-stage, uplift-related (telogenetic) meteoric dissolution, which aggressively created secondary moldic and vuggy porosity. In contrast, the mud-dominated facies were compacted and cemented, ultimately becoming effective seals, while stylolites introduced critical anisotropy, acting as vertical barriers but also as potential lateral conduits for fluid flow.
Crucially, these findings are not an isolated case. The Eocene Tethyan margin is a prolific hydrocarbon province, and this specific depositional and diagenetic model—a tectonically-influenced ramp dominated by LBFs, later enhanced by meteoric dissolution—serves as a powerful and widely applicable regional analogue. We see direct parallels in other major Pakistani reservoirs, such as the

Sakesar Limestone , as well as in global analogues like the El Garia Formation in North Africa. The true significance of this study, therefore, lies in the methodology proposed to unlock these insights. By moving beyond traditional, qualitative petrography, we have outlined a quantitative and predictive framework that fully honors the geological complexity.

By conceptualizing a workflow that integrates machine learning for automated facies classification with physics-based permeability modeling, this work provides a scalable template for "reimagining" the carbonate factory. This approach allows for the rapid, objective, and data-driven characterization of heterogeneous reservoirs, directly linking the micro-scale fabric identified in thin sections to the reservoir-scale fluid flow behavior. This quantitative linkage is the key to de-risking exploration and can be applied to complex carbonate systems globally, well beyond the confines of the Indus Basin.

REFERENCES

1. Alfonso Bosellini, 1989. "Dynamics of Tethyan Carbonate Platforms", Controls on Carbonate Platforms and Basin Development, Paul D. Crevello, James L. Wilson, J. Frederick Sarg, J. Fred Read. https://pubs.geoscienceworld.org/books/book/chapter-pdf/3791969/9781565761056_ch01.pdf
2. Davaud, E., & Jorry, S. (2006). Hydrodynamic behaviour of Nummulites: implications for depositional models. Facies. https://doi.org/10.1007/S10347-005-0035-Z.
3. Racey, A. (2001) A REVIEW OF EOCENE NUMMULITE ACCUMULATIONS: STRUCTURE, FORMATION AND RESERVOIR POTENTIAL. *Journal of Petroleum Geology*, 24 (1) 79-100 doi:10.1111/j.1747-5457.2001.tb00662.x
4. John D. Smewing, John Warburton, Tim Daley, Philip Copestake, Nazir Ul-Haq, 2002. "Sequence stratigraphy of the southern Kirthar Fold Belt and Middle Indus Basin, Pakistan", The Tectonic and Climatic Evolution of the Arabian Sea Region, P. D. Clift, D. Kroon, C. Gaedicke, J. Craig (Geological Society of London), https://doi.org/10.1144/GSL.SP.2002.195.01.15.
5. Hinsch, R., Asmar, C., Nasim, M., Abbas, M. A., and Sultan, S.: Linked thick- to thin-skinned inversion in the central Kirthar Fold Belt of Pakistan, Solid Earth, 10, 425–446, https://doi.org/10.5194/se-10-425-2019, 2019.
6. C. J. Wandrey, "Sembar Goru/Ghazij Composite Total Petroleum System, Indus and Sulaiman-Kirthar Geologic Provinces, Pakistan and India," Petroleum Systems and Related Geologic Studies in Region 8, South Asia, U.S. Geological Survey Bulletin 2208-C, 2000 (CD-ROM). https://pubs.usgs.gov/bul/2208/C/b2208-c508.pdf

7. Mohibullah, M. (2019). BIOSTRATIGRAPHY OF THE KIRTHAR FORMATION, MACH AREA, SULAIMAN FOLD-THRUST BELT, BALOCHISTAN, PAKISTAN. https://www.pjsir.org/editorial-process/articles/2388_20062934_Uddin-et-al--2018-Biostratigraphy--of-the-Kirthar-Formation-_Recovered_.pdf
8. Babar, N., Mohibullah, M., Kasi, A. K., Ali, N., & Khan, A. (2018). Foraminiferal Biostratigraphy of the Eocene Kirthar Formation, western Sulaiman Fold-Thrust Belt, Balochistan, Pakistan. *Journal of Himalayan Earth Sciences*, *51*(2), 66-77. Retrieved from http://ojs.uop.edu.pk/jhes/article/view/1860.
9. Muhammad Haris, Syed Kamran Ali, Syed Umair Kazmi, Shah Zeb Ali, Muhammad Zaheer, Shahzad Hussain, Khawaja Saad, Mubeen Islam, Tariq Mehmood, Malik Humza (2022); Surface And Subsurface Expressions Of Jacobabad Khairpur Highs, Southern Indus Basin Using Well Data: An Approach For Well Prognosis; International Journal of Scientific and Research Publications (IJSRP) 12(6) (ISSN: 2250-3153), DOI: http://dx.doi.org/10.29322/IJSRP.12.06.2022.p12654.
10. Akram, M.N., Khan, Z., Shahzad, R., Ahmed, S., Ahmed, S., Khan, I., & Awan, U.H. (2020). Tectono-stratigraphy, Structural Development and Hydrocarbon Potential of Khairpur-Jaccobabad High (KJH), Lower Indus Basin, Pakistan – An Overview Based on Seismic and Well Data.
11. Shah, F., Miraj, M., Ali, A. et al. Tectonics of Jacobabad–Khairpur High and Its Impact on Petroleum Fields of the Region, Southern Indus Basin, Pakistan: A Case Study. Geotecton. 57, 346–358 (2023). https://doi.org/10.1134/S001685212303007X.
12. Microfacies and Depositional Settings of the Eocene Nisai Formation, Pishin Belt, Pakistan.. (n.d.) >*The Free Library*. (2014). Retrieved Nov 06 2025 from https://www.thefreelibrary.com/Microfacies+and+Depositional+Settings+of+the+Eocene+Nisai+Formation%2c...-a0747020319.
13. Gingerich, P. D. (2003). Stratigraphic and micropaleontological constraints on the middle Eocene age of the mammal-bearing Kuldana Formation of Pakistan. *Journal of Vertebrate Paleontology*, *23*(3), 643–651. https://doi.org/10.1671/2409
14. AFZAL, J., WILLIAMS, M., LENG, M.J., ALDRIDGE, R.J. and STEPHENSON, M.H. (2011), Evolution of Paleocene to Early Eocene larger benthic foraminifer assemblages of the Indus Basin, Pakistan. Lethaia, 44: 299-320. https://doi.org/10.1111/j.1502-3931.2010.00247.x
15. Jones, R. W.: Aspects of the Cenozoic stratigraphy of the Northern Sulaiman Ranges, Pakistan, J. Micropalaeontol., 16, 51–58, https://doi.org/10.1144/jm.16.1.51, 1997.
16. Eames, F. E. (1951). A Contribution to the Study of the Eocene in Western Pakistan and Western India B. The Description of the Lamellibranchia from Standard Sections in the Rakhi Nala and Zinda Pir Areas of the Western Punjab and in the Kohat District. Philosophical Transactions of the Royal Society of London. Series B, Biological Sciences, 235(627), 311–482. http://www.jstor.org/stable/92425.
17. Asim, S. , Qureshi, S. and Khan, N. (2014) Study of an Uplift of Sargodha High by Stratigraphical and Structural Interpretation of an East-West Seismic Profile in Central Indus Basin, Pakistan. *International Journal of Geosciences*, **5**, 1027-1036. doi: 10.4236/ijg.2014.59088.
18. Shabeer Ahmed, Sarfraz Hussain Solangi, Muhammad Saeed Khan Jadoon, Adeel Nazeer, Tectonic evolution of structures in Southern Sindh Monocline, Indus Basin, Pakistan formed in multi-extensional tectonic episodes of Indian Plate, Geodesy and Geodynamics, Volume 9, Issue 5, 2018, Pages 358-366, ISSN 1674-9847, https://doi.org/10.1016/j.geog.2018.03.004.
19. Majid Khan, Yike Liu, Geodynamic evolution of the offshore Indus Basin Pakistan: the western Indian Plate Passive Continental Margin, *Geophysical Journal International*, Volume 217, Issue 2, May 2019, Pages 1366–1386, https://doi.org/10.1093/gji/ggz091
20. John D. Smewing, John Warburton, Tim Daley, Philip Copestake, Nazir Ul-Haq, 2002. "Sequence stratigraphy of the southern Kirthar Fold Belt and Middle Indus Basin, Pakistan", The Tectonic and Climatic Evolution of the Arabian Sea Region, P. D. Clift, D. Kroon, C. Gaedicke, J. Craig. https://doi.org/10.1144/GSL.SP.2002.195.01.15.
21. Lithofacies, Depositional Environments, and Regional Stratigraphy of the Lower Eocene Ghazij Formation, Balochistan, Pakistan - USGS Publications Warehouse, accessed October 26, 2025, https://doi.org/10.3133/pp1599.
22. JAWAD AFZAL, MARK WILLIAMS, RICHARD J. ALDRIDGE; Revised stratigraphy of the lower Cenozoic succession of the Greater Indus Basin in Pakistan. *Journal of Micropalaeontology* 2009;; 28 (1): 7–23. doi: https://doi.org/10.1144/jm.28.1.7
23. Malkani, M.S. and Haroon, Y. (2022) Lithostratigraphy, Structure, Geological History, Economic Geology and Paleontology of Mari Bugti Hills and Surrounding areas of Balochistan, South Punjab and North Sindh (Pakistan). Open Journal of Geology, 12, 13-56. https://doi.org/10.4236/ojg.2022.121002.

24. Ayyad, H.M., El-Moghny, M.W.A., Abuseda, H. *et al.* Sequence stratigraphy and reservoir characterization of the lower Eocene rocks (Thebes Formation) along the Tethyan Ocean's southern margin: biostratigraphy and petrophysical parameter applications. *Int J Earth Sci (Geol Rundsch)* **112**, 1091–1112 (2023). https://doi.org/10.1007/s00531-023-02291-9.
25. Amosu A, Mahmood H, Ofoche P (2018) Estimating the Permeability of Carbonate Rocks from the Fractal Properties of Moldic Pores using the Kozeny-Carman Equation. Research Ideas and Outcomes 4: e24430. https://doi.org/10.3897/rio.4.e24430.
26. Dalmasso, H., Montaggioni, L. F., Bosence, D., & Floquet, M. (2001). Numerical Modelling of Carbonate Platforms and Reefs: Approaches and Opportunities. *Energy Exploration & Exploitation*, *19*(4), 315–345. http://www.jstor.org/stable/43754840.
27. Srinivasan, S. (2009). Stochastic modeling of facies distribution in a carbonate reservoir in the Gulf of Mexico.
28. Bayat, A. , Asghari, O. , Bahroudi, A. , & Tavvakoli, M. (2016). Facies Modeling of Heterogeneous Carbonates Reservoirs by Multiple Point Geostatistics. *Journal of Petroleum Science and Technology*, *6*(2), 56-65. doi: 10.22078/jpst.2016.664.
29. Handoyo, N., Ronlei, B. C., Wibowo, A. S., Sigalingging, A. S., Nathania, E. Y., Fatkhan, F., Erdi, A., Avseth, P., Carbonell, R., Nugroho, P., Pandito, R. H. B., Nasibov, A., & Husein, A. a. A. (2025). Reservoir Characterization of Ngrayong Formation, Sandstone with Carbonate Intercalation, Using a Geostatistical Approach Based on Petrophysical Parameters, Northeast Java Basin, Indonesia. *Scientific Contributions Oil and Gas*, *48*(3), 237–251. https://doi.org/10.29017/scog.v48i3.1828
30. Almomen, A. T. Evaluating Machine Learning Techniques for Carbonate Formation Permeability Prediction Using Well Log Data. Iraqi Geological Journal. https://doi.org/10.46717/IGJ.56.1D.14MS-2023-4-23.
31. Aydın, İ., Şener, T. K., Kılıç, A. D., & Derviş, H. (2025). Classification of Thin-Section Rock Images Using a Combined CNN and SVM Approach. *Minerals*, *15*(9), 976. https://doi.org/10.3390/min15090976.
32. He Liu, Yi-Li Ren, Xin Li, Yan-Xu Hu, Jian-Ping Wu, Bin Li, Lu Luo, Zhi Tao, Xi Liu, Jia Liang, Yun-Ying Zhang, Xiao-Yu An, Wen-Kai Fang, Rock thin-section analysis and identification based on artificial intelligent technique, Petroleum Science, Volume 19, Issue 4, 2022, Pages 1605-1621, ISSN 1995-8226, https://doi.org/10.1016/j.petsci.2022.03.011.
33. "Vellappally, A. and Hou, S. and Emmings, J, Automated Grain Segmentation and Mineral Classification in Rock Thin Sections, European Association of Geoscientists & Engineers, 85th EAGE Annual Conference & Exhibition, Jun 2024, Volume 2024, p.1 – 5, https://doi.org/10.3997/2214-4609.2024101405.
34. Pereira Borges, H., de Aguiar, M.S. (2019). Mineral Classification Using Machine Learning and Images of Microscopic Rock Thin Section. In: Martínez-Villaseñor, L., Batyrshin, I., Marín-Hernández, A. (eds) Advances in Soft Computing. MICAI 2019. Lecture Notes in Computer Science(), vol 11835. Springer, Cham. https://doi.org/10.1007/978-3-030-33749-0_6.
35. Farmanov, Ravan, Feldmann, Felix, Mathew, Eric Sonny, Tembely, Moussa, Al-Shalabi, Emad W., AlAmeri, Waleed, Masalmeh, Shehadeh, and Ali AlSumaiti. "Application of Machine Learning for Estimating Petrophysical Properties of Carbonate Rocks Using NMR Core Measurements." Paper presented at the SPE Reservoir Characterisation and Simulation Conference and Exhibition, Abu Dhabi, UAE, January 2023. doi: https://doi.org/10.2118/212625-MS.
36. Pakhnevich, A., Nikolayev, D., & Lychagina, T. (2023). Local Crystallographic Texture of a Nummulite (Foraminifera) Test from the Eocene Deposits of the Crimea Peninsula. *Biology*, *12*(12), 1472. https://doi.org/10.3390/biology12121472.
37. Memon, F. H., Tunio, A. H., Memon, K. R., Mahesar, A. A., & Abbas, G. (2023). Unveiling the Diagenetic and Mineralogical Impact on the Carbonate Formation of the Indus Basin, Pakistan: Implications for Reservoir Characterization and Quality Assessment. *Minerals*, *13*(12), 1474.
38. Ala A. Ghafur, Osman Salad Hersi, (2023), Diagenetic evolution and its effect on the reservoir quality of Oligo-Miocene Kirkuk Group, Kurdistan Region, Northern Iraq, Geoconvention Calgary.
39. Shangfeng Yang, Zhidong Bao, Nan Wang, Xuefeng Qu, Yanbo Lin, Jinjiang Shen, Rizwan Sarwar Awan, Diagenetic evolution and its impact on reservoir quality of tight sandstones: A case study of the Triassic Chang 6 Member, Ordos Basin, northwest China, Marine and Petroleum Geology, Volume 117, 2020, 104360, ISSN 0264-8172, https://doi.org/10.1016/j.marpetgeo.2020.104360.

40. Magni, S., Martín-Martín, J. D., Bons, P. D., & Gomez-Rivas, E. (2025). Stylolites in Carbonate Rocks: Morphological Variability According to the Host Rock Texture. *Minerals*, *15*(2), 132. https://doi.org/10.3390/min15020132.
41. Nikbin, M., Moussavi-Harami, R., Moghaddas, N.H. *et al.* The role of stylolites as a fluid conductive, in the heterogeneous carbonate reservoirs. *J Petrol Explor Prod Technol* **14**, 2953–2971 (2024). https://doi.org/10.1007/s13202-024-01875-8.
42. E. Humphrey, E. Gomez-Rivas, D. Koehn, P.D. Bons, J. Neilson, J.D. Martín-Martín, J. Schoenherr,Stylolite-controlled diagenesis of a mudstone carbonate reservoir: A case study from the Zechstein_2_Carbonate (Central European Basin, NW Germany), Marine and Petroleum Geology,Volume 109, 2019, Pages 88-107, ISSN 0264-8172, https://doi.org/10.1016/j.marpetgeo.2019.05.040.
43. Swei, G.H. and Tucker, M.E. (2012), IMPACT OF DIAGENESIS ON RESERVOIR QUALITY IN RAMP CARBONATES: GIALO FORMATION (MIDDLE EOCENE), SIRT BASIN, LIBYA. Journal of Petroleum Geology, 35: 25-47. https://doi.org/10.1111/j.1747-5457.2012.00517.x
44. Rahim, H.-u.-, Qamar, S., Shah, M. M., Corbella, M., Martín-Martín, J. D., Janjuhah, H. T., Navarro-Ciurana, D., Lianou, V., & Kontakiotis, G. (2022). Processes Associated with Multiphase Dolomitization and Other Related Diagenetic Events in the Jurassic Samana Suk Formation, Himalayan Foreland Basin, NW Pakistan. *Minerals*, *12*(10), 1320. https://doi.org/10.3390/min12101320
45. Qamar, S., Shah, M. M., Janjuhah, H. T., Kontakiotis, G., Shahzad, A., & Besiou, E. (2023). Sedimentological, Diagenetic, and Sequence Stratigraphic Controls on the Shallow to Marginal Marine Carbonates of the Middle Jurassic Samana Suk Formation, North Pakistan. *Journal of Marine Science and Engineering*, *11*(6), 1230. https://doi.org/10.3390/jmse11061230.
46. Swati, M. A. F., Haneef, M., Ahmad, S., Latif, K., Naveed, Y., Zeb, W., Akhtar, N., & Owais, M. (2014). Diagenetic analysis of the Early Eocene Margala Hill limestone, Pakistan: A synthesis for thin section porosity. *Journal of Himalayan Earth Sciences*, *47*(2), 49-61. Retrieved from http://ojs.uop.edu.pk/jhes/article/view/1701.
47. Ahmad, R. and J. Afzal, 2002, Sequence Stratigraphy of the mixed carbonate-siliciclastic System of the Eocene Nisai Formation, Pishin Basin: **Distribution of source rocks and reservoir facies**. SPE-PAPG ATC 2002 proceedings. Hunting Survey Corporation.
48. Mazzullo, S. (2004). Overview of porosity evolution in carbonate reservoirs.
49. Viviana D. Diaz, Donald F. McNeill, Robert C. Goodin, James S. Klaus, 2019. "Porosity Distribution and Evolution in Pleistocene Reefal Limestone: Implications For Scale-Dependent Fluid Flow", Carbonate Pore Systems: New Developments and Case Studies, Donald F. McNeill, Paul (Mitch) Harris, Eugene C. Rankey, Jean C.C. Hsieh. https://doi.org/10.2110/sepmsp.112.07.
50. Lidz, B.H. (2011). Porosity Variability In Limestone Sequences. In: Hopley, D. (eds) Encyclopedia of Modern Coral Reefs. Encyclopedia of Earth Sciences Series. Springer, Dordrecht. https://doi.org/10.1007/978-90-481-2639-2_244
51. Khitab, U., Umar, M. & -, M. Microfacies, diagenesis and hydrocarbon potential of Eocene carbonate strata in Pakistan. *Carbonates Evaporites* **35**, 70 (2020). https://doi.org/10.1007/s13146-020-00601-9
52. Naveed Rehman, Shu Jiang, Syed Haroon Ali, Asim Falak Naz, Muhammad Tariq. Effect of Diagenetic Processes and Depositional Facies on Reservoir Quality of the Eocene Carbonate Sequence (Sakesar Limestone) in the Central Salt Range, Pakistan. *Journal of Earth Science*, 2025, 36(3): 1129-1148. doi: 10.1007/s12583-024-0105-1
53. Ehrenberg, Stephen & Morad, Sadoon & Yaxin, Liu & Chen, Rulin. (2016). Stylolites and Porosity In A Lower Cretaceous Limestone Reservoir, Onshore Abu Dhabi, U.A.E.. Journal of Sedimentary Research. 86. 1228-1247. DOI:10.2110/jsr.2016.68.
54. Fang Shaobo , Xi Dangpeng , Sun Qi , Li Dalei , Yang Zhangzhang , Liu Dan , Wu Yuyang , Jiang Tian , Wan Xiaoqiao, (2024), The bivalve-bearing carbonate platform on the east Tethys during the middle Eocene and its response to the Tethys transgression., Frontiers in Earth Science., 12, https://DOI=10.3389/feart.2024.1398474.
55. T.P. Burchette, V.P. Wright, Carbonate ramp depositional systems, Sedimentary Geology, Volume 79, Issues 1–4, 1992, Pages 3-57, ISSN 0037-0738, https://doi.org/10.1016/0037-0738(92)90003-A.
56. Kowal-Kasprzyk, J., Waśkowska, A., Golonka, J., Krobicki, M., Skupien, P., & Słomka, T. (2021). The Late Jurassic–Palaeogene Carbonate Platforms in the Outer Western Carpathian Tethys—A Regional Overview. *Minerals*, *11*(7), 747. https://doi.org/10.3390/min11070747.
57. Moradi-Doreh, F., Habibi, T., Ruban, D. A., & Hosseinzadeh, R. (2025). A Large Cenomanian Carbonate Ramp at the Transition Between Two Domains of the Zagros Sedimentary Basin, SW Iran: Cyclic Evolution and Its Eustatic and Tectonic Controls. *Journal of Marine Science and Engineering*, *13*(6), 1084. **https://doi.org/10.3390/jmse13061084**

58. Götz, Annette & Lenhardt, Nils. (2011). The Anisian carbonate ramp system of Central Europe (Peri-Tethys Basin): Sequences and reservoir characteristics. Acta geologica Polonica. 61. 59-70.
59. Khan, M.W., Ikram, M.F., Sultan, S.A., & Alam, I. (2019). Strata-bound Dolomitization in the Eocene Laki Formation, Matyaro Jabal Area Lakhi Range, Sindh, Pakistan.
60. Miclăuş, C., Tent-Manclús, J. E., Tosquella, J., Martín-Martín, M., & Serrano, F. (2025). Eocene Stratigraphic Sequences in the Prebetic of Alicante (SE Spain) and Their Correlation with Global Sea-Level and Climatic Curves. *Journal of Marine Science and Engineering*, *13*(6), 1031. https://doi.org/10.3390/jmse13061031.
61. Carbonate Seq Strat - SEPM Strata, https://www.sepmstrata.org/page.aspx?pageid=131
62. John D.S, John.W, Tim.D, Philip.C, Nazir U.H, (2002), Sequence stratigraphy of the southern Kirthar Fold Belt and Middle Indus Basin, Pakistan,
Geological Society, London, Special Publications, January,
https://doi.org/10.1144/gsl.sp.2002.195.01.15.
63. Raiees Amjad, M., Ehsan, M., Hussain, M., Al-Ansari, N., Rehman, A., Naseer, Z., Ejaz, M.N., Baouche, R., & Elbeltagi, A. (2023). Carbonate Reservoir Quality Variations in Basins with a Variable Sediment Influx: A Case Study from the Balkassar Oil Field, Potwar, Pakistan. *ACS Omega, 8*, 4127 - 4145.
64. Yang, C., Zhao, C., Meng, X., Dong, P., Chai, J., Wang, X., Nie, Q., Yang, J., & Yu, W. (2023). Reservoir Characterization and an Integrated Approach of Reservoir Modeling for Miano Gas Field, Middle Indus Basin. *Energies*, *16*(2), 856. https://doi.org/10.3390/en16020856.
65. Muhsan Ehsan, Rujun Chen, Muhammad Ali Umair Latif, Kamal Abdelrahman, Abid Ali, Jar Ullah, and Mohammed S. Fnais, Unconventional Reservoir Characterization of Patala Formation, Upper Indus Basin, Pakista*ACS Omega* **2024** *9* (13), 15573-15589, https://doi.10.1021/acsomega.4c00465.
66. Hafeez, M., Khan, N., Wadood, B. *et al.* Paleoenvironmental and Diagenetic Analysis of the Middle Palaeocene Ramp Carbonates in Northwestern Pakistan: Implications for Deciphering the Reservoir Potential. *Dokl. Earth Sc.* **515**, 609–623 (2024). https://doi.org/10.1134/S1028334X23603127.
67. Memon, F. H., Tunio, A. H., Memon, K. R., Mahesar, A. A., & Abbas, G. (2023). Unveiling the Diagenetic and Mineralogical Impact on the Carbonate Formation of the Indus Basin, Pakistan: Implications for Reservoir Characterization and Quality Assessment. *Minerals*, *13*(12), 1474. https://doi.org/10.3390/min13121474
68. Yuanyuan Chen, Luanxiao Zhao, Jianguo Pan, Chuang Li, Minghui Xu, Kejian Li, Fengshou Zhang, Jianhua Geng, Deep carbonate reservoir characterisation using multi-seismic attributes via machine learning with physical constraints, *Journal of Geophysics and Engineering*, Volume 18, Issue 5, October 2021, Pages 761–775, https://doi.org/10.1093/jge/gxab049.
69. Tian, X., Huang, H., Cheng, S., Wang, C., Li, P., & Hao, Y. (2022). A Carbonate Reservoir Prediction Method Based on Deep Learning and Multiparameter Joint Inversion. *Energies*, *15*(7), 2506. https://doi.org/10.3390/en15072506.
70. Said Hassaan, Abdulaziz Mohamed, Ahmed Farid Ibrahim, and Salaheldin Elkatatny, Real-Time Prediction of Petrophysical Properties Using Machine Learning Based on Drilling Parameters, *ACS Omega* **2024** *9* (15), 17066-17075, https://DOI.10.1021/acsomega.3c08795.
71. Zhao, J., Wang, Q., Rong, W., Zeng, J., Ren, Y., & Chen, H. (2024). Permeability Prediction of Carbonate Reservoir Based on Nuclear Magnetic Resonance (NMR) Logging and Machine Learning. *Energies*, *17*(6), 1458. https://doi.org/10.3390/en17061458.
72. Waqas Naseem, Irfan Ullah Jan, Khairul Azlan Mustahpa, Mohammed Hail Hakimi, Shabeer Ahmed, and Ali Y. Kahal, The Early Cretaceous Sembar Formation, Southern Indus Basin, Pakistan: Biomarkers and Trace Element Distributions to Investigate the Sedimentary Palaeoenvironment and Organic Matter Input, *ACS Omega* 2024 *9* (38), 39430-39451. https://DOI.10.1021/acsomega.4c02995.
73. Rehman, N., Jiang, S., Ali, S.H. *et al.* Effect of Diagenetic Processes and Depositional Facies on Reservoir Quality of the Eocene Carbonate Sequence (Sakesar Limestone) in the Central Salt Range, Pakistan. *J. Earth Sci.* **36**, 1129–1148 (2025). https://doi.org/10.1007/s12583-024-0105-1
74. Ali, A., Z, Rashid, H, (2016) 3D facies model of early Eocene succession southern Indus basin Pakistan. Abstract Publications. https://www.researchgate.net/publication/323627642_3D_facies_model_of_early_Eocene_succession_southern_Indus_basin_Pakistan
75. Sahy, Diana; Sasaran, Emanoil; and Tamas, Tudor (2008) Microfacies Analysis of Upper Eocene Shallow-water Carbonates from the Rodnei Mountains (N Romania), *Studia UBB Geologia* 53 (2): 13-24 http://dx.doi.org/10.5038/1937-8602.53.2.2.

76. Seyed Ahmad Babazadeh, Dominique Cluzel; New biostratigraphy and microfacies analysis of Eocene Jahrum Formation (Shahrekord region, High Zagros, West Iran). A carbonate platform within the Neo-Tethys oceanic realm. *Bulletin de la Société Géologique de France* 2023;; 194 (1): 1. doi: https://doi.org/10.1051/bsgf/2022016.
77. Muhammad Umar, Henrik Friis, Abdul Salam Khan, Akhtar Muhammad Kassi, Aimal Khan Kasi, The effects of diagenesis on the reservoir characters in sandstones of the Late Cretaceous Pab Formation, Kirthar Fold Belt, southern Pakistan, Journal of Asian Earth Sciences, Volume 40, Issue 2,2011,Pages 622-635,ISSN 1367-9120, https://doi.org/10.1016/j.jseaes.2010.10.014.
78. Lynton S. Land; Holocene Meteoric Dolomitization of Pleistocene Limestones, North Jamaica. *AAPG Bulletin* 1973;; 57 (4): 790. doi: https://doi.org/10.1306/819A43FA-16C5-11D7-8645000102C1865D
79. Hemphill, W.R. and Kidwai, A.H. (1973) Stratigraphy of the Bannu and Dera Ismail Khan Areas, Pakistan. Paper No. 716 B, United States Geological Survey, Reston, 1-36. https://doi.org/10.3133/pp716B
80. Asim, S., Khan, N., Qureshi, S. N., Hussain, F., & Bablani, S. A. (2014). Study of a Stratigraphic Trap of Paleocene/Late Cretaceous Age with the Help of Seismic Data in Sulaiman Foredeep and Kirthar Foredeep Area (Central & Southern Indus Basin, Pakistan). *International Journal of Geosciences*, *05*(10), 1049–1061. https://doi.org/10.4236/ijg.2014.510090
81. Wang Yan , Xie Pengfei , Zhang Huitao , Liu Yuming , Yang Aiying, (2024), Fracture-vuggy carbonate reservoir characterization based on multiple geological information fusion, Frontiers in Earth Science, Volume 11 – 2023, http://DOI.10.3389/feart.2023.1345028.
82. A. Mangione, H. Lewis, S. Geiger, Z. Jiang, G.D. Couples, J. Buckman, S. Beavington-Penney, S.A. Hall,
83. Estimation of pre-dolomitisation porosity and permeability of a nummulitic carbonate reservoir rock using the Multi-Component Architecture Method (MCAM), Marine and Petroleum Geology, Volume 132, 2021, 105196, ISSN 0264 8172, https://doi.org/10.1016/j.marpetgeo.2021.105196.
84. Amosu, A. A., & Sun, X. (2018). Estimating the permeability of carbonate rocks from the fractal dimension of pore networks modeled from thin section photomicrographs. *International Journal of Earth Sciences & Engineering*, *11*(01), 1-13.
85. Carman, P. C. (1937). Fluid flow through granular beds. *Transactions of the Institution of Chemical Engineers*, **15**, 150–166.
86. Folk, R. L. (1959). Practical petrographic classification of limestones. *AAPG Bulletin*, *43*, 1-38.
87. Embry, A.F. and Klovan, J.E. (1971). A Late Devonian Reef Tract on Northeastern Banks Island. *Canadian Petroleum Geology*, 19, 730-781.
88. Flügel, E. (2004) Microfacies of Carbonate Rocks, Analysis, Interpretation and Application. Springer, Berlin, 976 p.
89. Josep, Serra-Kiel & Martín Martín, Manuel & Mamoune, B. & Martín-Algarra, Agustín & Pérez, J. & Tosquella, Josep & Ferràndez-Cañadell, Carles & Serrano, Francisco. (1998). Biostratigrafía y litoestratigrafía del Paleógeno del área de Sierra Espuña (Cordillera Bética oriental, SE de España). Acta geológica hispánica; Vol.: 31 Núm.: 1 -3.
90. Hottinger, L., Halicz, E., & Reiss, Z. (1993). Recent Foraminiferida from the Gulf of Aqaba, Red Sea. Slovenska Akademija Znanosti in Umetnosti, Classis IV, Opera 33, Ljubljana, 179 p.
91. Wilson, J.L. (1975) Carbonate Facies in Geologic History. Springer Verlag, New York, 471p. https://doi.org/10.1007/978-1-4612-6383-8.
92. Bathurst, R.G.C. (1975) Carbonate Sediment and Their Diagenesis. Development in Sedimentology, Elsevier, Amsterdam, 658 p.
93. Flugel, E. (2010) Microfacies of Carbonate Rocks, Analysis, Interpretation and Application. Springer-Verlag, Berlin, 976 p.
94. Pape, H., Clauser, C., & Iffland, J. (1999). Permeability prediction for reservoir sandstones by use of fractal pore space characterization. Pure and Applied Geophysics, 156(1-2), 147-162.
95. Hottinger, L. (1983). Neritic macroid genesis, an ecological approach. In: Peryt, T.M. (Ed.), Coated Grains. Springer-Verlag, Berlin, pp. 38–55.
96. Hottinger, L. (1997). Shallow benthic foraminiferal assemblage as signals for depth of their limestones. Bulletin de la Société Géologique de France, 168, 491-505.
97. Burchette, T. P., & Wright, V. P. (1992). Carbonate ramp depositional systems. Sedimentary Geology, 79(1-4), 3-57.
98. Buxton, M.W.N. and Pedley, H.M. (1989) A Standardized Model for Tethyan Tertiary Carbonates Ramps. Journal of the Geological Society, 146, 746-748. http://dx.doi.org/10.1144/gsjgs.146.5.0746.

Appendix A: Mathematical Framework for Permeability Prediction in Heterogeneous Carbonates

(The Kozeny-Carman (85)(KC) equation provides a fundamental relationship between permeability (k), porosity (ϕ), and the geometric properties of a porous medium. For complex carbonate pore networks, particularly those with fractal characteristics, the standard KC equation can be modified to incorporate these complexities. This approach, outlined by researchers such as Pape et al. (1999) and applied by (84) provides a method to estimate permeability from parameters measurable in thin section images. (26)

The modified KC equation is given by:

$$k = \frac{\phi}{c T r_{eff}^2}$$

where c is a shape factor (often taken as 8 for cylindrical pores), T is the tortuosity of the flow path, and r_{eff} is the effective pore radius.
For a pore system that can be approximated by a fractal model (such as the pigeonhole model for moldic pores), tortuosity and porosity can be related to the fractal dimension (D) of the pore space and the average grain radius (r_{grain}). These relationships are valid for $2 < D < 3$:

1. Tortuosity (T):

   $$T = 1.34 \left(\frac{r_{grain}}{r_{eff}}\right)^{0.67(D-2)}$$
2. Porosity (ϕ):

   $$\phi = 0.5 \left(\frac{r_{grain}}{r_{eff}}\right)^{0.39(D-3)}$$

Application Workflow:

1. **Image Analysis:** A digitized thin section image is binarized to separate pore space from the rock matrix.
2. **Parameter Extraction:**
   - **Porosity (ϕ):** Calculated as the ratio of pore pixels to total pixels.
   - **Fractal Dimension (D):** Determined using the box-counting method on the pore space image.
   - **Average Grain Radius (r_{grain}):** Measured from the image.
   - **Effective Pore Radius (r_{eff}):** Can be estimated from pore size distribution analysis.
3. Calculation: By substituting a representative value for D (e.g., $D=2.11$ as used in 26), the equations for T and ϕ can be combined with the KC equation to derive a direct empirical relationship between permeability and porosity, constrained by the measured grain size:

   $$k = 4.3 \times 10^{11} r_{grain}^2 \phi^{7/5}$$

   This final equation allows for a physics-based estimation of permeability using readily obtainable petrographic data, providing a powerful tool for reservoir characterization.

Appendix B: A Conceptual Machine Learning Workflow for Automated Microfacies Classification from Thin Section Imagery

This appendix outlines a conceptual workflow for automating microfacies classification using a hybrid machine learning approach, combining a Convolutional Neural Network (CNN) for feature extraction with a Random Forest (RF) classifier. The workflow is described using a Python-based pseudocode structure, leveraging common libraries such as TensorFlow/Keras and Scikit-learn. (31)

Objective: To train a model that can automatically classify patches of a thin section image into one of the six defined microfacies (HR-MF 1 to HR-MF 6).

Python

```python
# Import necessary libraries
import numpy as np
import tensorflow as tf
from tensorflow.keras.applications import VGG16
from sklearn.ensemble import RandomForestClassifier
from sklearn.model_selection import train_test_split
from sklearn.metrics import accuracy_score, classification_report
# Assume 'load_images_and_labels' is a custom function to load data
# from a directory structure where each sub-directory is a microfacies class.

# 1. DATA PREPARATION
# ---------------------
# Load image patches (e.g., 224x224 pixels) and their corresponding labels (0-5 for HR-MF 1-6)
image_patches, labels = load_images_and_labels('path/to/labeled_data/')

# Normalize pixel values to the range
image_patches = image_patches.astype('float32') / 255.0

# Split data into training and testing sets
X_train, X_test, y_train, y_test = train_test_split(image_patches, labels, test_size=0.2, random_state=42

# 2. FEATURE EXTRACTION USING A PRE-TRAINED CNN
# ---------------------------------------------
# Load a pre-trained CNN (VGG16) without its final classification layers.
# This model, trained on millions of images (ImageNet), is a powerful feature extractor.
base_model = VGG16(weights='imagenet', include_top=False, input_shape=(224, 224, 3))
base_model.trainable = False # Freeze the layers to use it as a static feature extractor

# Function to extract features from a set of images
def extract_features(model, images):
    features = model.predict(images)
    # Flatten the output of the convolutional layers to create a 1D feature vector for each image
    flattened_features = features.reshape((features.shape, -1))
    return flattened_features

# Extract features for both training and testing sets
train_features = extract_features(base_model, X_train)
test_features = extract_features(base_model, X_test)

# 3. MODEL TRAINING USING RANDOM FOREST
# -------------------------------------
# Initialize a Random Forest Classifier. RF is robust and performs well on high-dimensional feature sets.
rf_classifier = RandomForestClassifier(n_estimators=100, random_state=42, n_jobs=-1)

# Train the classifier on the extracted features from the training data
print("Training Random Forest Classifier...")
rf_classifier.fit(train_features, y_train)
print("Training complete.")
```

```
# 4. PREDICTION AND EVALUATION
# ------------------------------
# Use the trained classifier to predict the microfacies for the test set features
y_pred = rf_classifier.predict(test_features)

# Evaluate the model's performance
accuracy = accuracy_score(y_test, y_pred)
print(f"Model Accuracy: {accuracy:.4f}")
print("\nClassification Report:")
print(classification_report(y_test, y_pred, target_names=))

# 5. APPLICATION (INFERENCE)
# --------------------------
# To classify a new, large thin section image:
# 1. Divide the large image into a grid of 224x224 patches.
# 2. Preprocess each patch (normalize).
# 3. Extract features for all patches using the 'base_model'.
# 4. Use the trained 'rf_classifier' to predict the microfacies for each patch.
# 5. Reassemble the predictions to create a classified microfacies map of the entire thin section.
```

This workflow demonstrates a powerful and scalable method for leveraging deep learning to automate a critical geological task, enabling quantitative, data-driven analysis of rock microstructures.

- MICROFACIES CREATED USING ML

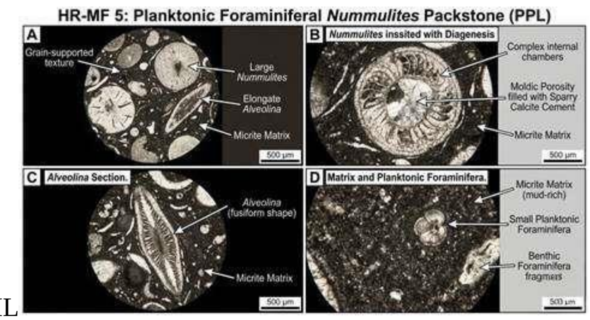

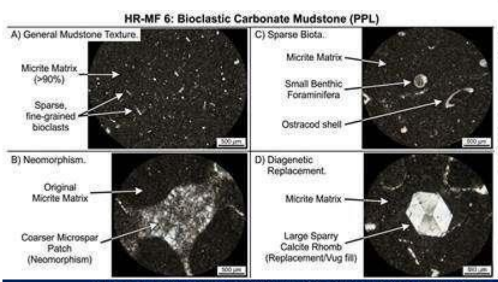

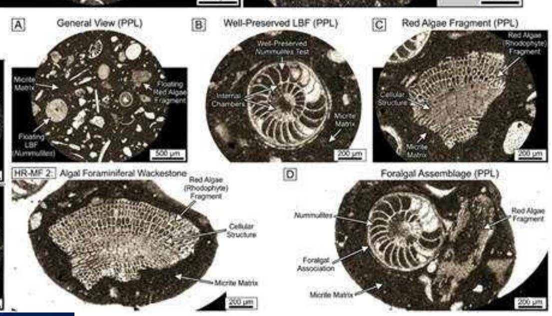

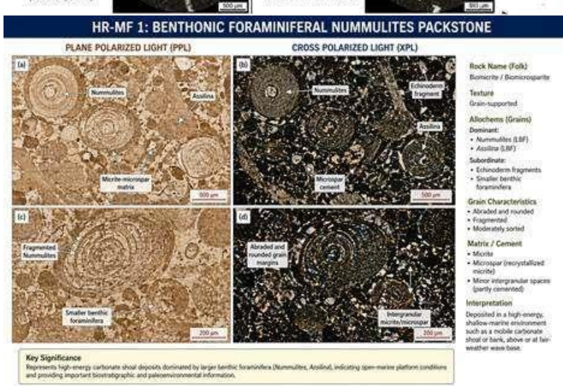

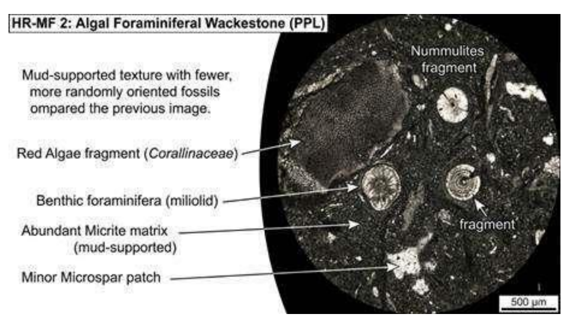

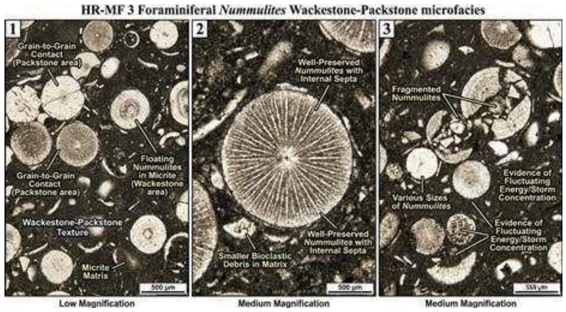
HR-MF 3 Foraminiferal *Nummulites* Wackestone-Packstone microfacies
1
Grain-to-Grain Contact (Packstone area)
Grain-to-Grain Contact (Packstone area)
Floating Nummulites in Micrite (Wackestone area)
Wackestone-Packstone Texture
Micrite Matrix
500 μm
Low Magnification
2
Well-Preserved Nummulites with Internal Septa
Well-Preserved Nummulites with Internal Septa
Smaller Bioclastic Debris in Matrix
500 μm
Medium Magnification
3
Fragmented Nummulites
Various Sizes of *Nummulites*
Evidence of Fluctuating Energy/Storm Concentration
Evidence of Fluctuating Energy/Storm Concentration
Medium Magnification